UNIVERSITY OF Southampton

University of Southampton Research Repository
ePrints Soton

Copyright © and Moral Rights for this thesis are retained by the author and/or other copyright owners. A copy can be downloaded for personal non-commercial research or study, without prior permission or charge. This thesis cannot be reproduced or quoted extensively from without first obtaining permission in writing from the copyright holder/s. The content must not be changed in any way or sold commercially in any format or medium without the formal permission of the copyright holders.

When referring to this work, full bibliographic details including the author, title, awarding institution and date of the thesis must be given e.g.

AUTHOR (year of submission) "Full thesis title", University of Southampton, name of the University School or Department, PhD Thesis, pagination

http://eprints.soton.ac.uk

MPhil Thesis
Transient Ground Effect Aerodynamics

Darren Coe

Aerodynamics and Flight Mechanics,
University of Southampton,
Southampton,
Hampshire
England

13th April 2015

Abstract

The aerodynamic development of vehicles in wind tunnels is currently performed via a series of static measurements. However, vehicles exploiting ground effect tend to be highly dynamic undergoing rapid changes in speed and attitude. Clearly therefore there is scope for an improvement in the fidelity of testing. At present the considerable difficulty of measuring body forces whilst simultaneously making variations to a model attitude prohibits transient investigations. Satisfying the demand for a dynamic testing capability formed the initial stages of the research. Having established the present performance of the hardware and software in use at the R.J. Mitchell wind tunnel an advanced data acquisition and motion control system was developed.

Experimental system identification methods were employed to determine the dynamic response of the force balance and pressure transducers. This knowledge was integrated into a data processing algorithm that effectively isolated the aerodynamic effects during the transient investigation.

As automotive vehicle models can be considered as bluff bodies their movement during dynamic testing has the potential to alter the test section wind speed due to varying blockage effects. To overcome this a controller was developed to maintain a constant wind speed. Tests were performed to allow the fan drive system and wind circuit to be characterised. The system was found to be non-linear a gain scheduling controller was therefore developed that improved the control of wind speed control without employing a complex non-linear controller.

Results from the dynamic test programme clearly demonstrated the transient aerodynamic effects upon a wing in ground effect. These results were dependent upon motion amplitude, frequency and mean ground clearance. Comparisons were made with static results and dynamic testing results out of ground effect.

Contents

List of Tables

List of Figures

Nonmenclature

a	amplitude
b	span
c	chord
C_D	Drag Coefficient
C_P	Pressure Coefficient
$\overline{C}_P$	Canonical pressure distribution
C_L	Lift coefficient
f	Frequency Hz
G	Transfer function
h	Height or ground clearance
h_τ	impulse response function
k	Reduced frequency, $\omega c/2U$
kh	Reduced plunge frequency with h non-dimensionalised with c
k_G	Garrick frequency, $\pi f c/U$
N	Newtons force
Re	Reynolds number
St	Strouhal number, $2fa/U$
t	Time
U	Freestream velocity
x, y, z	Cartesian coordinates, x positive downstream, y positive upwards
x_c	Canonical pressure length of chord from pressure rise to trailing edge
α	angle of incidence
ω	angular velocity, $2\pi f$

Glossary

ADC	Analogue to Digiatl Convertor
CNC	Computer Numerical Control
DOE	Design Of Experiment
DSP	Digital Signal Processor
FFT	Fast Fourier Transform
FPGA	Field Programmable Gate Array
F1	Formula 1
MDF	Medium Density Fibre board
NI	National Instruments
PID	Proportional, Intergral Derivitive
PIV	Particle Image Velocimetry
SISO	Single Input Single Output
SUV	Sports Utility Vehicle

Chapter 1

Introduction

1.1 General Overview and Objectives

The aerodynamic development of vehicles in wind tunnels is currently performed via a series of static measurements. However, vehicles exploiting ground effect are highly dynamic, undergoing rapid changes in speed and attitude. The dynamic nature of a racing car can be seen in figures 1.1 to 1.5. Variations of the attitude of a single seat, open wheel race car are shown over a single lap of the Donnington Park Grand Prix circuit. Data is acquired from freely available simulation software, Bosch LapSim.

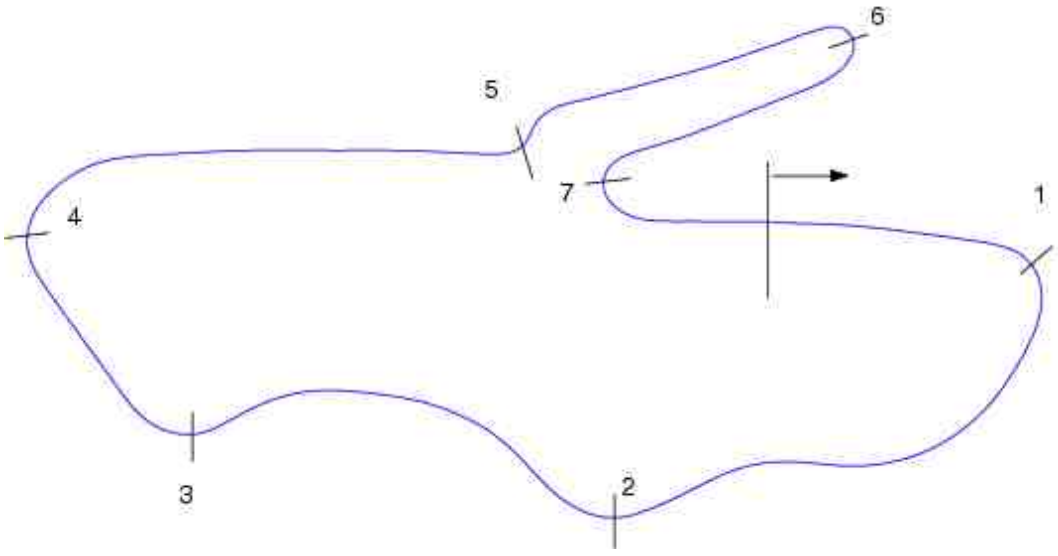

Figure 1.1: Donnington Park Grand Prix circuit, corner apexes and start line shown

From the strart line the vehicle accelerates toward the first corner. With the increasing speed the front and rear ride height reduces as the aerodynamic load builds and compresses the suspension. At the end of the straight the

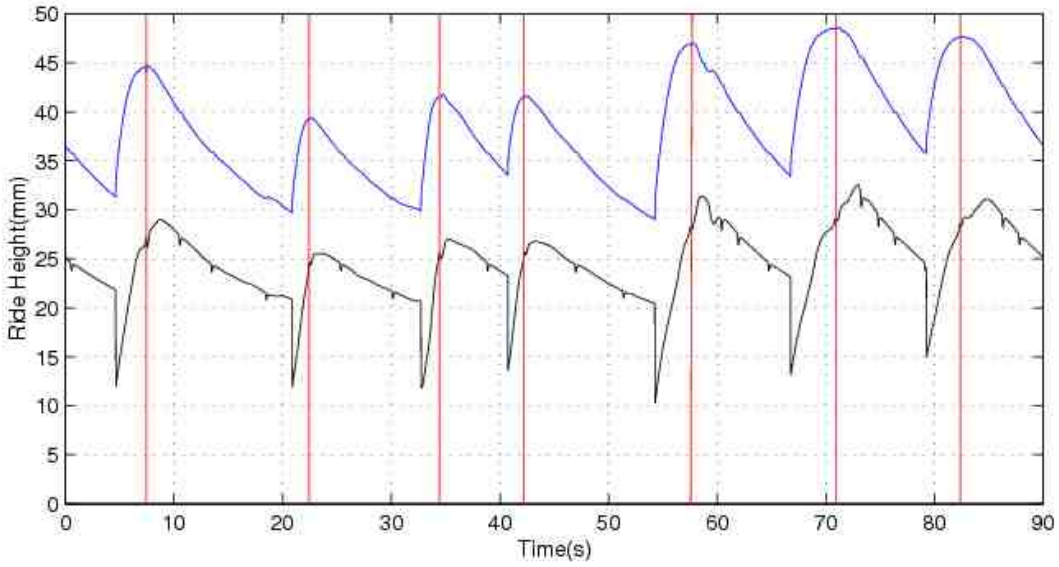

Figure 1.2: Variation of front (lower trace) and rear (upper trace) ride height during a lap of Donnington Park Grand Prix curcuit

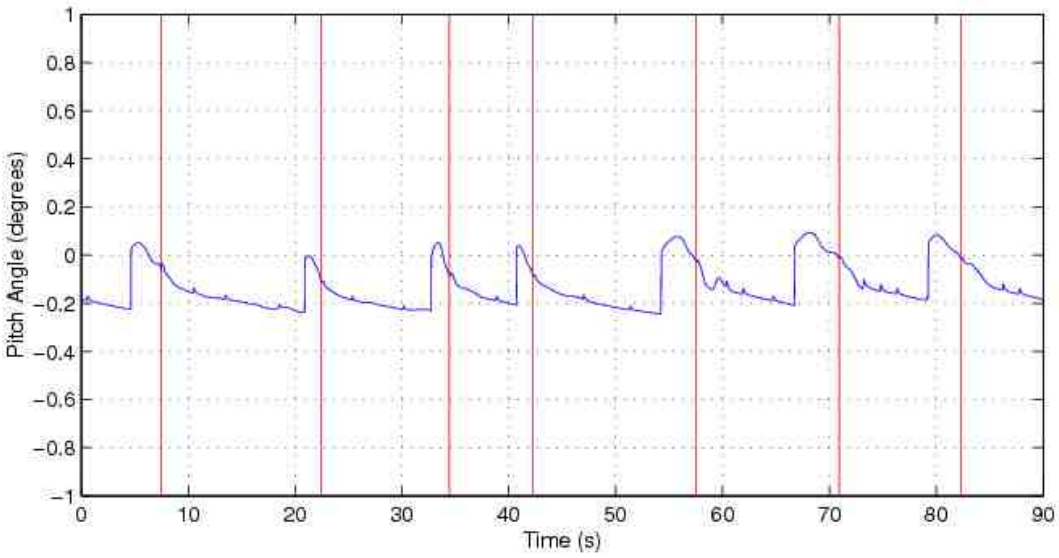

Figure 1.3: Variation of pitch during a lap of Donnington Park Grand Prix circuit

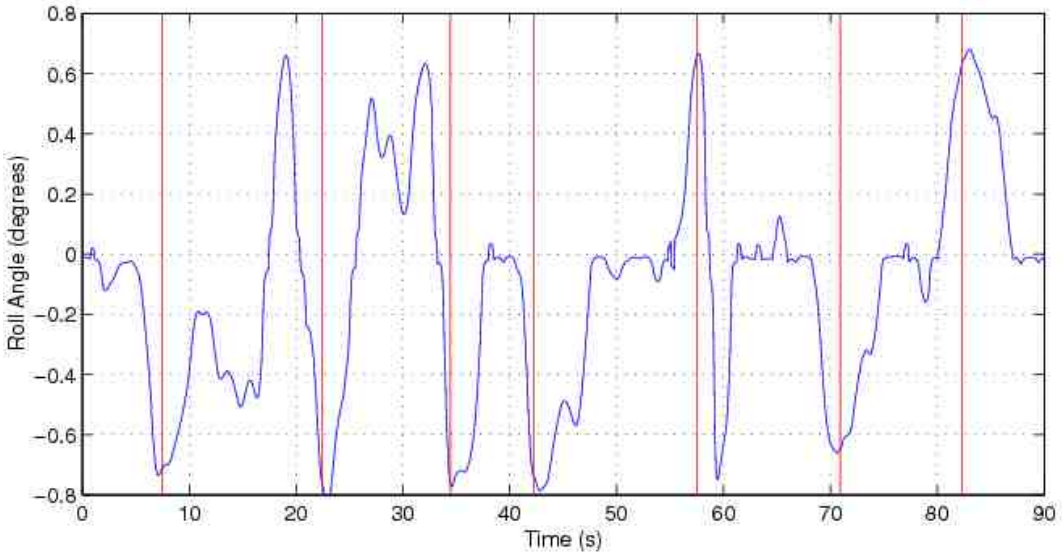

Figure 1.4: Variation of roll during a lap of Donnington Park Grand Prix circuit

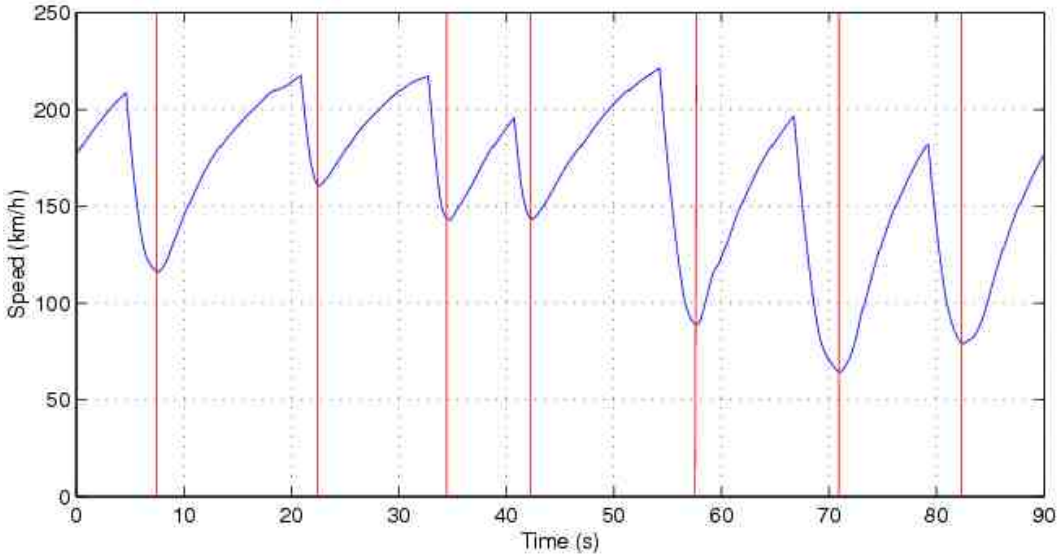

Figure 1.5: Variation of speed during a lap of Donnington Park Grand Prix circuit

corner phase begins as the brakes are applied. Speed dramatically reduces and the car pitches forward. once at the appropriate speed is reached the car turns into the corner. Along with pitch the roll attitude changes. At the corner apex speed is at its lowest. The final part of the cornering phase returns the car to an attitude where the maximum acceleration engine power can be applied. This results in maximum acceleration upto the following corner. This sequence is repeated at each of the 7 corners of the lap. The role of aerodynamics is to reduce the laptime by increasing the available grip, that is a function of tyre friction coefficient and vertical load, without increasing the mass of the car. In doing so it increases the performance envelope of the vehicle. It must achieve the increase in downforce with an acceptable level of drag.

Clearly therefore there is scope for an improvement in the fidelity of testing. However, it is difficult to measure body forces whilst simultaneously making variations to a model attitude and transient investigations are rare.

The need for dynamic testing of racing cars arises from the nature of ground effect aerodynamics. The flow is dominated by trailing edge separation and tip vortices with significant non-linearity and hysteresis effects. As the current method of testing requires that the flow settles and data averaging is employed, measurements are effectively steady state. Although static testing is presently employed to provide effective development of vehicles, the efficacy of such testing may be questionable. The present research will determine the extent to which transient aerodynamics affects the performance of vehicles.

The aeronautical industry identified the need for dynamic testing as aircraft performance increased. Time averaged static testing is used to remove unsteady measurements. This proves to be acceptable at low angles of attack. At higher angles unsteady effects increase, that in turn have a large effect on aircraft performance. This is especially true of modern highly dynamic military aircraft. Testing of such aircraft is performed at high angles of attack and in non-linear regimes. A good example is the wing drop problem of the FA/18 that prompted the abrupt wing stall programme [3]. Dynamic testing provided an insight into a complex aerodynamic problem.

The requirements of a dynamic testing system are not only synchronised continuous motion with data acquisition but also an understanding of the dynamic response of measurement devices. For dynamic investigations to provide insight it is imperative that there is a clear understanding of what is actually being measured. Not only are the sensors to be understood but one must also consider the effect the dynamic motion of the model will have upon tunnel flow conditions. During static testing it is often necessary to adjust the wind speed following a model position change due to changes the model imparts on

the test section flow conditions.

As the understanding of transient aerodynamics effects on automotive performance is extremely limited this research project will conduct an investigation that will provide an insight into transient ground effect aerodynamics. Specifically the research aims were to:

- Characterise the wind tunnel performance and develop a test velocity controller capable of maintaining wind speeds during dynamic testing.
- Determine, and extend where necessary, the capabilities of the existing experimental force and pressure measurement sensors.
- Develop dynamic testing techniques and technology.
- Perform an experimental investigation into the transient aerodynamic effects applicable to automotive vehicles exploiting ground effect.
- Provide an insight into any differences between static and dynamic testing caused by transient aerodynamic effects.

1.2 Thesis Outline and Principal Achievements

This thesis is divided into 8 chapters. Chapter 2 provides a review of investigations relevant to this project and outlines how it relates to other disciplines within the field of aerodynamics research. The development of automotive aerodynamics is summarised up to the current state of the art in transient investigations. The definitive ground effect aerodynamic and aeronautical transient investigations are detailed prior to the outlining of relevant publications of wind tunnels and testing techniques. In chapter 3 the R.J. Mitchell wind tunnel is investigated. The wind circuit and fan drive system are characterised. A controller that offers a significant improvement over that presently used is developed and analysed. Satisfying the demand for a dynamic testing capability is covered in chapter 4. Having established the present performance of the hardware and software in use at the R.J. Mitchell wind tunnel an advanced data acquisition and motion control system will be implemented. This included determining the dynamic response of the force and surface pressure measurement devices. A frequency response function was then developed that formed part of a data reduction algorithm that effectively isolated the aerodynamic forces and surface pressures from the measured data. The conditioning and uncertainty of this data is detailed in chapter 5. Once these systems were completed an investigation was performed into the static aerodynamic behaviour

of a wing in ground effect in chapter 6. An experimental examination was performed into the transient aerodynamic effects on a wing in ground effect with the key findings of the research being detailed in chapter **??**. Finally the thesis is concluded with recommendations of future work in chapter 7 The main achievements include

1. The selection and employment of an appropriate system identification method that allowed the characteristics of the R.J. Mitchell wind tunnel to be determined.

2. The design and implementation of a control system that significantly improved the performance of the R.J. Mitchell wind tunnel.

3. Performing a thorough investigation into the response of pressure and force measurement instruments and the subsequent development of a novel dynamic testing system.

4. The two proceeding points were combination to deliver a dynamic wind tunnel system capable of conducting experimental investigations into transient ground effect aerodynamics.

5. A test case was performed into the transient aerodynamics of a dynamic heaving wing.

Chapter 2

Background Review

The aim of this chapter is to plan this research in what with that of others in be at this and related fields. It reviews existing knowledge of results and methods that are relevant to the aims of the research. Specifically, methods of performing transient force measurements are considered. In doing so it provides guidance for the most suitable route and methods necessary to successfully achieve the research project aims. As this research project is fundamentally experimental in nature, this review will concentrate on experimental methods.

2.1 Automotive Aerodynamics

The effect that aerodynamics has upon the performance of cars was identified by manufacturers of racing cars around the turn of the twentieth century. Drag reduction was prioritised as it increased maximum vehicle speed. Solutions were borrowed from the marine industry, with for example boat-tailing of the rear bodywork used to streamline the vehicles. The streamlining of road vehicles was performed by eye. With the birth of the aeronautical industry came advances in the understanding of aerodynamics and development techniques. Automotive designers could thereafter follow this lead.

An abrupt end to automobile aerodynamic research occurred in 1935 when manufactures sought to clearly differentiate their vehicles from those of other manufactures. The belief was that aerodynamic development would lead all manufactures to one single optimal aerodynamic body shape. Market forces had come to be the priority of car manufactures. Styling and customer expectations led over engineering development. Toward the end of the 21st century fuel economy became a sufficiently important issue to reintroduce significant automotive aerodynamic research as part of the development process of a car. Manufactures of mass market vehicles had the resources to invest in advanced

facilities including wind tunnels. The quest for drag reduction brought vehicle design to the wind tunnel.

With the availability of wind tunnels, designers were able to also consider other aerodynamic effects such as cooling, vehicle soiling, visibility whilst driving in the rain, passenger comfort due to noise and high speed stability. All major vehicle manufactures now have their own full size wind tunnel facilities with some also having aeroacoustic tunnels. One of the largest vehicle manufacturing groups is the Volkswagen Audi Group; details of their wind tunnel used for vehicle aerodynamic design can be found in Lindener and Wickern [4].

The purpose of testing can range from initial shape evaluation to refinement of the final design. Tests can be performed on full size or scale models with a wide range of fidelities. Experimental techniques employed include: (i) the measurement of surface pressures,(ii) body forces with internal and external balances and (iii) flow visualisation, both surface and particle trace. Testing aims to discover surface flow paths, locations of flow separation and regions of recirculation. A concise account of the purpose and techniques of automotive testing can be found in the work of Hucho [5].

As already stated, the earliest considerations of race car aerodynamics were drag reduction and hence increased top speed. This changed markedly with the introduction of inverted wings mounted on race cars to improve cornering speeds. As a result motorsport aerodynamic testing is far more extensive then that employed for road going vehicles. The pinnacle of motorsport is Formula One (F1)with half a dozen manufacturers forming the largest investor in automotive aerodynamic testing. Modern F1 teams operate wind tunnels 24 hours a day with a number of teams having two such facilities. The requirement for such extensive testing can be seen by considering the nature of the race cars themselves. In addition to diffusers and multi element front and rear wings, extensive use is made of flow control devices. Allied with the need to produce differing aerodynamic configurations to tune a car for the demands of the differing circuits visited each season and the continual necessity to improve performance.

Wind tunnel testing of passenger vehicles is typically achieved through a series of time averaged measurements at fixed static attitudes. As the performance of motorsport vehicles is highly dependent on attitude, the number of points within the range is greater than that of passenger cars and may include additional effects such as steered front wheels. Testing is primarily concerned with the generation of downforce, efficiency of downforce in relation of drag and the location of the centre of pressure balance. As the aerodynamic features of a upper level race car are so numerous no attempt will be made to detail all

of them here. An excellent insight into race car aerodynamics can be found in Wright[6] and Millikin and Millikin[7].

2.2 Automotive Transient Aerodynamics

Other then traditional static testing the increasing popularity of the Sports Utility Vehicle (SUV) with its high sides and high centre of gravity and hence potential instability spawned a need for transient testing. Current transient automotive testing is concerned with vehicle stability during passing manoeuvres, gusting crosswinds and when in proximity to other vehicles.

Strong side-wind gusts have the potential to cause a vehicle to deviate from its intended course, having an alarming effect on the driver and being potentially extremely hazardous. An experimental investigation of transient side gusts was performed by Chadwick et al. [8]. Simplified vehicle geometries were employed. The surface pressure on a flat sided box with and without rounded corners was integrated to give side force and yawing moment. Models were moved on a track past a wind tunnel jet of approximately five times the length of each model. Results indicated that no steady state was found for the side force of the flat plate. Significant transient activity was found with the sharp-edged box, which had the highest degree of flow separation.

Passing manoeuvres can cause a similar effect on a vehicle as side wind gusts. Nodger et al. [9] investigated the transient effects of vehicle passing. A scale model was moved past another being held stationary. Forces were measured with internal piezoelectric balances. Passing manoeuvres were investigated by Abdel Azim [10] at model scale. A passenger vehicle was simulated passing an articulated commercial vehicle. Surface pressures were measured on both vehicles to provide information on side force and yaw moments of both vehicles for a number of separation distances. Both investigations illustrated that transient aerodynamic effects can influence vehicle stability.

Vehicles interact with each other's flow field when travelling in traffic, either following or leading. The transient effect of the movement of a vehicle in close proximity was studied experimentally by Tsuei and Savas [11]. Simplified vehicle geometries were used to represent a four car platoon. Forces were measured from all models whilst one was performing a sideways oscillation. Difficulties were experienced with producing valid data from the internal strain gauge balances used to produce force measurements. Of more relevance to this project is the recent increase in interest in transient aerodynamic effects caused by the motion of a vehicle. Although Summa [12] performed a numerical simulation of a vehicle undergoing a pitching motion in 1992 no experimental

investigations were published until 2004. Summa [12] is more a demonstration of a panel method's ability to perform an unsteady simulation of the surface pressure of a vehicle whilst in motion. No analysis of the aerodynamic effects is made.

In 2004 Wiedemann and Hucho [13] selected unsteady effects as the topic of the Progress in Vehicle Aerodynamics series in which the first published research into experimental model motion was made. Lock [1] recorded forces on a full-scale small hatch-back car being dynamically yawed. Results were compared to static results and a considerable lag was found during the motion. However this only occurs at one point on the plot, while the remaining results appear to follow the static line. As no insight is given into the apparatus used for force or position measurement or the motion control it is not possible to confirm this lag as being caused solely by an aerodynamic effect.

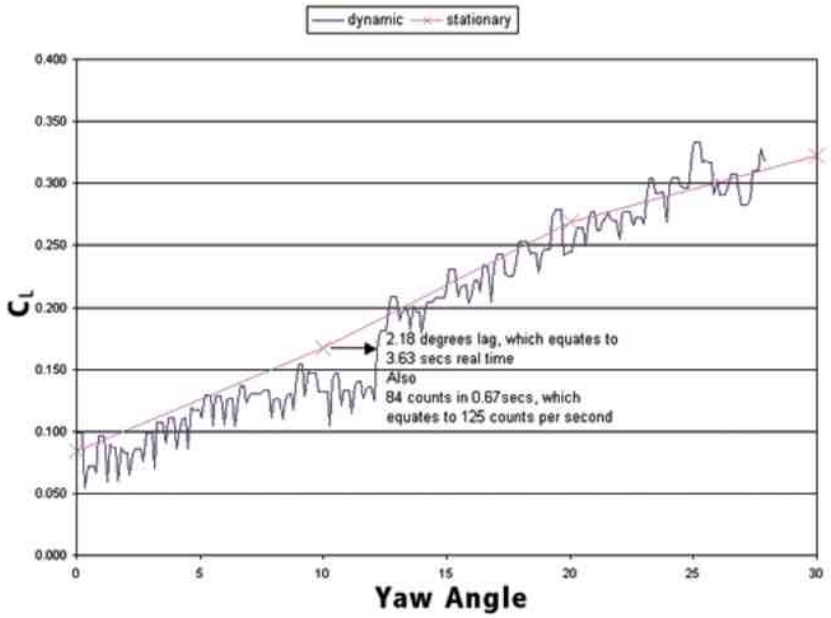

Figure 2.1: Dynamic results of full scale model yaw test, reproduced from [1]

Motorsport applications have proved to be the stimulus for recent dynamic model investigations. A series of investigations began by Knörnschild [14] performing a dynamic test with a scale model undergoing a pitching motion. Surface pressures were recorded on the underside of a third scale Le Mans car. Specific motion apparatus was used for the test and attempts were made to identify the effects that model motion would have on pressure measurement devices. Two motion velocities were investigated; both retained the overall pressure profile but minimum and maximum values were found to significantly

differ.

Aschwanden, Knörnschild and Müller [15] continued these investigations with a model shaker that was capable of producing changes in pitch and heave whilst measuring forces. Again differences were found between static and dynamic results, both in terms of downforce and drag and in terms of the resulting balance of the vehicle. Tests were performed at a number of different motion amplitudes and frequencies. The importance of isolating aerodynamic loads and accurately determining model position was highlighted.

The effects on vehicle performance due to transient aerodynamics have only recently been considered by the automotive industry. The clearest intention to evaluate transient aerodynamic effects caused by dynamic motion has been made by Formula 1 racecar manufacturers, whom are the biggest investors in automotive research. Due to the highly competitive, and hence secretive nature of motorsport, the only published research available is that performed by Knörnschild et al [15]

2.3 Ground Effect Aerodynamics

Motorsport began influencing the aerodynamic development of cars almost immediately after the production of the first petrol engine cars. This early development was concerned with drag reduction and cooling. In the late 1960s aerodynamic devices were introduced with the aim of improving overall vehicle performance by increasing the force acting through the tyres without increasing the vehicles mass. Increases in tyre force provide an increase in cornering ability and improved traction for braking and accelerating. Inverted aeronautical wings were attached to suspension arms with the inverted lift termed downforce. One of the first examples of this is the Lotus 49b Formula One car from 1968. Later the front wing was placed ahead of the front wheels and close to the ground. A dramatic improvement in performance was found and aerodynamic features were quickly introduced into the underside of the vehicle. The side pods that accommodate radiators became shaped like aerofoils and skirts were added to limit the flow entering from the sides. Ground effect plays a significant role in the performance of motorsport vehicles. So great is the benefit from aerodynamic devices that the governing body of motorsport constantly seek to maintain safe cars speeds by placing heavy restrictions upon their use.

Ground effect aerodynamics is characterised by its dependency on ground proximity. The flowfield contains strong three-dimensional effects such as vortices and in the case of a diffuser asymmetry of flow, even the regions con-

sidered as essentially two-dimensional can contain boundary-layer separation. The flow associated with ground effect devices is therefore highly complex with strong interaction of non-linear characteristics.

Academic research into motorsport ground effect did not begin until the mid 1980s. The early investigations used wind tunnels suited for aeronautical applications, i.e. having a stationary floor and hence incorrectly simulating the moving ground boundary. The first experimental investigations of ground effect conducted with a tunnel designed specifically for automotive testing with a correctly simulated ground was Knowles et al: A single element inverted wing was tested, with forces and surface pressure measurements made at a variety of incidences and a number of ride heights ranging from one chord down to 12% of the chord. Downforce was found to dramatically increase with reduced ground clearance and attributed to a venturi effect.

Zerihan and Zhang [16] have performed a series of wing in ground experiments at the University of Southampton. Surface pressures and body forces were measured for a single element wing, when the minimum ride height was reduced to less than $0.06c$. As with the previous investigations, aerodynamic force was found to increase with reducing ground clearance. At the extended lower ride height range a region was observed where downforce was found to reach a maximum and then reduce. The three regions were defined as the force enhancement, plateau and reduction regions. The force increase region is attributed to the ground constraining the flow causing it to accelerate to a greater velocity than that found in freestream. As the ground is approached this significantly reduced pressure beneath the wing produces an adverse pressure gradient that results in flow separation at the trailing edge of the wing. The area of separation continues to increase as ride height reduces. The loss of lift caused by separation balances the increase caused by ground proximity to produce a force plateau. A significant reduction is found at ride heights below the plateau, the force reduction phenomenon, where the region of separation has extended over a significant portion of the rear of the suction surface. All three force regions can be seen in figure 2.2. Drag behaviour can be seen to continually increase with reducing ground clearance in figure 2.3.

The wake and edge vortex of the same wing are investigated in [17] and [18]. A strong dependence is found between the properties of the edge vortex and the ground clearance and hence level of downforce. The behaviour of the wake is also dependant on ride height, with an increase in size and a downward shift of wake trajectory occurring with increased ground proximity.

It is common for racing cars to operate with multi-element wings. In [19] the aerodynamic behaviour of a double element wing in ground effect is in-

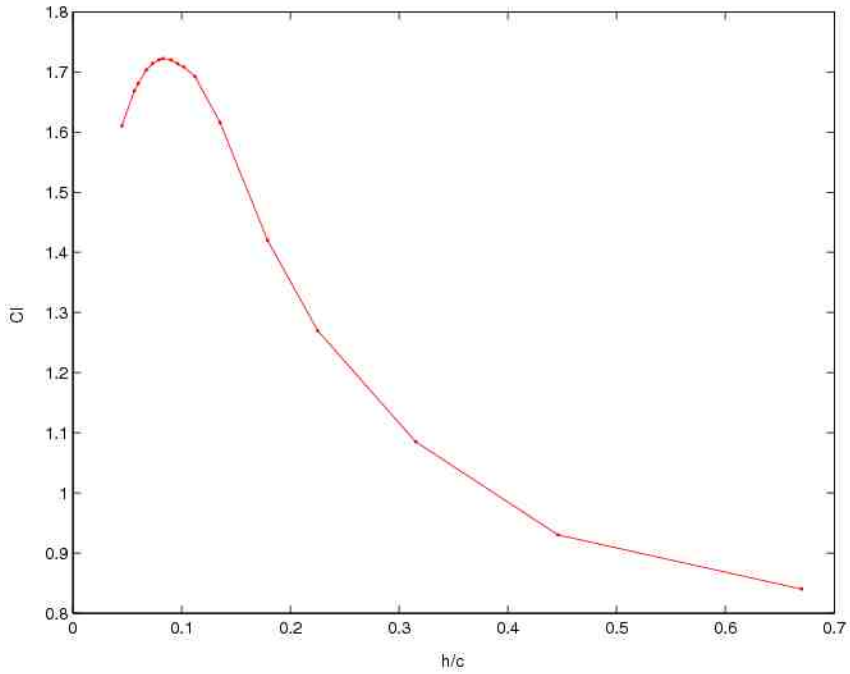

Figure 2.2: variation of downforce coefficient with ride height for a wing in ground effect

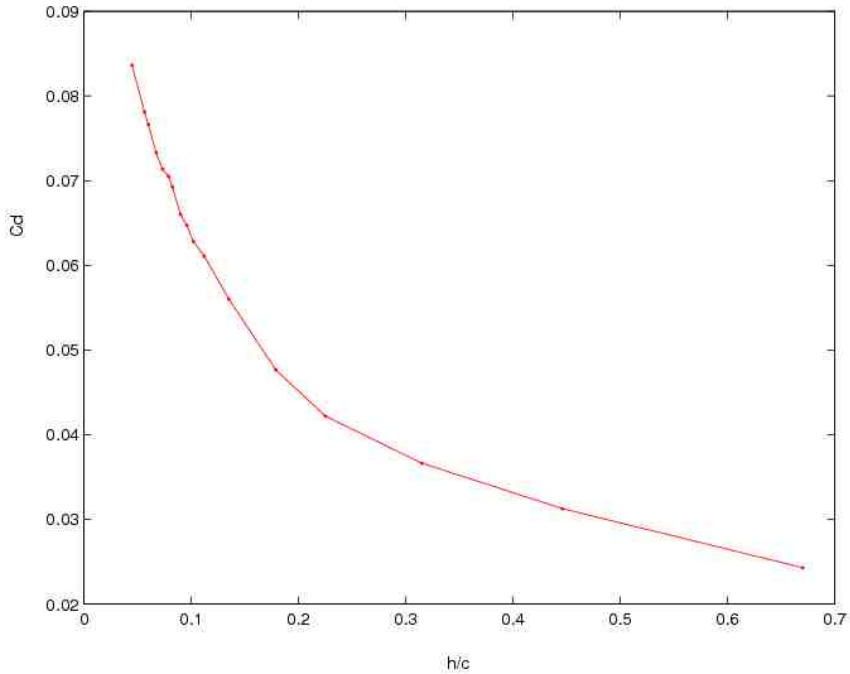

Figure 2.3: variation of drag coefficient with ride height for a wing in ground effect

vestigated. The effect of the positioning and angle of incidence of the second element or flap is potentially to greatly augment downforce, however with a high incidence the reduction in downforce in the force reduction region is of greater severity then for a single element wing. The second element also modifies the edge vortex and in [20] the relationship between the edge vortex, ground proximity and downforce is investigated.

Senior and Zhang [21] [22] investigated a diffuser in ground effect. As with a wing, reducing ground clearance increased downforce up to a maximum after which a reduction is found. Forces were found to be dependent on a highly three-dimensional flow dominated by vortices and boundary layer separation. Ruhrmann and Zhang [23] evaluated the effect that the angle of the diffuser has upon the generation downforce and the impact upon the flowfield. Zhang, Senior and Ruhrmann [24] then proceeded to investigate the vortices generated by the diffuser and Mahon, Gage and Zhang [25] investigated their development.

Wings in ground effect and diffusers have been studied in isolation, however the performance of a vehicle is dependent on these devices operating in conjunction with other aerodynamic and non-aerodynamic devices such as wheels and tyres and cooling apertures. As motorsport is a highly competitive business, little published work is available on the aerodynamics of an entire car configuration, the only work to date being a summary of previous isolated component testing by Zhang, Toet and Zerihan [26].

It is clear to see that the motivation for transient investigations is potentially strong for vehicles exploiting ground effect. They are highly dynamic and their flowfield consists of a number of interacting complex phenomena.

2.4 Transient Aeronautical Aerodynamics

Even though wind tunnel investigations have been performed with a model racing car in motion [15], no attempt has been made to identify the causes of differences between static and dynamic tests. The aeronautical industry identified the effects of dynamic motion as worthy of investigation as early as the mid 1930s. An increased understanding of aeroelastic stability served as the motivation for dynamic research. Research into phenomena such as flutter and aerodynamic behaviour caused by gusts evolved into investigations into developing aircraft with increased manoeuvrability.

As aeronautical transient investigations are at a more advanced state than those of automotive research the purpose of reviewing this area of research is to gain an insight into dynamic testing methods. In particular measurement

devices, testing techniques, data reduction methods and potentially useful dynamic parameters and the transient effect on flow features described in section 2.3 namely, vortices, wakes and the wing boundary layer will be considered.

Numerical, computational and experimental investigations have considered predominantly pitching aerofoils but also heaving and rolling. The earliest investigations considered the effect of motion, allowing the significant features of a dynamic flow to be identified. Subsequent investigations often concentrated on in-depth investigations of individual aspects of these key features.

One of the earliest publications to consider transient aerodynamic effects was von Karman and Sears [27] in which the theory of a two-dimensional wing undergoing a non-uniform motion was developed. Dore and Phil [28] extended this to three-dimensional applications for both rectangular and delta wings experiencing a sudden change of incidence, a sudden plunge as well as entry to a sharp edged gust.

One of the first dynamic wind tunnel investigations was performed by Landon [29] into a pitching and heaving wing. Surface pressures were measured on a two-dimensional NACA 0012 aerofoil. The effects of motion frequency, amplitude, initial incidence and Reynolds number were investigated. emphasis is on the re-production of data and experimental technique and less on analysis of results. A not insignificant deviation from static results was found, being dependant on motion frequency and amplitude.

Chang and Muirhead [30] performed dynamic wind tunnel investigations on a delta wing entering ground effect. The effects of a range of sink rates and incidence angles were evaluated similar to an aircraft during the landing phase. It should be noted that ground effect for an aircraft configuration is considered significant at h/c =0.3, this is a much larger ground clearance then already stated for race cars which is typically a minimum of h/c =0.05. Despite the title, no data is presented into the effect of sink rate on ground effect.

A numerical investigation of ground effect has been performed by Karkehabadi and Mook [31] with the aim of exploring the potential increase in performance of a wing in proximity to a wavy surface when applied to a large transoceanic wingship flying near waves. A wing in steady flight is modelled as travelling over a wavy surface represented by a harmonic sinusoidal heaving motion. The motion range was 25% to 75% of a chord with the effect of several oscillation frequencies being investigated. The mean aerodynamic forces on the oscillating wing were found to increase above those of the wing when stationary and increasing oscillation frequency produced higher forces.

A thorough experimental investigation into the boundary layer characteristics of a pitching wing was performed by Lee [2]. Hot-film sensor arrays were

employed and again a NACA 0012 aerofoil was dynamically pitched. The focus of the investigation was to document changes to the transition, separation and reattachment points caused by the dynamic motion. Unsteady boundary-layer separation was found to be one of the most important features and many of its key features were determined. An example of a hysteresis loop is shown in figure 2.4.

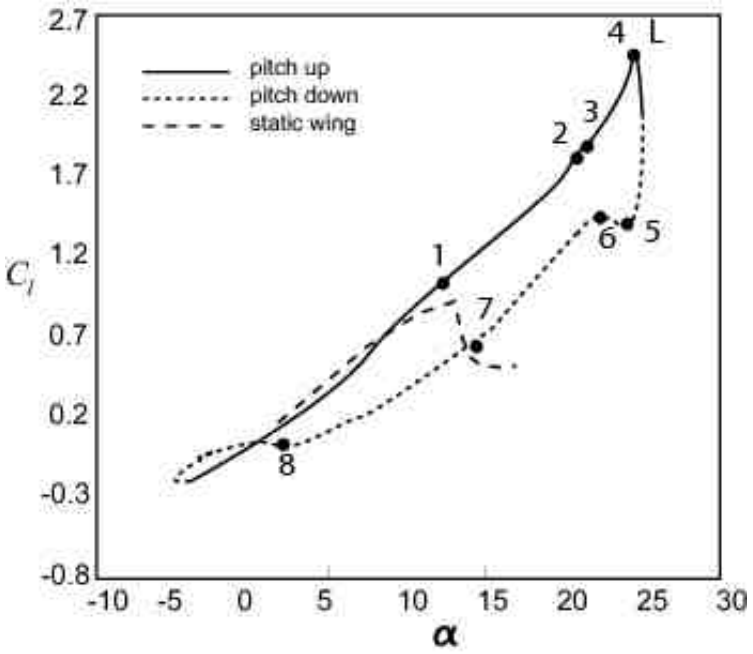

Figure 2.4: Hysterisis loop for a wing pitching about 10°with 15° amplitude reproduced from [2]. 1 flow reversal onset; 2 end of upward spread of reversal; 3 turbulent breakdown; 4 lift stall; 4-5 full stall; 6 onset of secondary vortex; 7 onset of flow attachment; 8 end of flow reattchment; L lift stall

As stated in section 2.3, an edge vortex is part of the complex flow field of ground-effect devices. Aeronautical investigations of the dynamic motion effect on a streamwise vortex can be found in research into delta-wing flows. Thompson et al. [32] investigated the vortex structure during the sinusoidal pitching motion of a delta wing. Smoke generators were used in conjunction with high-speed filming to visualise the flow during the wing movement. This allowed changes in the vortex location and its structure to be monitored. Although the range of pitching angle and the pitching rate were designed to be representative of those of an aircraft it is also of relevance to automotive ground effect aerodynamics. Dynamic results were compared to static results with a significant difference found between the two. As the performance of the wing is highly dependent on the vortices, differences were attributed to the particular susceptibility of vortices to hysteresis effects. At the end of the

transient motion a further time was required for the flow to settle to the static position.

Birch [33] carried out an experimental study of transient flow with vortices. Hot wire anemometry and a multiple pressure probe technique were used to investigate the downstream development of a tip vortex from a NACA 0015 aerofoil during deep stall pitch oscillations. Differences in vortex contour shapes and magnitudes were found between the pitch-up and pitch-down stages of the oscillation. Schrek and Helin[34] carried out a three-dimensional experimental investigation into the leading edge vortex dynamics during pitching of a NACA0015 wing. Initially the vortex, although unsteady, was essentially two-dimensional, however this rapidly changed with the vortex deforming across the entire span but being arrested by the wing tip and root, resulting in a highly three-dimensional flow. This had a marked effect on lift generation.

Transient effects on the vortex wake of a heaving wing were numerically studied by Katz and Weihs [35]. The development of the wake was found to be highly dependent on motion amplitude and frequency and a critical value was found above which the wake would break down. Interestingly, fluctuations in the wake occurred at a distance downstream of the wing and therefore had little overall effect on the instantaneous wings lift.

A numerical study has also shown a potential application for transient aerodynamic results. Tang and Dowell [36] extended an existing two-dimensional semi-empirical unsteady aerodynamics model to three-dimensions. Comparisons were then made to tests of a wing with a low aspect ratio of three, oscillating in pitch. Good agreement was found between the measured surface pressure and theoretical predictions for steady state and pre-stall and post-stall conditions. This indicates that the findings from transient research could possibly be incorporated into numerical simulations.

Grismer and Jenkins [37] performed an investigation centred on the transient flow and forces of a rolling delta wing. Considerable effort was required to isolate the body forces from those input by the motion drive. The development of a reliable method for data reduction was also necessary. Three critical states with two transition regions were found to exist in the flow over the range of angles tested. Once these were identified, measurements were taken either side and across the critical regions. The behaviour of the flow field was found to differ markedly when crossing regions.

Ensemble averaging is a commonly used technique for off-surface investigations. Fraser [38] highlighted the difficulties associated with this technique whilst using PIV to determine vortex properties on a pitching delta wing. When investigating vortex breakdown, data analysis must be carefully con-

ducted. Individual frames clearly showed vortex breakdown whilst ensemble averaging reduced the resolution of the vortex core.

The reduction of data is important with static testing but undoubtedly more so with dynamic testing. Lee and Tang [39] demonstrated an accurate method for the data reduction of strain gauge and pressure signals obtained from dynamic testing. These signals can show significant fluctuations with time and various filters can be applied to arrive at a mean value at a particular point in time or fluctuations can be used to indicate particular events.

2.5 Flapping Wings

Changes in pitch and heave are a main concern in the aeronautical industry, however the automotive requires mainly to heave, since pitch variation is only slight during the braking and accelerating motion of vehicles. Heave has been studied mostly concerned with flapping wing flows.

The aerodynamic mechanism of bird flight was first described independently by Knooler [40] and Betz [41] giving rise to the term for flapping wing aerodynamics, the Knoller Betz effect. It was theorised that flapping wings would produce oscillating lift and thrust forces. Later Garrick [42] developed inviscid equations to determine the level of thrust produced and the efficiency of an oscillating flat plate. Heave, pitch and combinations of the two were successfully modelled for small amplitude oscillations. Jones [43] developed an inviscid panel method of a heaving NACA0012 aerofoil and performed experiments for comparison. Good agreement was found within the wake structure suggesting the development of a reverse von Karman street is an invisid mechanism.

Inviscid investigations are limited to the smaller scale of birds as they are unable to correctly predict the flow separation that occurs at the leading edge of wings. As this feature plays a significant role in the performance of flapping wings other methods are required.

Experimental investigations and computational simulations have been performed into a wide range of aspects particular to low Reynolds number flapping wings. The effects of heave amplitude and frequency and the pitch amplitude and phase angle on the flow field have been investigated. Lai [44] performed an experiment with an aerofoil oscillating in heave in a water tunnel. At low oscillation frequencies the flow field is similar to that of a static aerofoil with a drag producing von Karman street downstream. As the oscillation frequency is increased the motion produces vortices. These motion induced vortices mix with the drag producing vortices in the wake. What happens as the frequency

increases is dependant upon the behaviour of this complex mix of vortices. Initially, a period of neutrality is reached were no drag is experienced. Above this frequency the motion vortices dominate and a reverse von Karmen street is produced. The wake becomes a thrust-producing jet with a velocity higher then the freestream velocity.

The behaviour of the jet was examined by Jones [43]. At increasing plunge velocities the axis of the wake changes and becomes upwardly inclined when vortices shed from the trailing edge begin to interact and the jet is deflected either upward or downward, depending on the direction of the initial motion.

When considering the production of thrust, the efficiency of the oscillations becomes important. This is the ratio of power required for flapping to thrust generated. Anderson [45] used a force balance and PIV to arrive at an optimum combination of the flapping parameters to produce the maximum thrust and the most efficient thrust. Hover [46] defined a range of Strouhal number above and below which the efficiency drops sharply. Investigations were also performed into motion type. A sinusoidal motion produced the highest efficiency whilst a sawtooth motion produced the highest thrust. Coupling heave with pitch was found to greatly increase efficiency. This increase in efficiency was also confirmed by Tuncer [47] and Pedro [48] and attributed to a reduction in the leading edge vortex.

Of particular interest to flapping wing research is hovering flight. Tests are performed at zero freestream velocity with the model in motion. Vandenberghe [49] demonstrated that thrust can be produced without forward flight and indeed without thickness or camber by heaving a flat plate in a stationary fluid. Lai [50]produced thrust with a heaving NACA0012 in stationary water. When a cylinder was put through the same motions no jet, hence thrust was produced.

2.6 Key Parameters

Research relevant to transient race cars aerodynamics is spread across a number of fields. To better understand how these areas relate it is necessary to understand the key parameters of each. The Reynolds number Re is a key parameter used throughout aerodynamic research. As well as the Reynolds number for flapping wing investigations the Strouhal number St is considered important, particularly in terms of vortex shedding and wake patterns. The Garrick frequency k_G is also an important parameter as it defines features of vortex shedding from the leading edge of wings. Flapping wing experiments can be considered as low Reynolds number and high Strouhal number.

Anderson [45] experimented with Strouhal numbers between 0.15 and 0.4 at Reynolds numbers up to 40,000. Lai [44] performed experiments with a range of Reynolds number of 500 to 21,000 and Garrick frequency of 4 to 16. Motion amplitudes are also important and can be in the region of 0.5c for heave and 15 degrees in pitch.

Aeronautical investigations are concerned with considerably higher flow speeds, often the key parameter being the Mach number. The non-dimensional parameter reduced frequency k, with $k = (\pi fc/2U)$ is used in preference to the Strouhal number. Grismer [37] performed tests at a constant Mach number of 0.3. Landon [29] and the accompanying work tests at Mach numbers from subsonic 0.5 through to transonic with shock wave 0.751 with Reynolds numbers of 1.7×10^6 to 11.4×10^6. Values of Reduced frequency are 0.049 to 0.301. Motion amplitudes can be similar to the range used in flapping wing experiments.

Static testing of wings in ground effect are conducted at a Reynolds number in the region of 5×10^5. Dynamic automotive testing has been performed at a Reynolds number of 3.3×10^6 when based on wheelbase and a 50 meters per second test velocity, by Knorschild [14]. Motions were up to 10Hz frequency and 8mm amplitude heave and half a degree pitch, equating to a reduced frequency of 0.126 and 1/375 of the wheelbase. When Lai [44] performed an experiment at 10Hz the reduced frequency was 10π. It is clear therefore that automotive transient research sits between the other two areas selected for comparison in terms of key parameters. Reynolds numbers are an order of magnitude above the highest flapping wing research and a similar amount below aeronautical investigations. Motion frequencies are two orders of magnitude below those of flapping wing testing and therefore of the same order as aeronautical investigations. Motion amplitudes are considerably below either of the other fields.

2.7 Wind Tunnel Technology and Control

Several groups have produced papers covering aspects of design and initial calibration or upgrade of their wind tunnel facilities. These include an upgrade of the drive motor speed control at the NASA Lewis research centre performed by Becks, Bencic and Blumenthal [51]. A new monitoring and control system was introduced to eradicate power spikes and surges during speed changes of a 87,000 hp fan. Results showed an improvement for constant speed over an rpm range for varying loads all within strict power limits: maximum 70MW, increase 10MW/min and decrease 15 MW/min.

Zhang, Chai and Shao [52] developed an autotuning adaptive feedforward strategy to control the transient and steady state Mach number in a wind tunnel test section. Nguyen and Ardema [53] developed a numerical model of the flow recirculation in a closed wind tunnel with a variable velocity input boundary condition. This was applied to the drive system to achieve minimum elapsed time during changes in flow speed.

Significant changes in model attitude can lead to variation of the flow in the tunnel, from increased blockage from the model or its wake. Pels [54] implemented a predictive controller to maintain a constant test section flow speed during testing of a model with increasing angle of attack beyond stall. Improvements were found over the existing PID controller allowing a more rapid change in model attitude.

As described in section 3 the fan speed system was identified as being nonlinear. Astrom and Wittenmark [55] proposed that for a process with dynamics that vary across the range of operation the use of a controller with varying parameters is recommended.If these variations are predictable then the most suitable adaptive controller is gain scheduling. This is a controller with adjustable parameters and a mechanism for adjusting the parameters. It is nonlinear due to the parameter-adjusting mechanism. Gain scheduling is an adaptive control method suitable for a wide range of applications from ship steering [56] to process control [57] and has become the standard for flight control systems [58]. Typically gain scheduling is concerned with maintaining control about some equilibrium with only a small or slow deviation from it. Methods to overcome this have been proposed by Leith and Leithead [59] [60]. Achieving the potential performance gains across the entire operating region is dependent upon the plant model, the division of the operating range and the treatment of off-equilibrium behaviour. The model can be derived from numerical methods [61] or from empirical data[62] and must balance complexity with conservatism [63]. The greater the number of subdivisions the more responsive the controller can be [64]. However this incurs an increase in development cost. Here, significant off-equilibrium effects during path tracking were successfully overcome with their inclusion in the model dynamics[65]. Gain scheduling has also been used for control of supersonic wind tunnels [66] and [67]. However unlike the current application where test duration is of the order of minutes, supersonic wind tunnels are intermittent in nature with tests lasting seconds.

The use of National Instruments hardware and software is of interest to this research programme as the wide use of it across the Universities experimental facilities makes it the primary choice for all data acquisition systems.

Okoro [68] upgraded an existing data acquisition and control system to be real-time for a supersonic facility. New hardware and software, both from National Instruments, were introduced, with the aim of allowing a single operator with little or no knowledge of the system, to safely perform tests and record data. Hodges [69] also used National Instruments products when introducing a model and probe position control and incorporated a user friendly interface. The new system was integrated with existing data acquisition equipment in a supersonic tunnel. Lau, Seet and Wing [70] installed a network set up to perform measurement tasks from pressure sensors, hot wire, laser flow visualisation, strain gauges, model and probe positioning, as well as fan control and data acquisition.

Of most significance here is the work of Graves [71] and Heim [72]. Both developed wind-tunnel systems to measure dynamic ground effect. Forces are recorded for a scale model of aircraft during the landing phase. Considerable emphasis is placed on the necessity to accurately remove model motion inertia from aerodynamic forces. Potential sources of error throughout the motion control and force measurement systems are defined.

The dynamic response of the force balance is of importance to the present research. There is little published work on the subject, however Parker and DeLoach [73] used a Design of Experiments (DOE) technique to improve upon existing methods of calibrating a wind tunnel force balance. This method consisted of applying a variety of loads on the six axis in a carefully defined sequence that encompassed to the full operating range of the balance. The identification of cross coupling between axes was found to be important and is therefore significant as this project will extend to simultaneous motion on multiple axes.

In summary a number of projects have been conducted that demonstrate the feasibility of upgrading a wind-tunnel facility to provide a significant increase in capability and performance. The dynamic motion of a model may lead to changes in the tunnel flow that have an impact upon the flow velocity in the test section and hence fan drive system. It is therefore necessary to perform an evaluation of any algorithm selected for use within the control system.

2.8 Chapter Summary

Experimental wind tunnel techniques have advanced from static testing to transient surface pressures and flow visualisation and then to dynamic testing with time accurate force measurements. This has allowed flow features

that greatly influence performance to be investigated. Dynamic testing has the potential to improve the fidelity of wind tunnel testing. Transient effects are highly dependant upon the amplitude, frequency, initial and final position, direction and type of motion. Boundary-layer properties such as position of transition and separation are all affected by motion as are off-surface features such as vortices and wakes. This combination of motion variables and susceptible flow phenomena provides a substantial and challenging research topic.

The testing technique employed to perform investigations plays an important role in the determination of transient effects. Due to the difficulties associated with measuring forces during dynamic motion, many previous investigations have used surface pressure methods to arrive at overall wing loading. Current Formula One cars bristle with aerodynamic devices, so it is necessary to use a balance to directly measure forces. As with aeronautical investigations the use of surface pressure measurements and any of the flow visualisation techniques can also be used to identify flow phenomena of interest.

Extensive research has been conducted into transient aerodynamic effects for a wide variety of applications. However, so far none has been conducted into wings in ground effect. The limited amount of research into transient automotive aerodynamics that has been published has made no attempt to determine the cause of any of the discovered effects.

Chapter 3

Wind Tunnel Development

This chapter considers the development of an improved wind speed control for the R.J. Mitchell wind tunnel. There are two aims for the improved controller. To improve the general performance of the wind speed control and investigate the feasibility of controlling the wind speed for dynamic testing. The chapter commences by outlining the former system in terms of hardware, software and performance. Following this, the methods and results of experimental system-identification tests performed to characterise the wind tunnel system are presented. Potentially suitable model types and representations are evaluated with the most appropriate being employed to create models that correctly describe the wind tunnel system. The chapter describes the controller design process, system simulation and the development of a suitable controller algorithm. Finally results are presented following controller implementation demonstrating the improved performance achieved by the new controller.

3.1 The R.J. Mitchell Wind Tunnel

The aerodynamic development of vehicles in wind tunnels is currently performed via a series of static measurements. However, vehicles exploiting ground effect are highly dynamic, undergoing rapid changes in attitude. In the case of elite track cyclists the variation is in speed. These provide the motivation for a drive toward dynamic wind tunnel testing. The need for dynamic testing of racing cars arises from the nature of ground effect aerodynamics. The flow is dominated by significant non-linearity and hysteresis effects.

The presence of a model within the test section has an effect on the wind tunnel flow termed 'blockage' [74]. The motion of a model during wind tunnel testing can cause sufficient changes in blockage that wind speed can be affected. As the flowfield about the model is modified then forces and pressures acting on

the model are also altered. A significant problem exists during dynamic testing when model motion leads to a change in wind speed that is not corrected. Dynamic measurements are typically compared to those derived from static testing[15]. This is not clear whether any deviation from static values be caused by transient aerodynamic effects or varying blockage induced changes in wind speed.

Typically a wind tunnel speed controller has two conditions to satisfy. Firstly, to reach the desired test wind speed and secondly to maintain the desired speed by compensating for disturbances. Often wind tunnel control systems, as is the current case are initially designed with mechanical safety limits as a key consideration and result in conservative performance. A dynamic testing system requires a controller that is adaptable, tuneable for a range of demands and able to cope with nonlinearities. Specifically for this research the desire it for a control system capable of maintaining a fixed wind speed with varying blockage and a varying speed to a prescribed trajectory. To achieve an increase in controller versatility requires a precise understanding of the capabilities of the system to be controlled. Yet knowledge of the existing wind tunnel system is often extremely limited, necessitating a system identification study.

It is typical for wind tunnels facilities to seek to improve performance. A new monitoring and control system was introduced to eradicate power spikes and surges during speed changes of a 87,000 hp fan in [51]. In [53] a numerical model of the flow recirculation in a closed wind tunnel with a variable velocity input boundary condition wasdeveloped. This is applied to the drive system to achieve minimum elapsed time during changes in flow speed. [68] upgraded an existing data acquisition and control system to be real-time for a supersonic facility.

An autotuning adaptive feedforward strategy to control the transient and steady state Mach number was developed in [52]. When applied to the drive system to achieve minimum elapsed time during changes in flow speed. Pels [54] implemented a predictive controller to maintain a constant test section flow speed during testing of a model with increasing angle of attack beyond stall. Improvements were found over the existing PID controller allowing a more rapid change in model attitude.

It will be shown that the wind speed system is nonlinear. The controller is therefore required to adopt a strategy that deals with this nonlinearity and allows adequate performance throughout the range of operating wind speeds. A number of suitable control solutions exist. The use of a general nonlinear controller is a possibility, however this is typically a complex method to design

and implement [75]. The desire is for a nonlinear controller that is a simple and efficient implementation that satisfies the demands of dynamic testing whilst maintaining plant safety limits. In accordance with Astrom and Wittenmark [55],a suitable controller is one that employs parameters that vary with the varying system parameters. This controller is gain scheduling as described in chapter 2

3.2 Assessment of Previous Performance

The R.J. Mitchell wind tunnel is based at the University of Southampton, England. It is a low speed, closed return, closed working section type with a 745KW axial fan providing a working wind speed range of 5 to 45ms^{-1}. The tunnel has a working section of 3.5m(11.5ft) width, 2.4m(7.9ft) height and 10.5m (34.5ft) length. The existing control system was formed of two control systems. The former control software is the outer control loop with the calculated wind speed within the test section acting as feedback. The fan drive has its own controller and forms an inner loop with the fan motor as shown in3.1. What is known of the existing controller is, output is based upon a calibration curve of command voltages relating to fan and wind speeds and a simple difference controller to compensate for wind speed error.

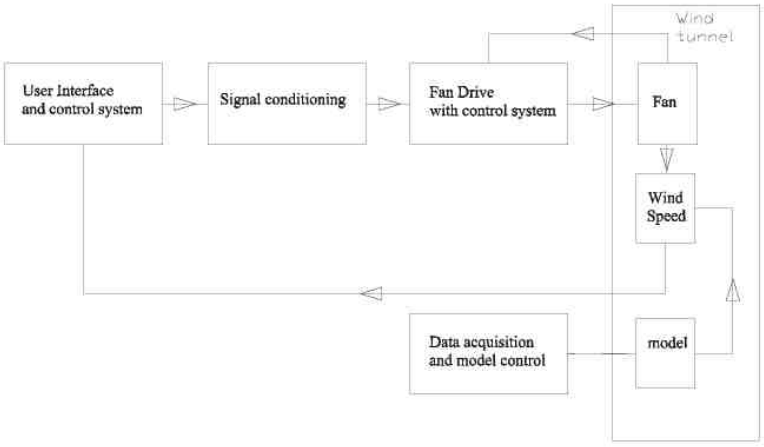

Figure 3.1: The R.J.Mitchell Wind Tunnel.

The behaviour of the RJ Mitchell wind tunnel and the former control system was monitored during a variety of tests. A 50% scale race car at 40ms^{-1} is used here as an example of the existing performance. The control strategy is evidently a fixed ramp rate to the calibrated point followed bya period of monitoringafter allowing the wind speed to settle. A correction is then made.

The wind speed error is a result of the model blockage and equated to 1% or 0.4ms^{-1} below the target wind speed. Overall the response of the fan and wind speed resembles an overdamped system. For data acquisition (to be triggered) the wind speed must remain within the tolerance of 0.2ms^{-1} or $\pm$ 0.05% of target speed for 5 seconds. The example test consisted of 14 changes in model attitude with some leading to changes in blockage sufficient to alter the wind speed in the test section. For almost half the settling time the system is outside data acquisition tolerance but operating at 99% of the commanded power. This incurs a financial penalty and, as motor power is proportional to the cube of wind speed, at higher test velocities this is a significant cost.

3.3 Characterisation of the Wind Tunnel

System identification is the first stage of controller design, its aim is to develop a mathematical model of the dynamic system that is to be controlled from observations or prior knowledge. Its accuracy is determined by the extent of prior knowledge and the observable variables [76].

A series of step inputs was employed to provide knowledge of the overall wind tunnel behaviour and set point tracking. These were 6 equidistant speeds across the operating range.It can be seen when increasing speed, the fan drive is rate-limited 3.2. This is at a fixed rate across the entire speed range, however it is a higher rate than that imposed by the existing system. The fan response varies from underdamped, with a 15% overshoot at low test speeds, to overdamped at mid to high test speeds. The corresponding wind speed response also appears overdamped from mid to high speeds. However at the lowest speeds, despite its underdamped nature, the wind speed initially responds rapidly but evolves into an overdamped response taking a similar time to reach its final value as the highest speed. This is a result of the low wind speed requiring a greater period of time to stabilise around the tunnel circuit.

The tests demonstrated that reducing speed has a markedly different and more complex response 3.3. Immediately obvious is the step in the highest two speeds, shortly after the reduction of the command signal. This is caused by the fan speed reducing much faster than at lower speeds.

The key finding of the system identification investigation is that the system is nonlinear. The process of designing a gain scheduling controller commences with the selection of operating points [77]. Rather than the six equally spaced regions used in the initial assessment, the wind speed range of operation was divided into quarters for the controller development. Steps were from a sta-

Table 3.1: Operational range division for increasing and decreasing wind speed

Increasing	I_{0-1} 0 - 10 ms^{-1}	
	I_{0-2} 0 - 20 ms^{-1}	I_{1-2} 10 - 20 ms^{-1}
	I_{0-3} 0 - 30 ms^{-1}	I_{2-3} 20 - 30 ms^{-1}
	I_{0-4} 0 - 40 ms^{-1}	I_{3-4} 30 - 40 ms^{-1}
Decreasing	D_{1-0} 10 - 0 ms^{-1}	$D_{1-1/2}$ 10 - 5 ms^{-1}
	D_{2-0} 20 - 0 ms^{-1}	D_{2-1} 20 - 10 ms^{-1}
	D_{3-0} 30 - 0 ms^{-1}	D_{3-2} 30 - 20 ms^{-1}
	D_{4-0} 40 - 0 ms^{-1}	D_{4-3} 40 - 30 ms^{-1}

tionary fan to each of the target speeds and a staircase sequentially through each target speed both increasing and decreasing. This was found to be sufficient to adequately describe the system and provide the necessary knowledge for the controller development. Test conditions are shown in table 3.1.

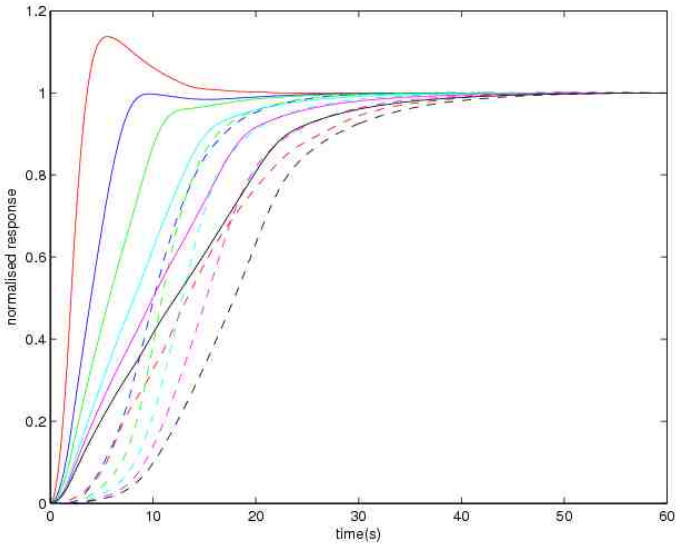

Figure 3.2: Normalised wind tunnel response during increasing speed from lowest speed, red to highest, black. Solid lines fan speed, dashed wind speed.

In-terms of potential dynamic car testing another significant finding was the feasibility of controlling the wind speed rapidly enough for dynamic testing. Exploratory tests were performed with sine and square wave stimulus across a range of frequencies and amplitudes. The maximum rate of change is wind speed was found to be 0.46ms^{-1} per second. An event is shown in 3.4 during

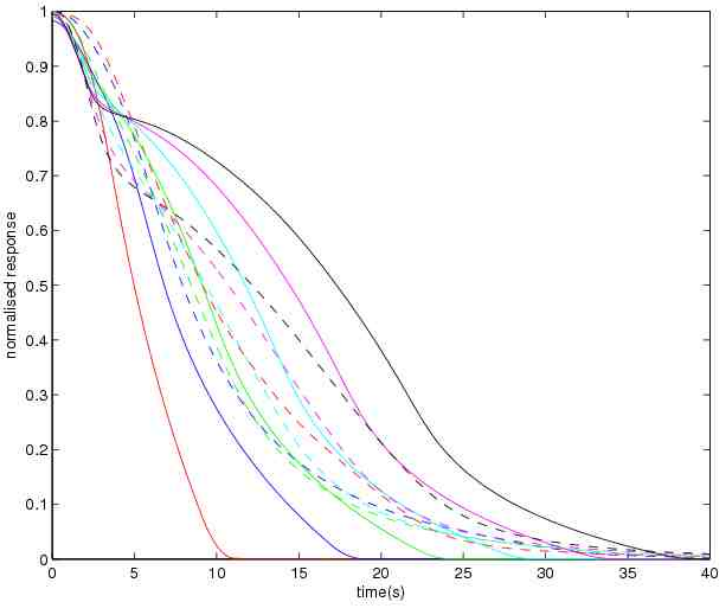

Figure 3.3: Normalised wind tunnel system response during decreasing speed from lowest speed, red to highest, black. Solid lines fan speed, dashed wind speed.

a test at 40 ms^{-1} with the addition of 0.56 ms^{-1} square waves with a duration of 2 seconds. The response of both fan and wind speed is clearly seen as an increasing trend toward a settled mean value. This point is reached after approximately 30 seconds. Along with the drift in mean value the wind speed response reduced to less than half of that commanded, 0.6% at 1/4Hz. The result indicated that, with an appropriate controller, the system offered the potential for dynamic testing for both elite cyclist and yawing vehicles.

3.3.1 Dynamic Model Development

The Matlab system identification tool was used to construct the plant model. Pre-processing of data consists of visual inspection, digital filtering and down-sampling to remove unwanted frequency content. This gives a sample rate that allows the system dynamics to be captured without undue numerical complexity or burden.

Stimulus and response signals were used to identify the plant dynamics as if it were an open loop system. This method is suitable for a wide variety of modelling methods including transfer functions and general linear polynomials. Although the system contains a closed inner loop feedback component, this approach is valid as the behaviour of that subsystem is contained within

Table 3.2: Model order and fitness

model	order	fitness $\Sigma\frac{(y-\hat{y})^2}{n}$
ARX	2210	97.20
ARX	4210	98.88
ARXAX	4321	97.50
ARMAX	5421	99.12
T.F.	2nd order	98.8
T.F.	3rd order	99.6

the behaviour of the entire system. It would be preferable to perform an indirect identification approach to determine the closed loop behaviour, however this requires knowledge of the closed loop controller. The direct approach is not suitable for identifying all closed loop systems and can lead to incorrectly identifying the model. It is however suitable if the reference signal from the controller to the plant is unknown. The suitability of the fit is the least complicated model that provides an adequate representation of the system dynamics [78]. In the case of the lowest test speed, a model order of three gave a system description with fourth order offering a worthwhile improvement. The best fit was achieved with an increase to 5 poles and 4 zeros and a single noise coefficient of the form 3.1. Model orders and corresponding fitness are presented in table 3.2.

$$\begin{aligned} A(z)y(k) &= z^{-n}B(z)u(k) + C(z)e(k) \\ &= B(z)u(k-n) + C(z)e(k) \end{aligned} \tag{3.1}$$

Models were designed to meet two proposed conditions: firstly for dynamic model testing with disturbances from a moving model with an amplitude of 1/4 ms^{-1} and a frequency of 1/4 Hz at a mean wind speeds of 40 ms^{-1} and secondly, for a possible method of elite cyclist testing, where the wind speed is dynamically varied at an amplitude of 2 ms^{-1} at a frequency of 1/7 Hz at a mean speed of 17 ms^{-1}. The latter offers the possibility of exploring transient aerodynamic effects of a track cyclist. Transfer functions for the first two conditions are shown in (3.2) and (3.3).

$$G = \frac{0.9997}{(1 + 2 \times 0.6361s + (1.82s)^2)(1 + 4.12s)} \tag{3.2}$$

$$G = \frac{0.9289}{(1 + 2 \times 0.507s + (1.82s)^2)(1 + 1.58s)} \tag{3.3}$$

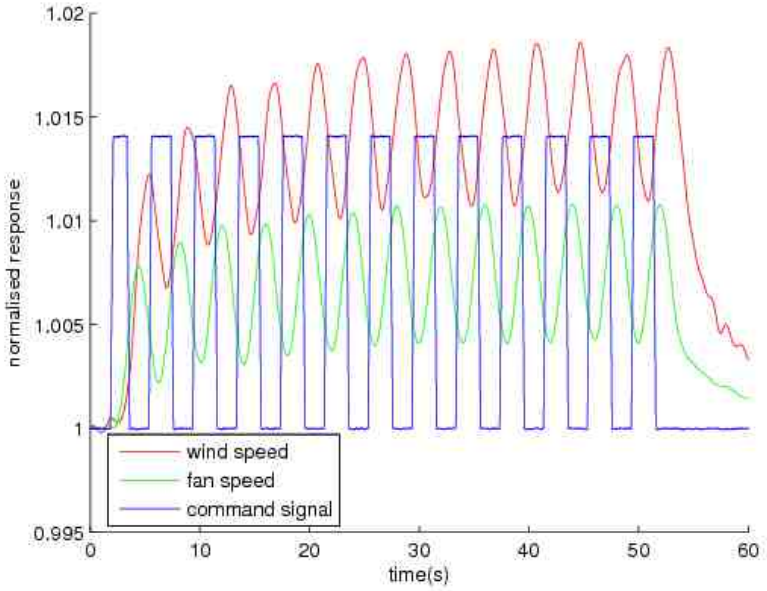

Figure 3.4: Normalised wind tunnel stimulus and response for square waves of 2 second duration.

3.4 Development of a Wind Tunnel Control System

The requirements for the improved controller are:

- A reduction of settling time.
- Ideally being critically damped/having minimal overshoot.
- Improvement in disturbance rejection for general testing.
- The ability to maintain a constant wind speed during dynamic model testing.
- The ability to perform sinusoidal wind speed variations.

The first requirement of an improvement in settling time, aims to reduce the time taken to achieve the final 10% of demanded wind speed. This will reduce the amount of time spent at near full power (for that test). The controller should be capable of simultaneously compensating for disturbances and reference point changes.

3.4.1 Control Strategy

Gain scheduling is considered as having two control loops. Firstly the process feedback loop and secondly the parameter adjuster loop. Often the second loop is slower than the first. Simulation is used to determine performance, particular attention being paid to transitions between operating conditions. The difficulty associated with gain scheduling is that it is often difficult to find a suitable scheduling variable, i.e. one that effectively equates the variables with the process dynamics. This is not the case for this application. Advantages include the control parameters being changed quickly in response to process variation, although dependant on the response of the measurement system. It is also relatively simple to implement. Disadvantages include the absence of feedback in the parameter loop for incorrect scheduling. It is a time consuming design process due to the requirement of a controller for each operating condition and extensive simulation and more so if interpolation is required to smooth transition between controller sections.

This application requires the capability to control at a wide range of operating points and also to traverse across and within the entire speed range. Typically gain scheduling is concerned with maintaining control about some equilibrium with only a small or slow deviation from it. Methods to overcome this have been proposed by Leith and Leithead [59] [60]. To develop a controller that performs as required, a method similar to that employed by Johansen et.al. [79] will be adopted here.

3.5 Controller Design and Analysis

With a suitable plant model and gain scheduling operating points identified, the next stage in the controller design process is to develop a linear controller for each of the operating point listed in table 3.1. If the plant model is well know, then an optimisation process can be used to control this process, possibly accommodating multiple performance criteria as with Griffin et.al.[80]. The controller design process for increasing wind speed requires several iterations of the design steps. Particular difficulty was experienced with achieving a suitable transient response, the more so with the two higher wind speeds. The initial response and the linear increase at the maximum ramp rate was ideal. The difficulty lay within the final stage. Placing the system output within the region between an underdamped 5% overshoot and an overdamped knee at 85% proved relatively straight forward. Fine adjustments to the root locus and PID coefficients resulted in jumps in the system response. The

system was considered settled if the output was within 1% of demand. The controller transfer function for I_{3-4} is shown in (3.4). The final design produced a transient response as desired with very small, if any, overshoot. The aim of improving settling time is also achieved. All controllers share the same general form of root locus and similar PID coefficients, however gain is higher for decreasing wind speed.

$$c = 0.14722 \times \frac{(1 + 0.6s)(1 + 3.5s)}{s} \tag{3.4}$$

3.5.1 Noise

The feedback sensor signal contains a considerable level of noise due to cabling length and electrical power required. Filtering was used to remove the noise for system identification processing as it has the potential to distort the resulting model. The noise from the sensor enters the system in the feedback loop. The error and hence command signal are affected by the noise. However, the dynamics of the system do not respond, therefore the system acts as a low pass filter. Despite this it is undesirable to allow high frequency content to have an effect on the control system as a noisy command signal can lead to potentially damaging demands upon system hardware. A pseudo-random binary sequence (PRBS) and band limited white noise was added in the simulation feedback loop. Comparisons were made to controller response in terms of stability, rise and settling times. If noise does have an adverse effect on the control system it will be necessary to include a filter in the feedback loop when deploying the controller [81] [82]. As expected the modelled system response showed a limited effect with an initial undershoot of less than 0.7%. The settling time was unaffected by noise on the feedback signal as can be seen in 3.5.

3.5.2 Disturbances

To examine the controller's performance when dealing with disturbances, an additional input node was placed between the controller and plant. A number of conditions were tested to explore the behaviour of the controller during long period disturbances from changes in environmental conditions and to rapid disturbances caused by model motion. The results of a simulated rapid disturbance created by increasing the setpoint by 5% at 30 seconds in region I_{3-4} can be seen in 3.6. The step is inserted into the simulation between the compensator and the plant model. The disturbance produces an overshoot in wind speed commencing at 32 seconds and achieving a maximum overshoot of only 4%. This peak occurs at 37 seconds and remains constant for 4 seconds.

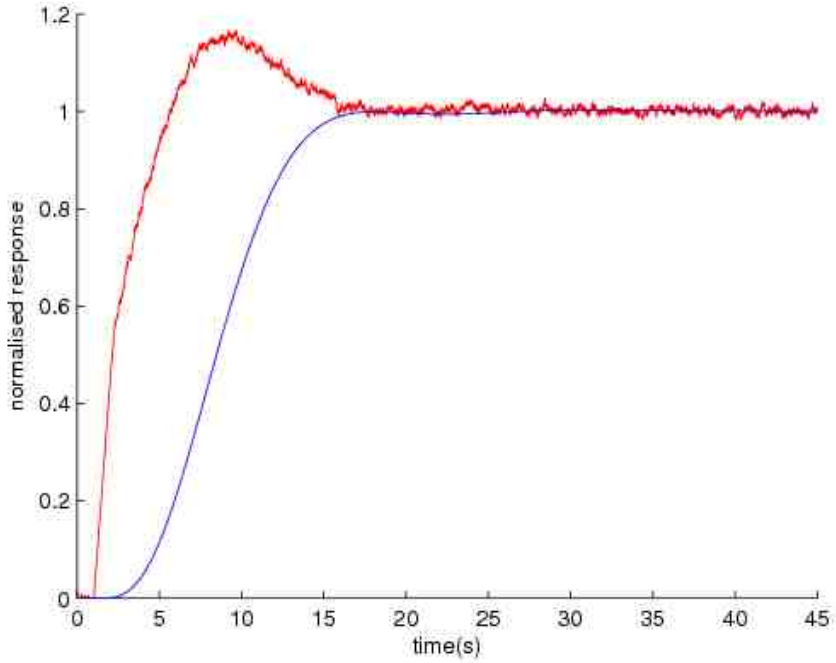

Figure 3.5: Comparison of model and measured system response with noise Model output blue, command signal red.

The control begins its response 4 seconds after the disturbance input. A progressive increase in control output is seen and is responsible for restraining the wind speed overshoot to 4%. The control reaches a steady state at 45 seconds. The wind returns to the reference value of 1 at 53 seconds. A very similar result was found when applying a disturbance that reduced wind speed. This indicates that the controller is capable of rejecting disturbances of moderate amplitude about an equilibrium point.

3.6 Gain Scheduling Algorithm

A key factor in gain scheduling is the development of a control law that transitions between controllers. Typically, some method of interpolating is adopted [83], ideally with a smooth transition [63]. The absence of hard boundaries between regions of operation can ensure this [79]. A weighting function for each controller assures smooth transitions occur at boundaries enablingcontrollers to perform well across their entire region. A Simulink model was employed to determine the most suitable interpolation method for the gain scheduling algorithm. When blending the controllers linear interpolation was used as $u = (1 - L)K1 \times y + L \times K2 \times y$. Controllers are switched by configuring the look up table to implement the gain value below or equal to each quarter set

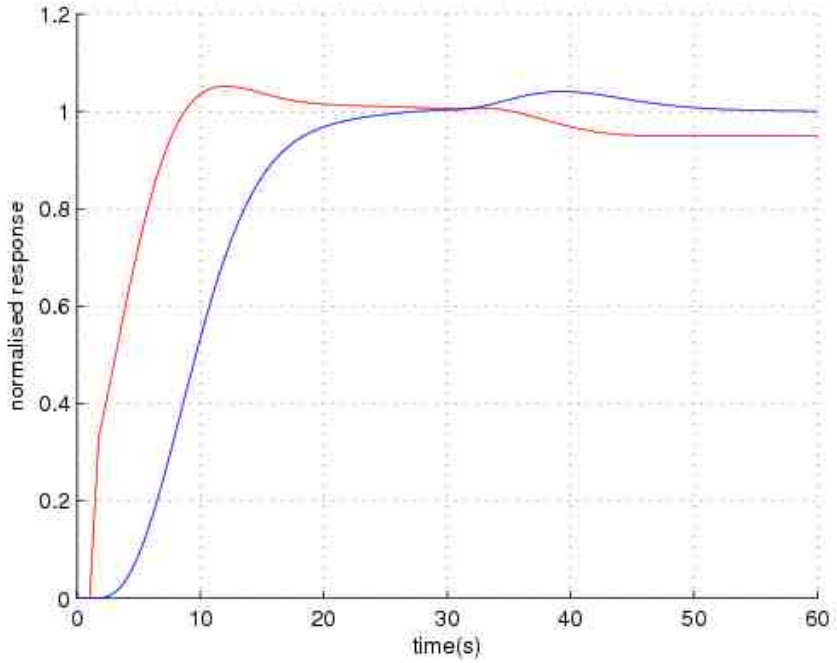

Figure 3.6: Control command and system response during increasing wind speed disturbance.

point. In the same manner as [79] a Simulink switch block is used to select the appropriate system model. Two simulation models were used, one each for increasing and decreasing wind speed. A matrix of reference wind speed profiles was simulated based on those to be tested during controller validation following installation. Particular attention was paid to transitions from one system quadrant to another. The difference between switching and blending controllers can be seen in 3.7. This is based on the maximum wind speed. The effect on the command signal is that during the gain increase up to the first transitions the blended profile is higher than the switched profile resulting in a marginal but clearly faster response. The blended profile now falls sharply below the switching profile with a resultant reduction of controller command. The gradient of system response therefore reduces. The switching gain profile by contrast remains constant with a greater command output that allows the system response to remain at a constant rate. The slower response in the latter half of the blended controller produces a greater error causing the controller output to increase, leading directly to a larger overshoot then the switching method.

The main conclusion to be drawn from this result is that the blending method is directly affected by the profile of the variation in controller parameters. Blending, even on increasing transitions, does not reduce sharp changes in

controller output. This would imply a greater number of equilibrium points are required to satisfactorily smooth the gain profile and hence command signal. As switching performs adequately in terms of system response whilst blending requires a more complex controller algorithm for no advantage, a direct switching method was therefore employed. The marginal increase in response offers little overall improvement. The main difficulty as highlighted in section 3.5 is the final third of transient response, the desire is to improve settling time with the possibility of reducing ramp rate to reduce load on hardware. Blending therefore offers precisely the opposite to the desired effect. The main purpose of the algorithm is satisfied with gain switching.

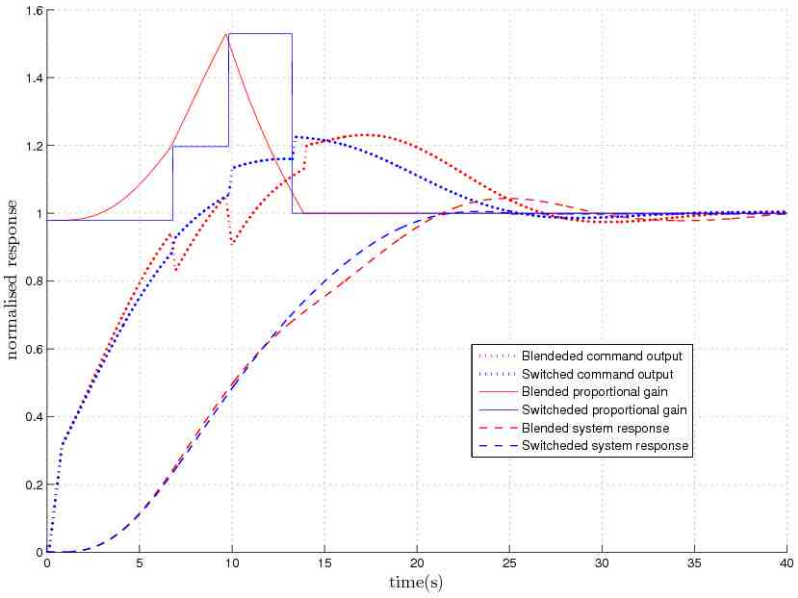

Figure 3.7: Comparision of gain scheduling methods during simulation of wind speed increase from minimum to maximum speed.

3.7 Results

This section presents the experimental results following the deployment of the controller on the R.J. Mitchell wind tunnel. Extensive simulations were performed to confirm controller performance prior to implementation. Firstly, modelled results are compared to experimental findings in 3.8 and 3.9. Initial trails performed during controller implementation were used to establish key parameters including steady state error, rise and settling time. The gain scheduling algorithm is tested before finally the controllers suitability for dynamic testing is evaluated.

3.7.1 Predicted and System performance

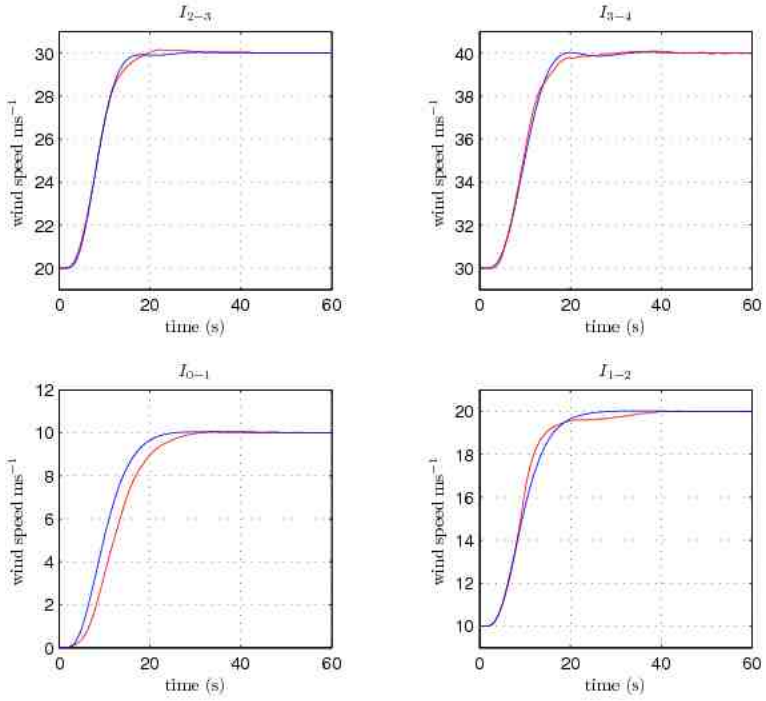

Figure 3.8: Comparison of model and achieved increasing wind speed controllers.

I_{0-1} $0 - 10\text{ms}^{-1}$ Displays a slower rise then that modelled following the start producing a lag during transient response. This was due to a greater delay in starting the actual controller due to the logic employed to overcome the dead time. With the exception of the delay the achieved performance is in excellent agreement with that modelled.

I_{1-2} $10 - 20\text{ms}^{-1}$ Model and controller are in agreement up to mid rise. At this point the implemented controller continues at the maximum limited rate whilst the model had begun to reduce output. This results in a mildly overdamped response reaching the setpoint 10 seconds later then the model. The condition proved to be the hardest to tune.

I_{2-3} $20 - 30\text{ms}^{-1}$ Agreement was found up to 28.2 ms^{-1}. The model is marginally overdamped whilst the implemented controller experienced overshoot. However this resulted in a near identical settling time for both.

I_{3-4} $30 - 40\text{ms}^{-1}$ Again the transient response is in agreement up to 85% of the rise where the implemented controller continues, overshooting. Again the model is overdamped and both reach the setpoint at the same time.

D_{4-3} $40 - 30\text{ms}^{-1}$ When decreasing wind speed from the highest setpoint the model is near critically damped. However the achieved performance has

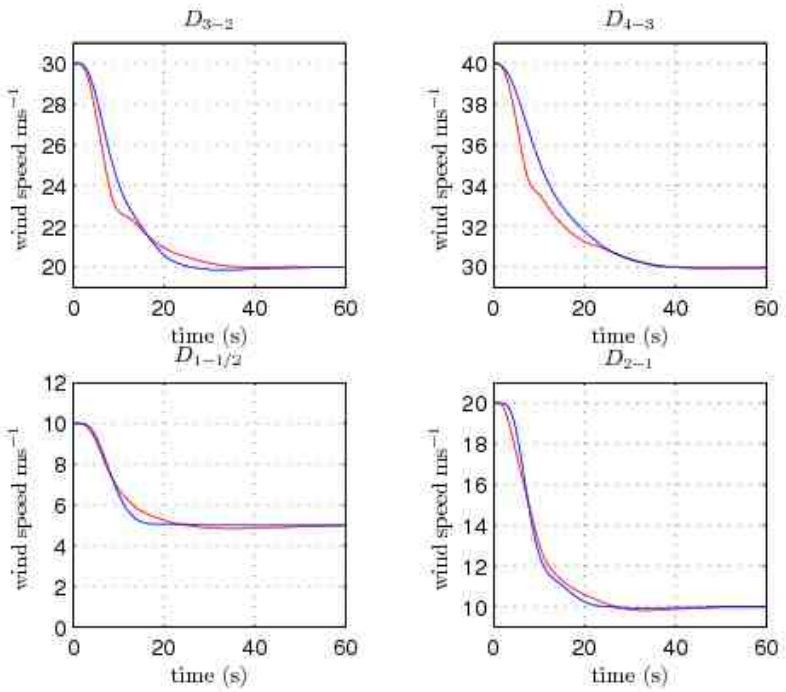

Figure 3.9: Comparison of model and achieved decreasing wind speed controllers.

a faster initial reduction before an adjustment is made, forming a 'kink'. The two converge at 85% of the setpoint.

D_{3-2} $30 - 20\text{ms}^{-1}$ The kink found for condition D_{4-3} is exaggerated to form a distinct step at 70%. From here the reduction in speed is much slower then modelled being underdamped, achieving the setpoint 4 seconds later than themodeled performance. Of the speed reduction controllers this region proved the most demanding to achieve a satisfactory performance when implementing.

D_{2-1} In contrast to increasing wind speed the reduction from 20-10ms^{-1} proved to agree with modelled extremely well.

$D_{1-1/2}$ $20 - 10\text{ms}^{-1}$ The achieved performance proved much harder to achieve at 5ms^{-1}, changes in wind speed proved very hard to achieve due to the slow fan speed and lag in increasing speed through the wind circuit. Although this was captured by system identification and present in the model, the implemented controller proved very sensitive to changes in PID values. Any undershoot resulted in an considerable delay in settling time. The final performance was a compromise between achieving a sufficiently fast transient response whilst minimising undershoot. The implemented controller reduced speed slower during the final half of the speed change whilst suffering an undershoot of 6%, 0.3ms^{-1}, and reaches the setpoint in more than twice that predicted.

3.7.2 General performance

Tests were then performed to directly compare the new controller to the former system in terms of operational performance. Results with a 50% scale race car model test at 40ms^{-1} can be seen in fig 3.10 and table 3.3. The transient response of both systems is identical up to 35m/s. The formersystem then slows to reach a speed of 39.5 ms^{-1} at 65 seconds. An adjustment is made at 72 seconds that results in an initial sharp increase of 0.25 m/s and 99% of the setpoint, 39.6 ms^{-1} is achieved. A gradual rise follows and the setpoint is achieved at 110 seconds. However the rise continues overshooting the setpoint and resulting in a steady state error 0.05 ms^{-1}. The new controller doesn't begin to slow for a further 4 seconds than the former system at 40 seconds where it has reached 36.9 ms^{-1}. The rise to 99% of the setpoint, 39.6 ms^{-1} is achived in 53.2 seconds, 19.8 seconds faster then the former system. The wind speed is seen to overshoot by 0.12 ms^{-1} before the controller reaches the setpoint at 87 seconds and remains within ± 0.01 m/s for the remainder of the test. The new controller therefore reaches the setpoint 23 seconds sooner and maintains a lower steady state error.

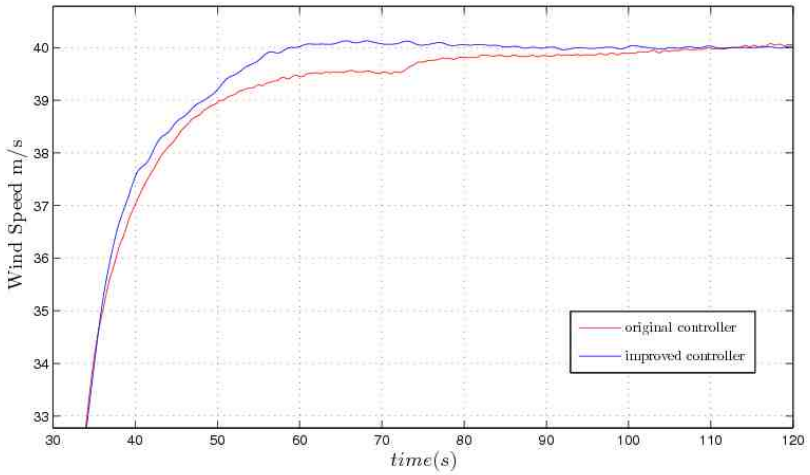

Figure 3.10: Comparison of improved and original controllers achieving 40ms^{-1} setpoint during model car test.

Table 3.3: Steady state error, rise time and settling time, former and Gain Scheduling controllers during 40ms^{-1} scale race car test.

Controller	99% Rise	Settling time	steady state error
Former controller	73s	110s	0.05ms^{-1}
Improved controller	53.2s	87.8s	0.01ms^{-1}

3.7.3 Disturbance Rejection

In order to assess response to a disturbance a test was performed with a varying blockage. The model support and shroud was placed in the test section. With the wind speed settled at 40ms^{-1} the shroud was yawed to create a significant blockage and hence reduce wind speed by over 1.5%. This blockage increase and the resultant wind speed error is much greater than the difference between the presence of the model itself and is far greater than that required for dynamic testing. The variation of wind speed and controller output can be seen in 3.11. Following the error detection the controller begins to correct the loss in wind speed by increasing command output. Yet the controller shows its capability to correct the exaggerated loss off wind speed immediately on detection. It is reached within noise levels and with minimal overshoot 40 seconds after the disturbance was initiated.

After the flow has settled back to 40 ms^{-1} the model is yawed back to the position in which it began. With the blockage reduced the wind speed increases markedly. The magnitude and rate of change is greater than when increasing the blockage. When the controller responds to the change in speed it results in a slight undershoot but reaches the setpoint in the same time as increasing blockage of 40 seconds.

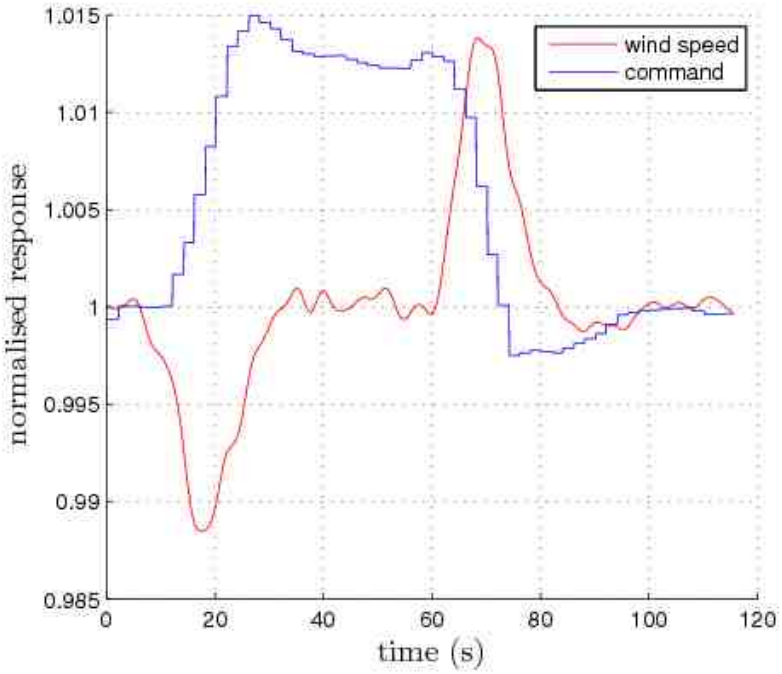

Figure 3.11: Disturbance rejection by improved controller

3.7.4 Gain scheduling transition

Several scenarios were tested when determining the behaviour of the gain scheduling algorithm. These explored the relationship between the setpoint and the transition points, either when crossing, very close to, both above and below, and coincident. Results during implementation demonstrated that switching when traversing boundaries to set points far away from transition values had no influence as command output is at maximum due to rate limiting. When the transition point fell between the region of rate limited output and the setpoint a very mild effect was discovered. It was found that by monitoring the command output the point of switching could be detected. However, little noticeable effect could be found in the wind speed response. When the set point was set to the transition point a minor oscillation occurred in command output as the wind speed fluctuated due to signal noise. This was particularly noticeable when transitioning from region I_3 to I_4. Again the wind speed showed no adverse response. This is due to the systems dynamics and the construction of the PID algorithm that has a limited change in output when the error is small.

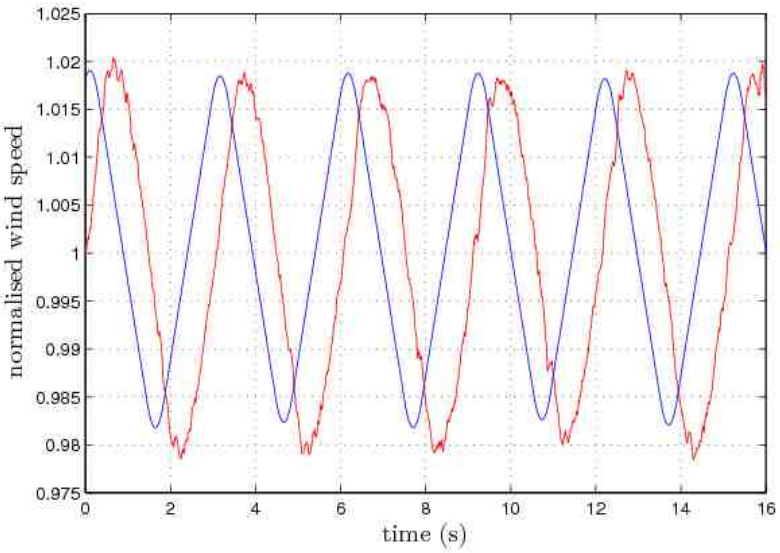

Figure 3.12: Normalised sinusoidal wind speed variation, command signal blue, wind speed red.

3.7.5 Dynamic Wind Speed Control

In order to support dynamic testing an additional feature was developed within the control software that allowed the command input to be entered as a pre-

defined sequence. The controller was capable of exceeding the initial targets for yawing car and cyclist testing. The maximum sinusoidal wind speed frequency achievable being 1Hz at a peak to peak amplitude of 0.005%, 0.2ms^{-1} at 40ms^{-1}. Results for a test with peak to peak amplitude of 0.8ms^{-1} with a 3 second period can be seen in fig 3.12. The system was capable of controlling an oscillating wind speed. The response to varying blockage was limited by the rate of detection of the wind speed variation. Further gains in performance may be found if the controller is developed to include a predictive capability.

3.8 Conclusion

This paper considered the development of the wind tunnel control system. Having adopted a gain scheduling algorithm to overcome the nonlinearity of the wind tunnel system, a set of controllers were designed. This was achieved by incorporating results from system identification into controller design. When implemented, good agreement was found between predicted and achieved performance. The performance of the controller was analysed in terms of ability to meet design criteria whilst achieving stability and other controller specific metrics. A main outcome was the improvement over the former system in terms of operational performance. Settling time, disturbance rejection and steady state error were greatly improved. The commercial value to the operation of the wind tunnel is the gain scheduling controller's ability to reduce the amount of time spent at near full power and hence cost whilst still being outside the tolerance for data acquisition. A significant performance enhancement was also made as the implemented system meets the requirement of performing dynamics testing with sinusoidal wind speeds variations. Although this additional capability was specifically designed to increase the fidelity of elite track cycle and yawing vehicle testing it maybe suitable for a wider range wind tunnel test activities. Overall the use of gain scheduling provided a unique low cost, linear control solution for a large scale non-linear plant whist increasing performance and meeting strict hardware safety limits.

Chapter 4

Transient Aerodynamics Experimental Apparatus and Techniques

This chapter details the techniques and apparatus and their development necessary to perform transient aerodynamic investigation. The requirements of a system capable of performing an experimental investigation into transient aerodynamics can be summarised by the following:

1. A suitable model
2. Accurate motion control
3. Continuous synchronised force, pressure and position measurement
4. An understanding of the dynamics of the measurement devices
5. Isolation of aerodynamic forces with effective removal of inertia forces

4.1 The Model

Although transient ground effect aerodynamics research is driven by the race car industry in the present research an entire car model won't be tested, due to the highly complex flow field. It is the aim of the research to explore any transient effects and if possible their likely cause. To achieve this, a device that has determinable flow features is necessary. Ideally one that is already well known in the static state, possesses the relevant flow features and crucially has the potential to provide an insight into any transient effects. Therefore a single element rectangular wing was used. This offered a greater likelihood of determining any mechanisms driving transient effects, it also provided an

achievable time scale for the model design and manufacturing along with the implementation of the necessary system enhancement.

The wing is a low speed aerofoil originally designed by NASA for general aviation applications, specifically the GAW(1) LS-17 [84]. It has been employed as a racing car front wing and, in its 17 % thickness to chord variant, has the advantage of offering robust mounting and sufficient internal space for sensing devices. The wing dimensions are dependent on several factors. Maximising test Reynolds number determines chord length whilst span is limited by the dimensions of the wind tunnel, specifically the width of the moving ground. Wing thickness is dependent upon the size of the sensors. With the moving ground belt having a width of 2 metres and the pressure sensors minimum dimension being approximately 50mm the final model dimensions are a span of 1035mm and chord of 293.5mm. With 3mm thick endplates this gives an aspect ratio of 3.5.

The design of the wing addressed several factors. Principally the ability to provide reliable and repeatable data. The wing must accommodate pressure tapings and associated tubing, allow access to in-model sensors whilst maintaining a faithful representation of the wing profile. The model was constructed in 4 sections. The main section forms the suction surface and is machined from a single billet of aluminium ensuring model rigidity. In to its internal surface the sting mounting interface is machined as are pockets for pressure transducer modules. The model is mounted to a sting and strut attached to the overhead balance. A smaller aluminium section forms the upper section of the leading edge of the wing. Care was taken to avoid the split lines occurring at the stagnation point or inducing premature separation due to proximity to the leading edge. The pressure surface is formed from two interleaving carbon fibre sections, bolted front and rear. All joints are filled with a compound that results in a completely smooth continuous surface.

From an understanding of the pressure distribution of wings in freestream and in ground effect, regions of the wing surface were identified where the flow was potentially of interest to this research. Pressure tappings were formed in 4 chordwise and 3 spanwise rows. Chordwise rows are at the semi span, quarter span, 0.1b and 0.025b respectively. As the wing is mounted on the centreline the semi span row is located at 0.45b. These rows consist of 19 taps on the lower surface and 9 on the upper surface.

Three spanwise rows are at the quarter chord, three quarter cord and 0.95c and are formed of 18 ports of which 4 are coincident with the chordwsie rows. All these pressure tapping's are on the starboard side of the wing. The port side of the wing contains 4 reference tappings. The arrangement of the pressure

tappings and both the mounting register and transducer pockets can be seen in figure 4.2.

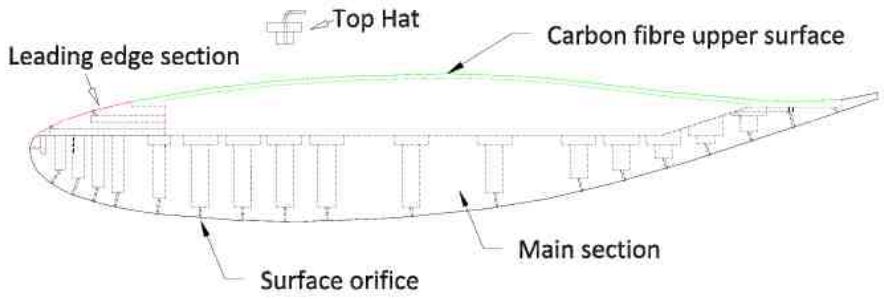

Figure 4.1: Section view of wing at 0.45b.

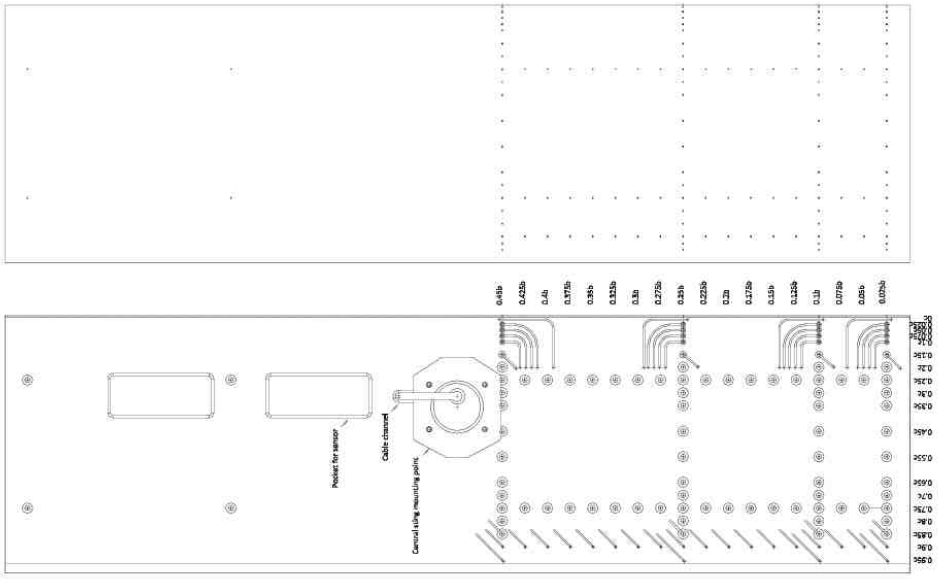

Figure 4.2: View of inside lower wing section and pressure tappings locations.

The surface pressure tapping is an orifice of 0.6mm diameter leading to a larger borehole A top hat is placed into the top of the bore hole which has a 1mm diameter tube, flexible tubing is attached to the free end and connects the tapping to the transducer. A bonding solution is applied to the surface that forms an airtight seal. Figure 4.1 shows the pressure tapping design and the components of the model.

The model is mounted to the overhead balance with the sting used for scale model automotive model testing. The sting is large enough to support the mass of the model, its aerodynamic loads and the force of the flow in the test section. To reduce its aerodynamic effect upon the model being tested its surface is streamlining with a fairing.

As the wing utilises the overhead balance the aerodynamic forces acting on the strut is measured along with those of the wing. Due to the size of the fairing the tare drag was significantly higher than that of the wing. The fairing used for automotive testing reduces interference effects it is however mounted directly to the sting. To isolate the forces acting on the model it was necessary to produce a fairing that shrouds the sting but makes no contact to it during testing. An extension plate was added between the sting and carriage to allow the wing to reach the desired ground proximity as the existing sting restricted ground proximity of 0.15c. The resulting tare drag reduction can be seen in table 4.1.

Wing drag	29.6N
Existing fairing drag	51.7N
New fairing drag	7.9N

Table 4.1: Tare values

4.2 The Dynamic Testing System

4.3 Motion control

The dynamic testing system must provide accurate motion control and continuous synchronised force, pressure and position measurements. The importance of accurate motion control was outlined by Knoschild [15]. Equally as important is knowing the actual model position. The primary motion factors were determined as the method of trajectory input, type of trajectory, accurate position feedback and the ability to follow a desired trajectory. The existing motion system consisted of a PC running a user interface where position commands are entered. A motion controller, Mitsubishi Melsec-FX2 formats trajectoriesfor the motor, Mitsubishi HA-FF63B-EC. The motor drives a gear head that drives a ballscrew that runs the length of the strut onto which a carriage is driven. The sting is mounted to the carriage.This system was found to be extremely limited as it was only possible to enter a single target position and maximum motion velocity with no accurate measure of model position.

The motion system hardware and fairing is shown in figure 4.3. The side and front views show the sting with and without the extension plate respectively. The increase in ground proximity is clearly illustrated.

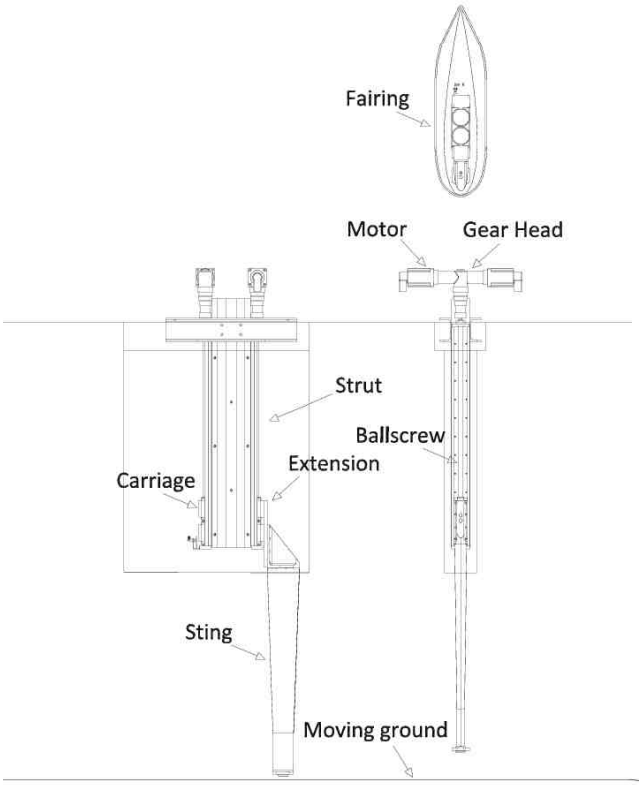

Figure 4.3: Improved fairing and motion hardware front elevation shows maximum proximity to ground without extension plate.

To overcome this limitation and take greater control of the model motion a National Instruments (NI) motion controller PXI-7358 was added to the data acquisition system. Tests were performed during the system development with motion trajectory being calculated by the NI system and output as a sequence of waypoints at fixed time intervals. This system did provide adequate motion feedback that could be incorporated into the data acquisition software and was used for an initial investigation [85]. Motions were of the order of 0.15c, single direction ramp and hold and half sine wave at frequencies up to 0.25Hz.

Although the initial trial adequately demonstrated the worth of dynamic testing the performance of the motion system required improvement to allow thorough investigations into automotive transient aerodynamics. A new motor system was specified that was capable of performing transient investigations. Suitable motors were 75E2C301 servoswith motion control performed by the

NI based system.

The improved motion control was performedby the National Instruments system. This utilises an FPGA and a Digital Signal Processor (DSP) and is used for all closed loop control with PID calculation, position tracking, and trajectory generation. The FPGA acts as a high speed trajectory generator and calculates instantaneous position command. Motor velocity is then calculated based upon the position command and current position using a PID controller. It was necessary to tune the closed loop PID parameters to meet the desired motion control.

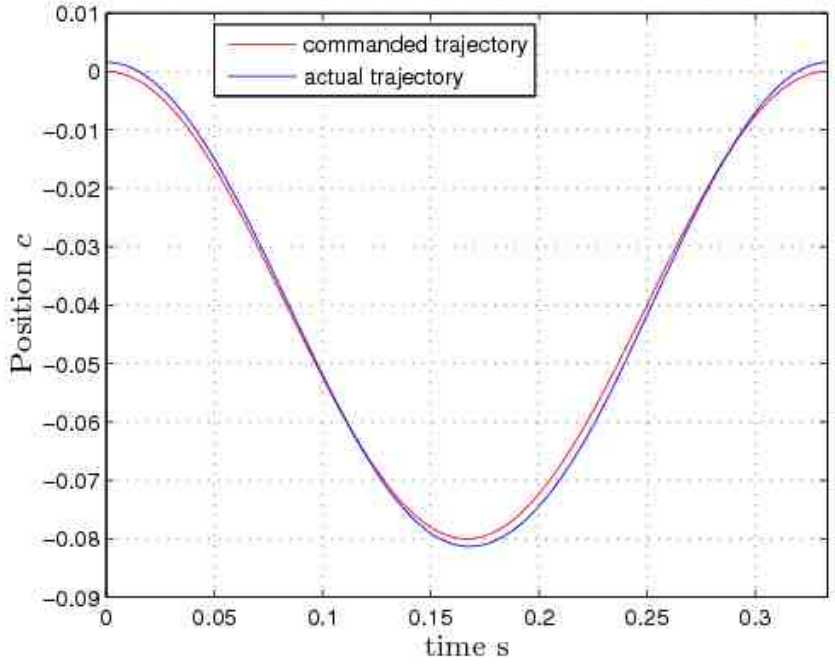

Figure 4.4: Achieved and commanded trajectory.

Results for a 3Hz sinusoidal motion of 0.08c can be seen in figure 4.4. The actual position is taken from a single cycle from the midpoint of an oscillation sequence. The overshoot at the peaks of the wave can be clearly seen. These are of similar magnitude and are the greatest error through the motion profile. They are less than 2% of the total amplitude. Following the overshoot the motion controller regains the commanded trajectory approximately half way on the downward stroke. Two thirds of the upstroke is complete before the trajectory is in line with that commanded.

Finally the effect of the aerodynamic load on the motion profile was explored. It is also necessary to consider the effect the aerodynamic load has upon the trajectory. Tests were performed with the wind and moving ground at test speed. Position profiles were compared to those without wind. The

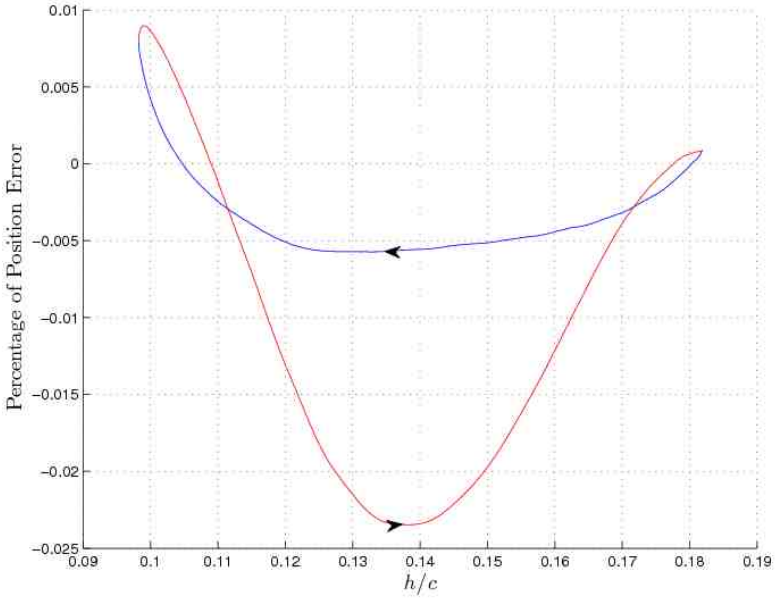

Figure 4.5: Variation of trajectory between wind on and wind off tests.

difference between wind on and wind off motion position profiles expressed as a percentage of peak to peak motion amplitude can be seen in figure 4.5. Beginning at the top of the motion at $0.18c$ the error is at a minimum. On the downstroke the wind on trajectory leads that of the wind off trajectory by a near constant value until the bottom off the oscillation where the wind on motion experiences a greater overshoot. The wind off trajectory is again lower on the upstroke, however as this in the opposite direction it therefore lags behind the wind on motion. These tests served to confirm that the motion trajectory could be considered to be sufficiently accurate to conduct dynamic testing.

4.4 Synchronisation

A system for dynamic testing must be capable of outputting anyone of a variety of motions upon command whilst measuring forces, pressure and position logged to a single data file. The present system employed to acquire measurements from the overhead balance is based upon the National Instruments family of hardware and software primarily a PXI-1044 chassis.

The six forces are received from the balance amplifier as a voltage and are measured with a low channel count high resolution simultaneous data acquisition card, PXI-4472. Each channel having its own analogue to digital converter. Model position is received on the PXI- 7358 motion card from the

motor encoder as incremental quadrature counts. As these two devices are part of the National Instruments based system it is possible to write a LabVIEW programme to acquire both forces and position on the PC. Motion commands are directed to the motion controller again with a LabVIEW programme on the same PC.

The pressure module, ScanivalveZoc 33, is interfaced with a high speed multifunction data acquisition card, PXI-6251. This card was selected as it is optimised for extremely high accuracy at high sample rates having a fast settling time afforded by a high speed onboard amplifier. A digital port is used to output the binary address of the required pressure transducer. Following the desired settling time of the pressure modules Analogue to Digital Converter, ADC, the analogue voltage from the pressure transducer is measured on the analogue input channel.

Following extensive development a LabVIEW programme was created that controlled motion and all data acquisition. Measurements were synchronise using the NI systems 10MHz reference clock. A trigger was devised that is sent from one card aligning all others. Both force and position measurement cards are triggered from the pressure system card when a measurement is taken. This also allows each card to sample at different rate whilst synchronising data acquisition.

The maximum pressure sample rate of pressure measurements is dependent on settling time of the ADC, the manufacturer recommend minimum of 20 micro seconds this is a 50KHz sample rate, using all 64 ports this results in a sample rate per port of 781.25Hz. Tests were performed with varying settling periods from 40 to 10 micro seconds. To bring samples into line with the force measurements on the PXI-4472 card which has a minimum sample rate of 1KHz a settling time of 14.5 micro seconds was used. With programme iteration loop requiring a further 0.076 micro seconds the final sample rate is per port of 1072Hz.

4.5 Dynamic System Response

In order to perform transient investigations it was necessary to develop a dynamic testing technique. To produce meaningful data a detailed understanding the dynamics of the system was required. The balance is a mechanical device, loads applied to the model cause deflection that result in a displacement within the relevant load cell. The load cell responds by producing an electrical output proportional to the applied load. How this mechanical system responds to a variable input and what effects it may have on the aerodynamic loads on the

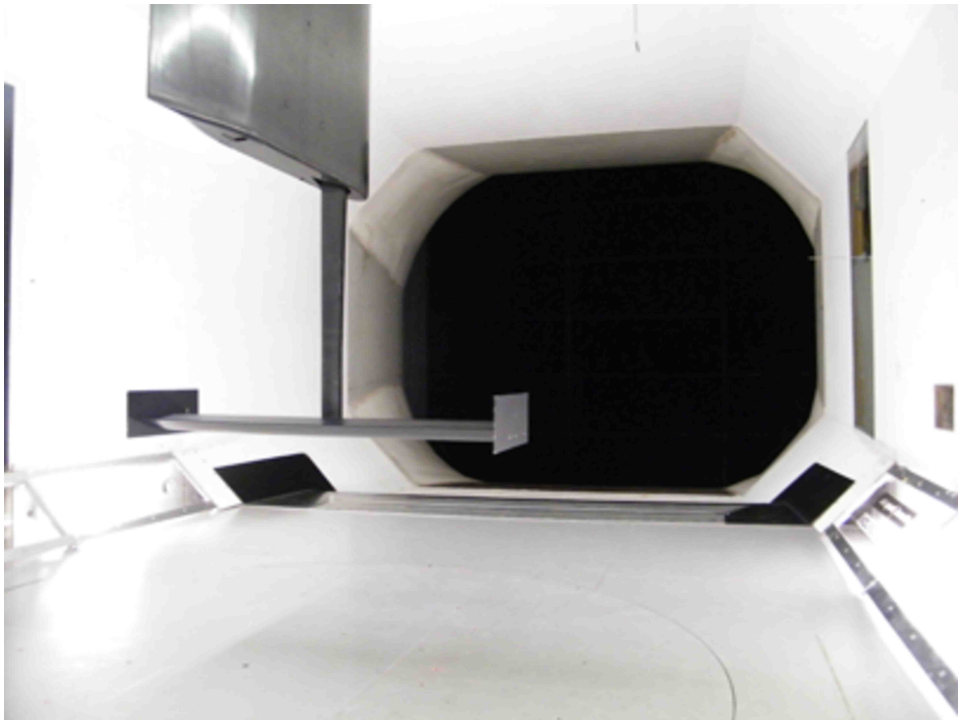

Figure 4.6: Wing shownin highestconfiguration with original fairing.

model must were determined. In a similar manner a pressure on the wing surface is transmitted via tubing to the pressure measurement system. The frequency response function for both systems must be established. A single input single output method was used to determine these response functions.

The frequency response function can be derived in terms of the unit impulse response function $h(\tau)$. This is the systems response to delta function input.

The dynamic properties of the physical system can then be described in terms of a transformation of the unit impulse response function. A Fourier transform is typically the preferred transformation as it provides a frequency domain description. The frequency response function is defined as:

$$H(f) = \int_0^\infty h(\tau) e^{-j2\pi f\tau} d\tau \tag{4.1}$$

Typically this is a complex number with real and imaginary parts or in complex polar form.

$$H(f) = H_R(f) - jH_I(f) \tag{4.2}$$

$$H_R(f) = \int_0^\infty h(\tau) \cos 2\pi f\tau d\tau \quad H_I(f) = \int_0^\infty h(\tau) \sin 2\pi f\tau d\tau \tag{4.3}$$

$$H(f) = |H(f)| e^{-j\phi(f)} \tag{4.4}$$

The magnitude $|H(f)|$ is the system gain factor and the phase $\phi(f)$ is the system phase factor.

$$|H(f)| = [H_R^2(f) + H_I^2(f)]^{\frac{1}{2}} \tag{4.5}$$

$$\phi(f) = \tan^{-1}\left[\frac{H_I(f)}{H_R(f)}\right] \tag{4.6}$$

The frequency response function for an ideal system with a sinusoidal input at frequency f produces sinusoidal output at some frequency f. However, the amplitude may differ and the phase may be shifted.

$$x(t) = X\sin 2\pi ft \quad y(t) = Y\sin(2\pi ft - \theta) \tag{4.7}$$

The dynamic response of the pressure transducer is the least complicated of the measurement devices. The development of a method to determine sensor frequency response will therefore commence with the surface pressure measurement device.

4.6 Unsteady Pressure Measurements

The aim of this section of the research was to determine if the pressure system is capable of performing dynamic testing without modification. In [15] a sound source was used to determine the frequency response of pressure sensor. Experiments were conducted accepting the small error found and without making compensation for it. The measurement of surface pressures are made with an orifice at the wing surface as detailed previously. The response of both the transducers and ADC are the limits of the system. The steady state calibration of a pressure sensor is achieved by applying a number of constant pressures across the transducers range of operation. A calibration curve is then determined from the mean value of each of the applied pressures.

Dynamic testing is primarily concerned with the measurement of fluctuating pressures as well as the mean pressure. It is therefore necessary to determine the dynamic response of the complete pressure measurement system. Theoretical approaches have been made to determining the system transmission characteristics, notably by Bergh and Tijdeman [86]. Experimental methods include those of Knorschild [14] in which a chambered loud speaker for the same purpose. However this only allows calibration in the laboratory. For this project it is deemed necessary to allow calibration with the system installed in the model so that the transport characteristics of the entire system can be determined. Paniagua and Dnos [87] successfully used a similar technique to

determine the dynamic response of a pressure probe, although an exploding balloon was used to provide the varying pressure source. A digital method was employed to compensate for the response of the pressure system that was based on an $m-$order linear system.

This research used an experimental technique similar to that used by Williams [88]. A single input single output system identification method was used to determine a frequency response function describing the actual pressure fluctuation at the model surface from the measured pressure signals, as a function of time. A proven method is employed for this purpose. A sealed chamber having a speaker on one side and a pair of adjacent pressure tappings on the other. The speaker provides a sinusoidal pressure input signal up to the maximum pressure transducer sample rate. The tappings contain a high response pressure transducer, that is used to provide a reference signal, and a connection to the pressure transducer under test.

The chamber was constructed from 3pieces of 15mm thick Medium Density Fibreboard (MDF). The sensor side piece has the two tappings. The speaker side piece has an orifice to accommodate the speaker, a 200W Alpine 6203. The high dynamic response pressure transducer used was a Kulite model XCQ-093-5D. This is placed into the chamber flush to the inner surface and sealed on the outer surface. A thin walled steel tube is inserted in to the second tapping, protruding 20mm. Again it is flush with the inner surface and sealed on the outer surface. The pressure transducer is connected to the steel tube via flexible tubing.

The sine wave is generated by a PXI-6251 as an analogue signal that is passed to a preamp, Soundlab G097, that in-turn drives the speaker. Measurements are made with a PXI-4472 card. The Zoc signals are received via the new system detailed in section 4.4. The reference signal from the Kulite are amplified by a Vishay 2120B set to match the input range of the Zoc, $\pm$ 2.5V, taking advantage of the PXI-4472s adjustable input range to allow measurements to be taken at the full dynamic range. The speaker, chamber and Zoc pressure module can be seen in figure 4.7.

An exploratory test was conducted with frequencies held at 10, 50, 100, 200, 300 and 400Hz for 20 seconds. This served to provide some insight into the capabilities of the pressure sensor and the dynamic calibration system. Following this, tests were performed with a sine wave staircase with 2 seconds at each frequency in the range 2-400Hz. This was greater than the expected maximum response rate of between 200Hz and 300Hz. This is acceptable as the sampling frequency of each pressure port is approximately 1KHz. To satisfy the Nyquist criteria of sampling at a minimum of twice the highest frequency

Figure 4.7: Pressure sensor, calibration chamber, speaker and Zoc33 module.

of interest. For practical applications this is typically extended to 2.5 times that.

The Zoc module is factory fitted with tubing 200mm in length. Extensions are necessary as the pressure module is located on the port side of the model, the opposite side to the tappings. The wing has a total of 165 pressure tappings, with the Zoc module containing 64 ports it is therefore necessary to perform tests in three different configurations, switching between them. To avoid damaging the air tight seal each tapping has a tube permanently attached. This results in a significant quantity of tubing inside the model. It is possible to use tubing of differing lengths to reduce this amount. To determine the effect of tube length tests were performed with this standard length and with extensions of a further 400 and 60mms.

A bandpass filter restricted data to 400Hz. The Matlab System Identification tool was used in to produce a frequency response function. Results can be seen for the 3 lengths of tubing in figure 4.9. The standard tube length has an initially flat response that, from 30Hz this develops into a distinct broad resonance curve with a gain in amplitude of 67% peaking at 165Hz. The response levels off at 350Hz where it has fallen by 20%. The phase response is again relatively flat up to 30Hz followed by a progressive increase in lag reaching a maximum of 180°s.

Both the extended tube lengths display a good response up to 25Hz. At

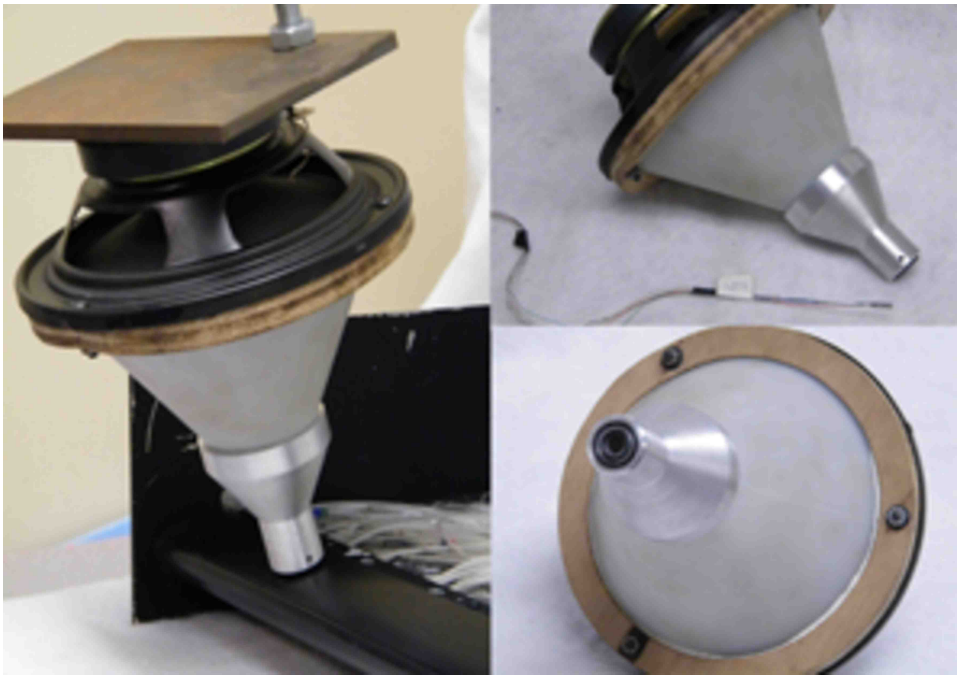

Figure 4.8: Wing mounting pressure calibration device.

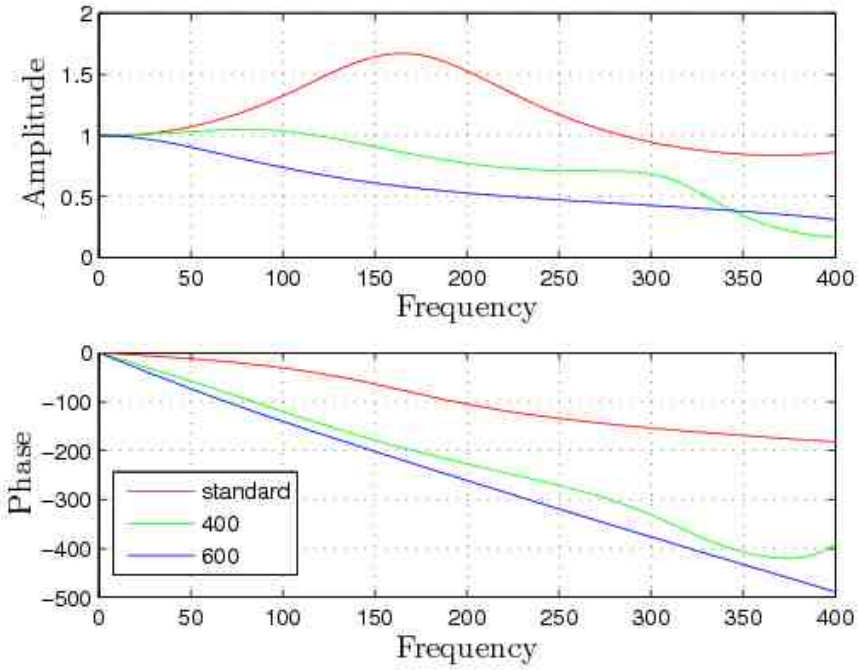

Figure 4.9: Response of pressure system for varying tube lengths.

this frequency the longer extension tube begins a steady loss dropping to approximately a half at 200Hz. By contrast the 400mm extension rises to less than a 5% gain up to 100Hz where it steadily decreases to 69% at 300Hz. Here a sharper drop occurs, falling rapidly to 16%. The phase shift for both extensions is very similar and unlike the standard tube commences with an immediate delay that continues to the maximum frequency. In the case of the 600mm tube this lag is essentially linearly, whilst that of the 400mm extension levels off at a frequency corresponding to the anti-resonance.

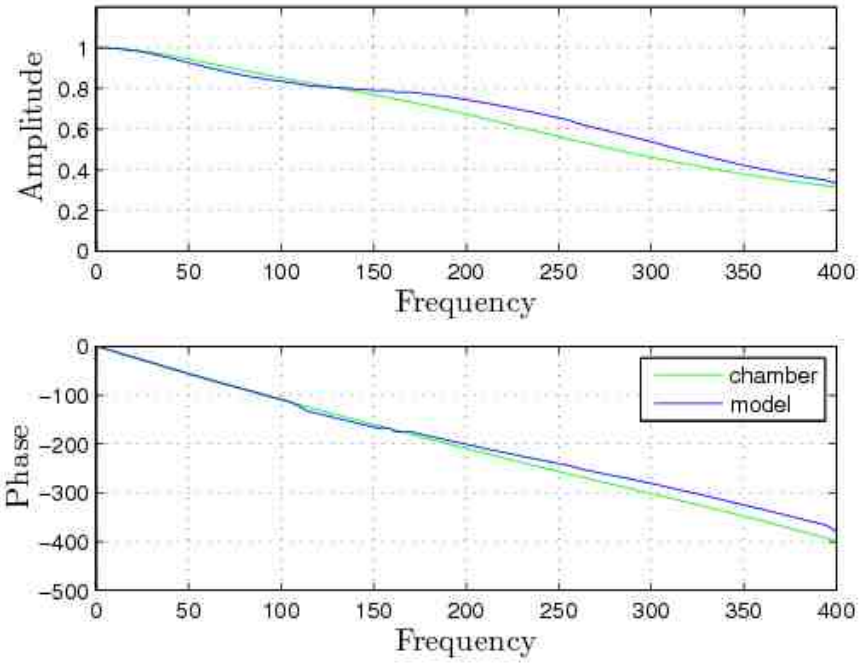

Figure 4.10: Comparison of pressure system response with 400mm tube in model and chamber.

The effect of tube length is to cause an attenuation of higher frequency pressure measurements. At lower frequencies in the case of the shorter extension tube this was a positive effect, reducing the gain in amplitude experienced by the standard configuration to less then 5% greater than unity. The phase response the increased tube length has the effect of introducing a consistent lag across 3/4 of the test bandwidth.

These results exceeded expectations and as such were highly encouraging. The response of the module is sufficient to capture a wide frequency spectra of pressure data. It was decided that a single tube length would be used throughout the model, 400mm. Each sensor therefore simple requires its own conversion factor to engineering units and the application of a common dynamic calibration function.

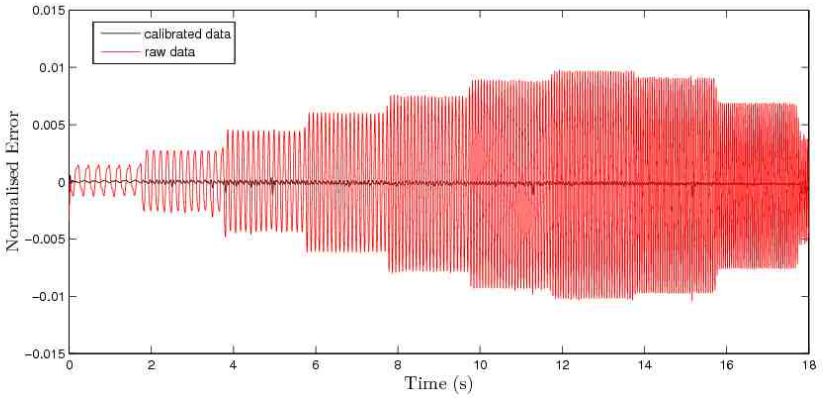

Figure 4.11: Calibrated and raw pressure data error normalised to reference pressure.

The same approach as the bench test was adopted with the fluctuating pressure being applied to the model surface to characterise the entire pressure transport system. The chamber was therefore replaced with a vesselwith an orifice for the Kulite,that channelled the pressure wave into the pressure tapping on the model. Tests were performed with an extension tube length of 400mm.

The response of a single sensor tested with the chamber and, again when installed in the model can be seen in figure4.10. It can be seen that any difference between the two is minimal. This was true of all tappings at a variety all the locations tested on the model.

A dynamic calibration algorithm was developed that compensating for the response of the pressure measurement system. In [88] compensation up to the maximum sensor response is achieved in the frequency domain with the use of a Fast Fourier Transform, FFT. In contrast for the test cases being conducted as part of this research a method was developed to allow dynamic calibration in the time domain and over a restricted frequency bandwidth. As [87]a parametric model is employed to determine a transfer function of the pressure systems response. Compensation of dynamic pressure measurements was achieved via an algorithm based on the inverse transfer function.

Using the experience gained in chapter 3 the Matlab System Identification software was employed to develop a series of models of the pressure system response. From the bench test data a 4th order ARX model provided a suitable transfer function. A Matlab based post processing algorithm inverts the function. Validation results are shown in 4.11.The calibrated measurements can be seen to have reduced both the amplitude and phase shift to near zero.

This portion of the research was conducted with few difficulties and pro-

duced good results. It was found that the pressure measurements system had an excellent range of response and the model pressure transportation system had little effect upon the transducer frequency response. This allowed 'true' pressures to be recreated from measurements. These results indicated the system was suitable for use in dynamic testing.

4.7 Transient Force Measurements

This is a highly challenging task and critical to achieving the desired outcome of this experimental investigation. Previous investigations have struggled to satisfy this requirement, see chapter 2. To perform transient aerodynamic investigations with force measurements it is vital to understand the dynamic response of the measurement systems. The validity of force data is dependent on the development of a method of identification that allows both frequency and magnitude response to be determined and the creation of a calibration algorithm.

The force measurement device used during the research is an external pyramidal or virtual centre balance as seen in photograph 4.12. Forces are determined at a resolved centre, separated into 6 components and measured with six individual load cells. As previously stated, this is a mechanical system and is of significantly more complex design than the pressure sensor and therefore is a far more demanding task. Along with measuring forces this system has the added complication of providing the model motion. Enacting an appropriate system identification method is therefore also challenging. As with the pressure transducers the single input single output system identification method will be used to determine the systems dynamic response.

Static calibration of external balances is typically performed by the balance manufacturer as part of the installation process. Specific equipment is employed to allow the application of a full combination of loads to provide interaction matrices. Once completed it is necessary to periodically apply check loads to confirm continued accuracy. The forces of principal interest to this research are downforce (negative lift) and drag, with the former an order of magnitude greater than the latter. These forces are positive measurements downward and in the direction of the freestream flow. For static testing check weights can be suspended from the bottom of the sting and via a pulley to the rear. For system identification purposes a stimulus is required that replicates transient input during dynamic testing. The input can be made with either the addition of a known mass or by a device that causes a displacement. In both cases it must provide a varying force.

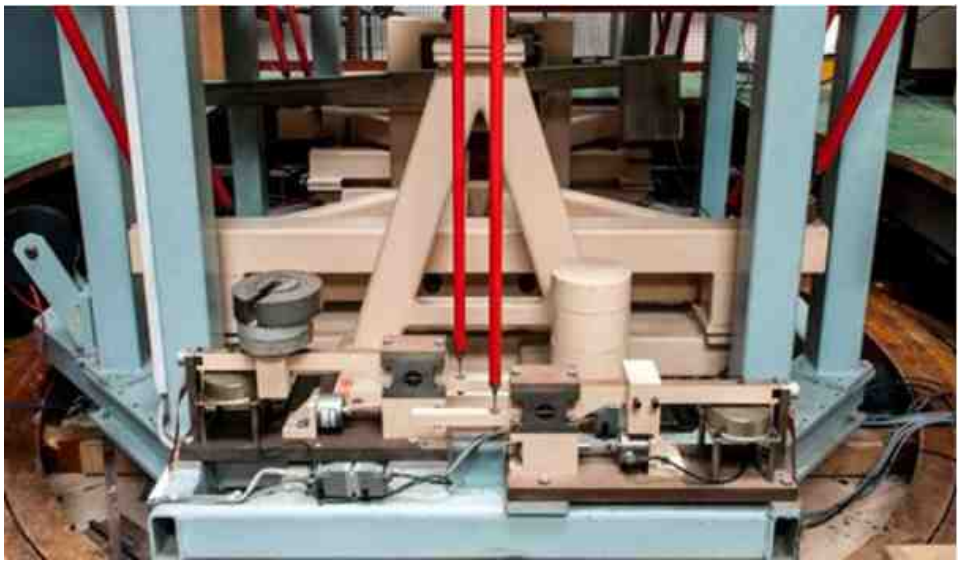

Figure 4.12: Overhead Balance

At the outset of this research the dynamic capabilities of the overhead balance were unknown. Prior to performing a detailed examination of the balance a preliminary test was performed to determine the extent to which the overhead balance was suitable for transient investigations. The simplest method for the determination of the response to a sudden change in force was to remove or apply a load. The use of impact loads to calibrate force transducers was performed by Bruns [89]. A mass is rapidly applied to a load cell with a single impact proving capable of identifying its response to a change in load.

Toproduced an instantaneous reduction of forcea mass was suspended from the foot of the strut, allowed to stabilise before the attachment was released. With an accelerometer attached to the mass an accurate measurement of the time detachment of the mass and the time of force measurement response, the systems time delay could be determined. Measurements showed that the balance was capable of adequately responding to rapid changes in load. Some oscillation was detected in the response. To fully evaluate the systems natural frequency a complex excitation was applied to the foot of the strut in the form of a hammer blow. This served to provide a wide range of frequency components. In accordance with resonance theory the system responds at its natural frequency by acting as a filter and removing all other frequency components. By repeating tests with a variety of impact forces the natural frequency of the strut, sting and balance was found to lie with the region of 20 to 22Hz. This is above the frequency of motions to be investigated.

A method of system identification was devised, based on a displacement

stimulus displacement rather than a forcethat fully established the systems dynamic response. A static load test was conducted with the applied mass, deflection of the strut and resulting force measurement recorded. Results be seen in figure 4.13. The test showed that to produce a force equal to the level of downforce developed by the wing in ground effect required a displacement of only less than 0.1mm.

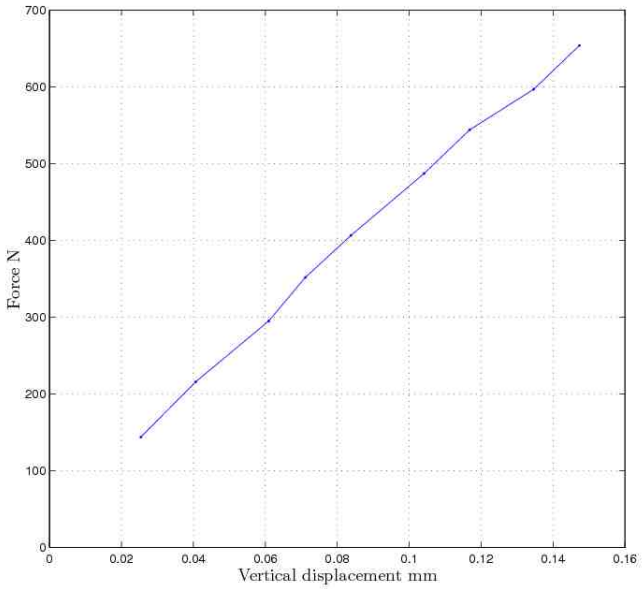

Figure 4.13: Overhead balance lift response to displacement.

The controlled varying displacement was provided bya cam and follower arrangement driven by a variable speed motor. Two cam's were used, a single and a five lobe. With the motor speed ranging from 2 to 28Hz this provided an excitation frequency range of 2 to 140Hz on a single axis. Each axis was tested separately. A spring is attached to the follower ensuring contact is maintained between the strut and the exciter. A shear accelerometer was mounted to the base of the strut to provide the reference signal, PCB Piezotronics model 353B32. A second accelerometer was placed at the interface of the strut and balance to provide an insight into the behaviour of the strut.

As with the pressure system the stimulus signal was intended to be a swept sine wave. However unlike the pressure system where a single continues data file was employed to perform system identification, data was dissected into clear frequency components.These frequencies were 3, 4.8, 7, 9, 13, 15, 17 and 22Hz.

It was felt that a possible limitation of this approach is that the amplitude of the force input is not known and therefore has to be derived from accel-

eration data. This relies on the acceleration being transformed firstly into a displacement then into a force. Aside from difficulties with the derivation of displacement data, this method relies on the static deflection calibration to determine force input. This is the precisely what this experiment aims to overcome (therefore seems contradictory). To overcome this a spring mass system was therefore employed to provide a know force input that could be compared to the force output of the balance.

Three spring of varying stiffness were suspended from the strut with a range of masses that reflected the variation of aerodynamic force found during the region of ground effect likely to be tested in the transient investigation. The frequency range was 3, 5 and 7Hz and loads of up to 60N.

Typically, difficulty is found when using accelerometers at such a low frequency. However, unlike typical accelerometers those chosen for this research have an excellent operational range of frequencies with an 95% accuracy at 1Hz and 90% at 0.7 Hz. Great care was therefore taken to ensure with tests being repeated several times for each spring. At these frequencies the force input is not simply a product of mass and acceleration. The system can be considered as being 'springy' rather than 'massy'. Inertia does not singularly provide the force input the spring itself makes a contribution. $F = m\ddot{x} + kx$. The potential difficulty with this method is that the again the displacement is not directly measured it is derived from the accelerometer data. However using $x = \ddot{x}/-\omega^2$ and $\omega^2 = k/m$ with k determined from a static test, results were found to be in excellent agreement down to all but the lowest amplitudes experienced as the sinusoidal motion decayed. This was due to there being insufficient displacement to provide excitation of the shear accelerometer.

Data analysis was performed on measurements in the time domain and in the frequency domain via Fourier transformation. A number of features were identified. The system responds to a instantaneous change in applied force with a fixed dead time of lessthen 10 milliseconds. Following this, a finite time is required to reach the new value where an oscillation occurs with relatively small amplitude that decays to within noise levels in approximately 5 seconds. This is typical of a strain gauge load cell. During sinusoidal experiments a fixed phase shift exists up to 17Hz, above this it progressively increases. A sharp increase in force response was found between 18 and 20 Hz. The accelerometer exhibited no sign of this indicating that the lowest resonant frequency of the system lies within that range and emanates from the overhead balance. Results from displacement tests can be seen in figure 4.14 and sprung mass tests in figure 4.15. The error in amplitude is within experimental uncertainty at the lowest tested frequency and increases to 2% at 7Hz.

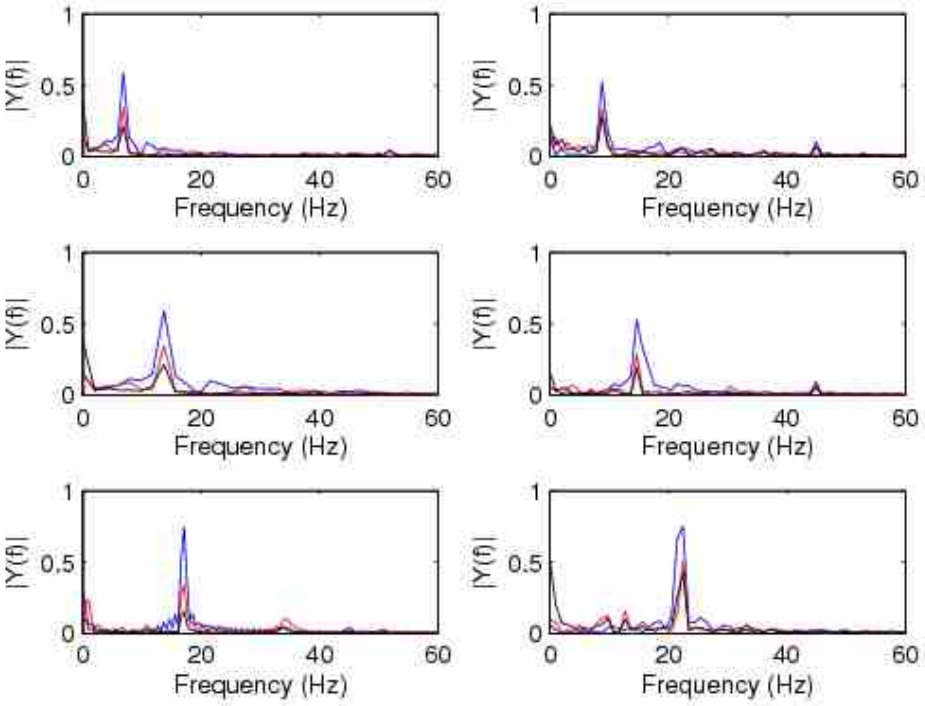

Figure 4.14: Frequeny response of overhead balance.

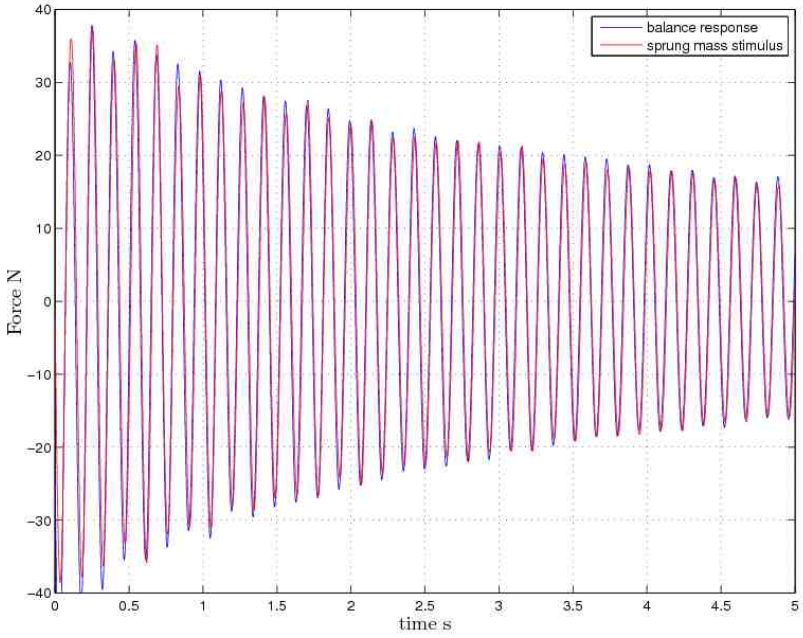

Figure 4.15: Overhead balance response to sprung mass stimulus.

Using a displacement as an input method proved successful in determining the response in terms of frequency and phase but not the amplitude. Although the amplitude mass damper tests did not extend to the same frequencies as the motorised excitation testing results they did exceed the test frequency and the balance was found to respond within measurement uncertainty. The combination of the two tests demonstrated the balances ability to correctly measure force during transient investigations and allowed a frequency response function to be developed.

These tasks occupied a considerable portion of the project. With the combination of each of these tests the response of the system was determined. Dynamic calibration will require the removal of the fixed dead and correction of phase shift based upon data sample rate.

4.8 Isolation of Aerodynamic Loads

The final requirement of the dynamic system is the effective isolation of aerodynamic loads. The method used for the isolation of the aerodynamic loads is that used successfully by [37]. Tests are performed without wind or road to determine the inertia of the motion. The test is then repeated with the wind and road. Ensemble averaging is then employed on each set of data and the aerodynamic force is found by removing the inertia determined from the first test from the wind on test. Sufficient repeats are made of each experiment so that the inclusion of an additional repeat does not change the average value. This value is highly variable being dependant on the stability of the flow that is in turn dependant on the motion type, frequency, amplitude and mean ground proximity.

The ability to employ this method is dependent upon a number of factors. The most critical being accurate motion control. In [14] a 0.1mm error in position between wind on and inertia tests during 20Hz motions results in a force measurement error of 47N. If this is true then unable to use wind off tests for inertia removal. To overcome this problem [14] utilised 6 accelerometers to determine inertia.

Although not presented here another factor that may influence using wind off technique for inertia removal is added mass. This was evaluated numerically with the assistance of Newman [90]. It was found to make no measurable contribution to aerodynamic effects at the reduced frequencies under consideration.

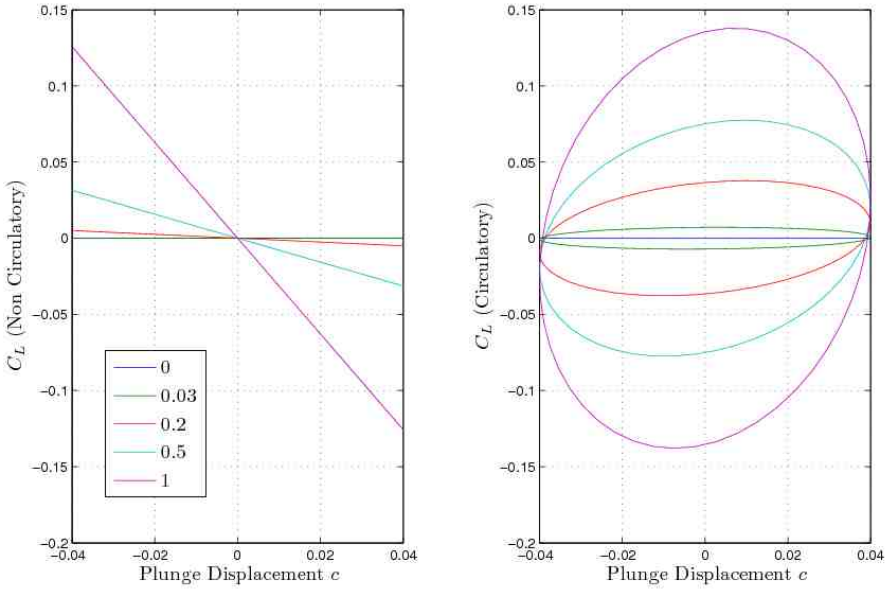

Figure 4.16: Theoretical lift variation due to added mass during to pure heaving motion for k varying between 0 and one.

4.9 Chapter summary

This chapter detailed the steps taken to satisfy the requirements of a dynamic experimental testing system. The selection, design and construction of a model suitable was followed by the development of a combined motion and data acquisition system capable of controlling the desired motion profiles whilst measuring synchronised data. An extensive investigation into the dynamic response of force and pressure measurements systems was performed. Determining the response of the overhead balance was identified as the most challenging task of this section of the research. With the completion of the final stage with the effective isolation of aerodynamic loads it is possible to consider and analyse the data produced by the dynamic system.

Chapter 5

Signal Conditioning and Data Reduction and Uncertainty

With a suitable system of measurement in place,the final requirement of a transient investigation is the development of a data reduction algorithm.The approach adopted and subsequent results of data reduction are detailed. Signal conditioning methods, both physical and digital are highlighted. An accurate method was determined to derive the aerodynamic behaviour from multiple cycles of a dynamic experiment. Finally experimental uncertainty analysis will be presented.

5.1 Signal Conditioning

Signal conditioning is concerned with three properties namely amplification, filtering and electrical isolation. During data acquisition the signal is acquired from the source transducer measuring the physical phenomenon. The signals are transmitted to a conditioning device via two or more wires. The length and path of these wires varies by application. The wind tunnel building contains many sources of high voltage and electromagnetic hazards. Most interference and signal degradation occurs in the signal connection.

The National Instruments data acquisition system performs processing prior to digitising in an attempt to clean the signal. In some cases of this research signals are in microvolts, and ideally amplification needs to be performed as close as possible to the source. Amplification close to the sensor increases the signal above noise levels. Conversely, noise acquired prior to the amplifier is then amplified along with signal.

Signal conditioning is the transformation of a physical property to an electrical signal. Isolation, and effective grounding is used to prevent noise from entering the measurement system. The data acquisition cards employed are isolated as signal is passed through a transducer. In this case it is a capacitive

coupling device that breaks the ground loop, rejecting common mode voltage.

Lowpass filtering ideally completely attenuates signal above a cut off frequency, whilst leaving the passband unaffected, and possess a linear phase shift. In reality a filter employs a mathematical function and therefore will have ripples in both the passband and stop band, a finite transition region and non-linear phase response. Analogue filters are the hardware, having both input and output as analogue. Digital filtering has a number of advantages over analogue filters, however they cannot be employed to exclusively compensate for poor signal conditioning. As such, a digital filtering formed only the final stage of the signal conditioning process.

Throughout this research noise has presented a challenge. Noise frequency content was evaluated in a wide variety of conditions. Measurements were taken from the overhead balance and pressure system with the tunnel in quiescent state, with wind on, with wind and road and road only to identify the sources of noise. Several sources were found and wherever possible were neutralised. To reduce the unavoidable noise two filters were evaluated, Butterworth and Chebyshev. Seeking a sharp transition, minimal attenuation and ripple in the passband and near absolute attenuation in the stopband. Pressure data was filtered with a 40Hz passband while force measurements were filtered to retain the second octave of the highest motion frequency at 15Hz. Matlab was employed to design the filters that are shown in figure 5.1. The Butterworth filter was chosen in preference to the Chebyshev at it best achieved the design criteria by avoiding ripples in the passband and by, employing a higher order, matching the sharpness of transition.

5.2 Data Reduction

To understand the transient or time dependant measurements of dynamic testing it is first necessary to have a grasp of the steady measurements from static testing. During a static test forces are measured against time to produce a time history record. Data averaging techniques are then employed to provide a static value. Experiments can be repeated to obtain an ensemble of time history records. During these tests every effort is made to maintaining constant experimental conditions. For wind tunnel testing this is rolling road and test section flow velocity, flow temperature and model attitude. The data produced can then be considered stationary data, that is, the average value does not change with time. The mean, mean square and variance for a single time history of stationary data can be calculated by equations 5.1, 5.2 and 5.3.

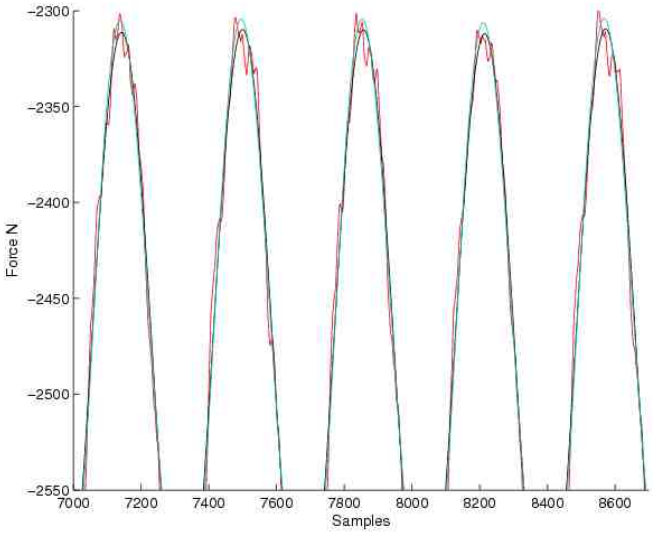

Figure 5.1: Comparisons of filtering of lift measurements. Raw data red, Chebyshev blue, Butterworth cyan.

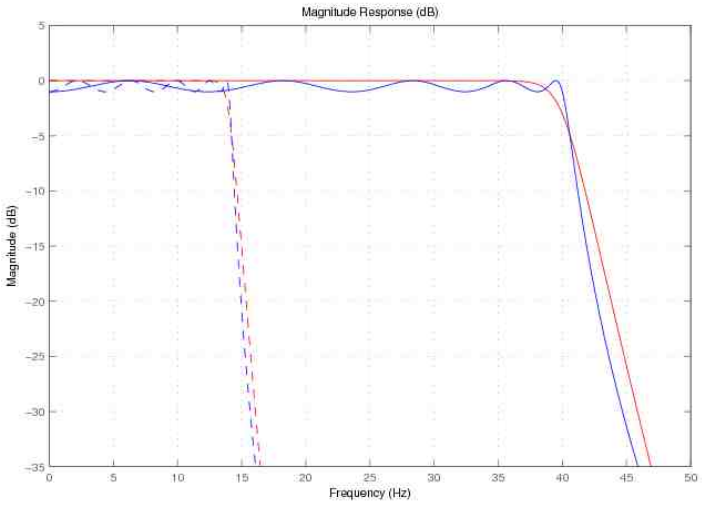

Figure 5.2: Comparisons of filter design response for type 1 Chebyshev red and Butterworth blue with cutout frequencies of 14Hz dashed and 40Hz solid.

$$\mu = \lim_{T\to\infty} \frac{1}{T} \int_0^T x(t)dt \tag{5.1}$$

$$\psi^2 = \lim_{T\to\infty} \frac{1}{T} \int_0^T x^2(t)dt \tag{5.2}$$

$$\sigma^2 = \lim_{T\to\infty} \frac{1}{T} \int_0^T \{x(t) - \mu\}^2 dt \tag{5.3}$$

The standard deviation is derived from the variance.

$$\sigma = \sqrt{\sigma^2} \tag{5.4}$$

In the case when data is stationary, an average value for the entire time history can be computed from the ensemble average at a single time. Dynamic testing is employed to provide transient effects that are time dependant. As the average value varies with time data is non-stationary. If this transient data results from a short duration event with clearly defined beginning and end then averaging techniques can be employed similar to used with stationary data. By repeating the experiment N times an ensemble of time histories is produced with the value at any particular time t_1 being computed by averaging over the ensemble of time histories.

The ensemble mean, mean square value and variance then become:

$$\mu(t_1) = \lim_{N\to\infty} \frac{1}{N} \sum_{i=1}^{N} x_i(t_1) \tag{5.5}$$

$$\psi^2(t_1) = \lim_{N\to\infty} \frac{1}{N} \sum_{i=1}^{N} x_i^2(t_1) \tag{5.6}$$

$$\sigma^2(t_1) = \lim_{N\to\infty} \frac{1}{N} \sum_{i=1}^{N} \{x_i(t_1) - \mu(t_1)\} \tag{5.7}$$

Data reduction was performed post test, commencing with filtering, tares and offsets are then removed and dynamic calibration is applied to pressure and force measurements. Data is segmented and an array of each wave is created. Tests were performed over a number cycles. Several of the first waves are removed from the array to allow the flow to develop into full transient state. The ensemble average is then computed and the inertia is removed. Finally data is converted to engineering units and non-dimensionialised.

Every individual sinusoidal test is preceded and followed by a period with the model stationary and static data is acquired. Statistics are determined for position, pressure and forces in the form of the data mean value, standard

deviation and variance for each data point in every wave in the ensemble array and the pre and post oscillation static data. These statistics are saved in a file and allow a measure of uncertainty to be determined.

5.3 Experimental Uncertainty

It is essential that the integrity of data acquired during experimental investigations is assessed and the uncertainty of measurements determined. There are standards for wind tunnel testing methods and data integrity AIAA, SAE and ARGARD. Uncertainty or experimental is formed of two types, systematic and random. Systematic can be considered as accuracy of instruments making measurements and produce a fixed deviation from the true value, hence the term bias being used to also describe these errors. Random errors typically contribute a small deviation, both additive and subtractive, to repeated experiments with all other variables held constant.

Systematic uncertainty is a more complex challenge then random. Sources include the speed of moving ground, wind speed that includes measurement of ambient and dynamic pressures and temperature, force and pressure transducers, position control, model installation, measurement device capability and numerical issues. Prior to conducting tests sources of potential systematic error were considered and evaluated. Where possible steps were taken to reduce these errors. With the exception of the temperature gauge all sensors were calibrated. All pressure sensors were calibrated with a Druck DPI 615 Pressure Calibrator.

Test conditions are controlled as closely as possible with the wind tunnel being run for a period to raise the test section air temperature to 20°. It is then maintained at that temperature with a chiller. Wind and road speeds are maintained to within $\pm$ 0.1 m/s during tests. The dynamic pressure is measured along with force and surface pressure data throughout each test and used to non-dimensionilise.

Calibration of the overhead balance was achieved with a static loading check of all components over the range experienced during dynamic test. The masses used for calibration were in kilograms, as the output of the calibration matrix is in Newtons to double check the assumption of $F = ma$ with gravitational acceleration assumed to be 9.8001 calibrated weights in Newtons were applied on the lift and drag axis prior to the test. The calibration of sensors does not totally eradicate error as there is uncertainty both the measurement devices in the form of quantisation and in the regression used to determine calibration coefficients of the transducers. Where possible the highest resolution data

acquisition cards are used, up to 24bit for forces with the lowest being 16bit wind tunnel environmental conditions.An in-intimate working knowledge of the overhead balance was acquired by the author whilst supporting extensive commercial and academic wind tunnel tests. On numerous occasions load checks were performed with one particular application requiring the resolution of the balance to de determined to its finest scale. It was demonstrated that employing this method and employing sufficient care and sample length allowed a repeatable resolution of one gram.

There is a certain degree of uncertainty is associated with the model itself. Sources include the accuracy of the wing profile, model installation and model positioning. The design and material of the model ensures that there is no measurable deformation under aerodynamic load. Model installation is achieved by setting the wing position with an electronic height gauge accurate to within $\pm 0.01mm$. Additionally a digital inclinometer is used to ensure pitch and roll is negligible. Changes in wing height during testing is achieved with the dynamic motion control system. This measures position to with a hundredth of a millimetreand maintained static ground clearance to within $\pm 0.001c$. During the highest reduced frequency motions the wind on data acquisition position was found to progressively increase by a total of 0.21mm. This drift equates to $0.9c$. Much uncertainty of previous investigations was overcome with the development of an accuracy of the motion system.

Having established and made an effort to reduced the systematic errors the uncertainty of the data must be considered. From the static data acquired pre and post oscillation the uncertainty during an individual test run and over the duration of the test programme can be determined. Along with the uncertainty of a single experiment or test, the variation from multiple experiments over an extended period of time. The model acts as the wind tunnel calibration wing therefore it is possible to establish long term repeatability. Short term, as would be expected from such a uncomplicated model, is excellent. Long term was also found to be excellent at 0.39 Netwons over three separate experiments. The repeatability of pressure measurements is determined via the reference ports. These allow assessments to be made between the port and starboard sides of the model. They are used throughout everytest allowing repeatability to be determined. The repeatability of reference ports was within twoPascals for short term and three Pascals long term.

Random error is also termed noise and it is this contributing to force and pressure measurements that makes the most significant random uncertainty. Statistical approaches can be employed to deal with this. Assuming a Gaussian distribution , which is known to describe experimental variation extremely well,

random variations will form the distribution population curve. By using the standard deviation as defined in 5.4 and that provided sufficient samples are taken we can be 95%confident that a value will lie within $\pm 1.96\sigma$ of the mean value.

Most important is the spread of data within each ensemble. The standard deviation of an ensemble of 25 cycles of measurements of: surface pressure at the mid-span suction peak, $0.45b$, $0.25c$, lift and drag during a single test at 3Hz with a peak to peak displacement of $0.08c$ and mean $h/c = 0.18$ are used to asses this and are shown in figure 5.3. It should be noted that position is the $cos(x(t))$, commencing at $t = 0$ i.e. at the top peak with the model at maximum ground clearance. Commencing at the top of the motion the standard deviation of the lift ensemble is at its greatest. It progressively reduces by a 1/4 prior to the midpoint of the downstroke where it remains essentially constant until the bottom of the motion is reached. Upon the commencement of the upstroke it increases to a gentle hump with a peak in the region of the initial, value shortly after the midpoint. The variation of the standard deviation of the pressure tapping is similar to the behaviour of lift in that the minimum is found midway through the downstroke, this is again followed by a hump. Unlike the lift measurement there is no levelling off with the result of the peak in the hump occurring earlier and is 1/3 greater then at the outset of the motion. Drag measurements also exhibit an increase in standard deviation on the upstroke.

The confidence interval formed from the standard deviation for the lift ensemble average varies from ± 3.03 to 2.19 Newtons whilst drag varies between ± 0.42 and 0.33 Newtons and pressure measurements range from ± 0.0038 to 0.0023 C_p. The individual waves, mean value and confidence interval of each ensemble of are shown in figures 5.4, 5.5 and 5.6. These clearly illustrate the variation within the lift and pressure ensemble is greatest in the region of the peaks of each oscillation. These are the points in the motion where the trajectory is at its slowest. The minimum is found during the downstroke, close to the midpoint. Also visible an effect created during data processing. The sample length of each cycle could vary by one sample. The ensemble average was therefore calculated over the shortest sample length of the data array. This truncation and a number of outliers, particularly in the lift and drag data, was evaluated and had minimal effect on the derived average.

The same equipment is used for static and dynamic measurements therefore full time histories are acquired for all static data. Static data acquired at the mean ground clearance during the same test as that employed to determine dynamic uncertainty experienced confidence levels of ± 0.89 Newtons for

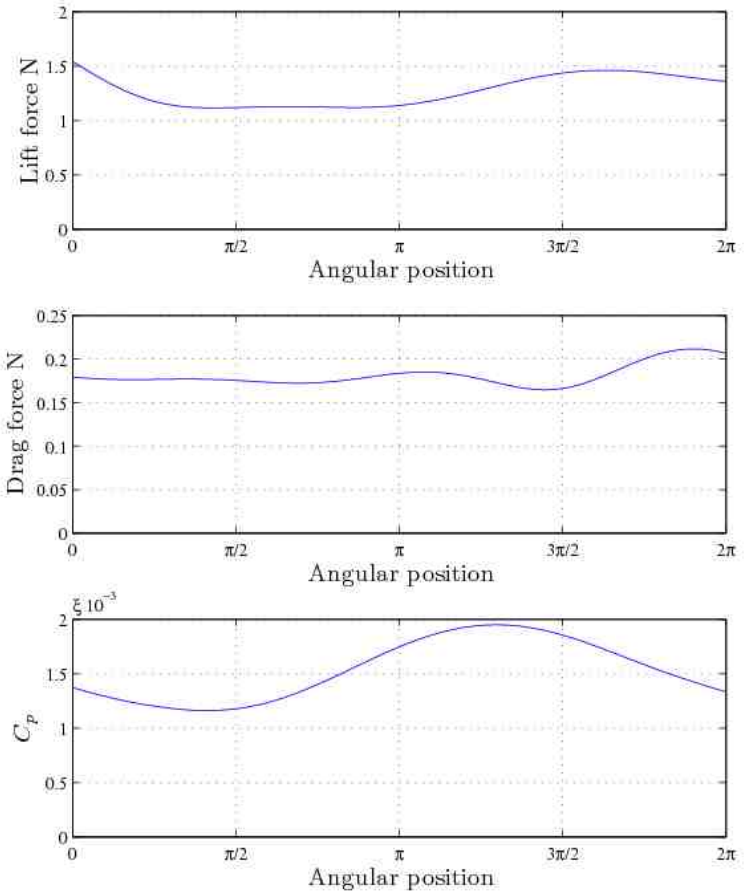

Figure 5.3: Variation of standard deviation for ensembles of lift and drag forces and pressure coefficient.

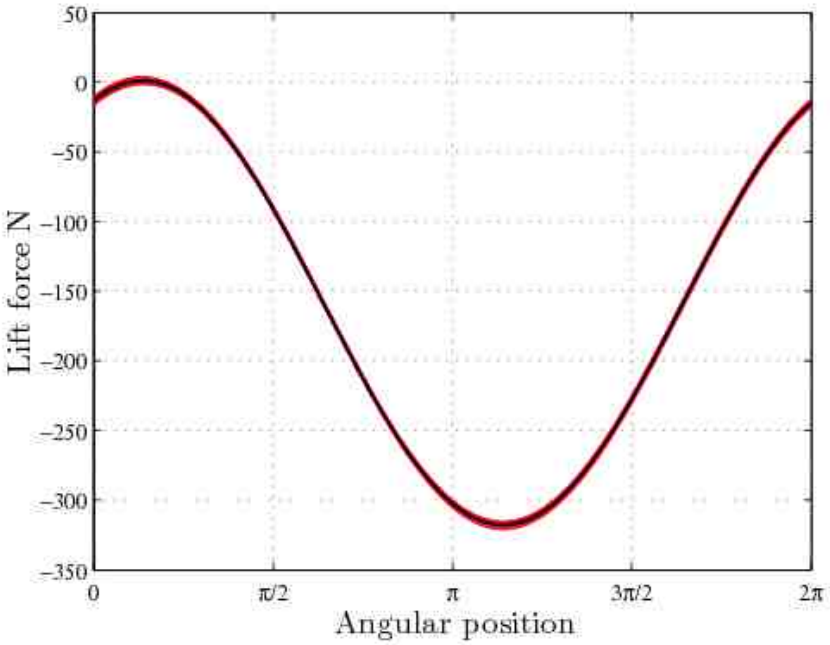

Figure 5.4: Ensemble of lift force cycles at suction peak 0.45b, 0.25c during 3Hz 0.08c oscillations. Red individual waves, blue 95% confidence bounds and black ensemble average.

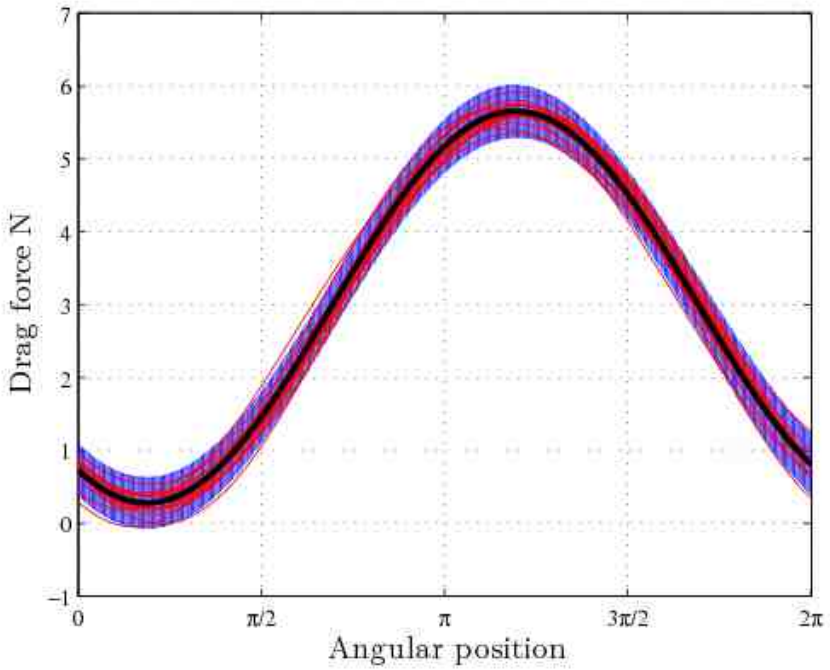

Figure 5.5: Ensemble of drag force cycles at suction peak 0.45b, 0.25c during 3Hz 0.08c oscillations. Red individual waves, blue 95% confidence bounds and black ensemble average.

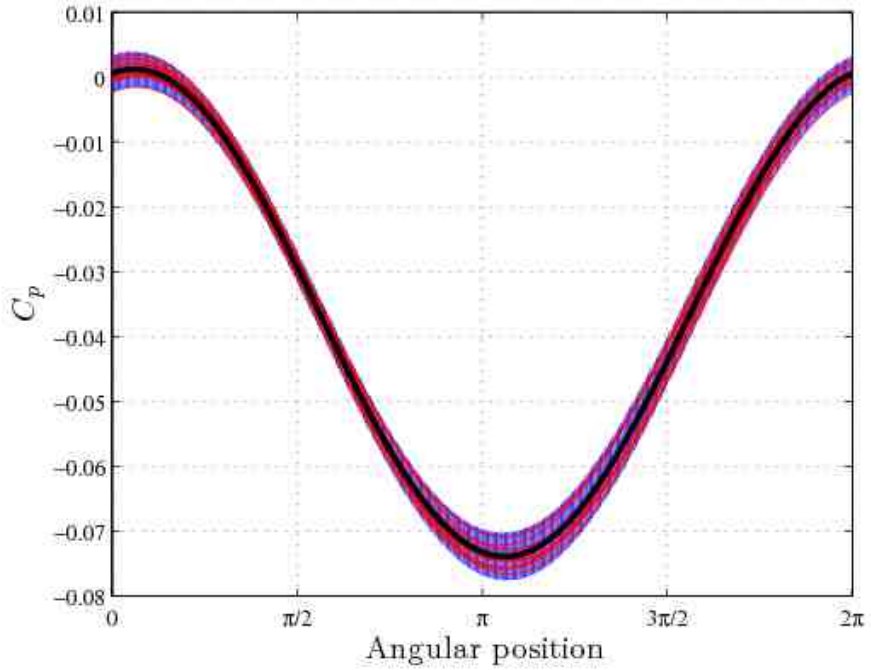

Figure 5.6: Ensemble of pressure cycles at suction peak 0.45b, 0.25c during 3Hz 0.08c oscillations. Red individual waves, blue 95% confidence bounds and black ensemble average.

lift, ±0.42 Newtons for drag and ±0.0013 Pascals for pressure measurements. These lower values can be attributed to the greater sample length of 107,200 from 10 seconds of data and having allowed the flow to have reached a steady state prior to acquiring data.

The total uncertainty U, is a combination of the systematic S, and random errors R, as defined in equation 5.8.

$$U = \sqrt{S^2 + R^2} \tag{5.8}$$

Applying the order of magnitude estimates, those below 1/5 of the largest can be considered negligible [91]. The total uncertainty of lift, drag and pressure measurements as force and coefficients are shown in table 5.1.

C_L	±4.74 N	±1.48%
C_D	±0.58 N	±10.7%
C_P	±4.67 Pascals	±6.36%

Table 5.1: Total Uncertainty

These levels of uncertainty, along with the resolution of sensors and measurement devices and in combination with the long and short term repeatabil-

ity of experiments, are more then sufficient accuracy for dynamic testing.

5.4 Chapter summary

This chapter introduced the approach adopted for signal conditioning, including the properties of measurements devices and filtering. The methodology of reduction of data and uncertainty of experimental measurements was detailed. Sources of bias and random errors have been highlighted and their treatment, where it was not possible to eradicate them, was minimised. This has fulfilled the last requirement of a dynamic system and allow dynamic testing to be performed.

Chapter 6

The Aerodynamic characteristics of the Static GAW(1)

To allow the investigation of any possible effect dynamic motion imparts upon the aerodynamic features of a wing in ground effect, a static test was first performed. This allowed the aerodynamic behaviour of the wing in ground effect to be characterised. Of particular interest was the variation with changes in ground proximity of lift and drag, the structure of edge vortices and the presence and extent of trailing edge separation. To achieve this the ground clearance was varied in a number steps from $h = 1c$ down to $h = 0.05c$. Lift and drag forces were measured along with surface pressures and surface flow visualisation was also performed. The effect of Reynolds number was also explored.

6.1 Experimental procedure

Experiments are conducted with the wing installed as outlined in chapter 4.Ground clearance is defined as the closest point of the wing to the ground as shown in figure 6.1. The 3.45° reference incidence of the wings rotated chordline and the endplates configuration can also be seen in figure 6.1. Testing was principally conducted at a wind and moving ground velocity of 40 ms^{-1} with a resultant Reynolds number based on chord length of 7.77×10^5. For the purpose of exploring Reynolds number affects, both wind and moving ground speeds were altered to match the required reduced test speed.Force and surface pressure data was measured simultaneously during each test. Each test consisted of a sweep through a range of ground clearances. A number of heights are repeated to determine the extent, if any, of drift during the test. A total of three tests were required to capture data for all pressure tapping con-

figurations. Surface flow visualisation was performed at a number of ground proximities. For these tests the pressure sensors are removed to avoid the possibility of contamination.

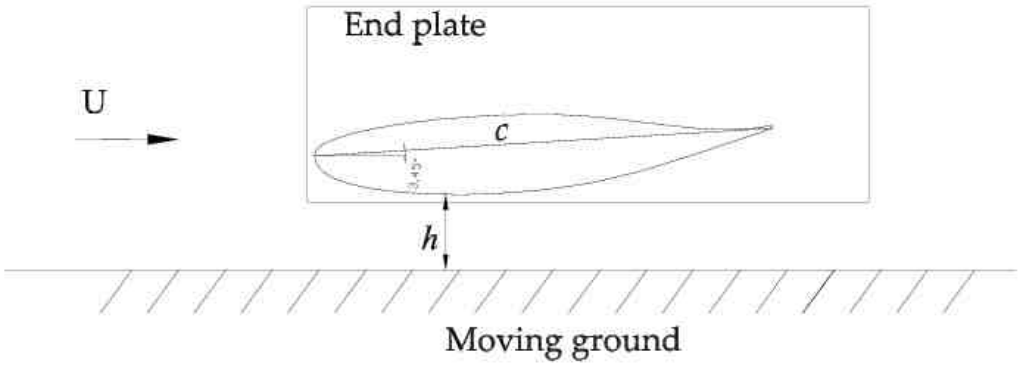

Figure 6.1: Wing schematic showing ground clearance definition

Data is processed as described in the preceding chapters. Results are presented in agreement with the Society of Automobile Engineers (SAE) convention of aerodynamic forces with lift being positive in the direction away from the ground and drag positive in the direction of the freestream. The aerodynamic force acting in the opposite direction of lift is termed downforce or negative lift.

6.2 Wing at $h = 1c$

Prior to exploring the behaviour of the wing in ground effect the general characteristics of the wing at a ground clearance of $h = 1c$ is established. The aerofoil section was designed for low speed, general light aircraft wings, detailed by research at NASA Langley[84]. A number of features were developed with the intention of improving performance over pre-existing wing designs. These include: a blunt nose to increase the peak negative pressure coefficient to delay stall, an increased trailing edge camber to develop a chordwise uniform load distribution and equal upper and lower surface profile at the trailing edge to delay stall. The stall mechanism is a gradual trailing edge type. The section performance achieved was a C_L of 0.4 at a cruising Reynolds number of 6×10^6, a peak C_L of 2 during climb and an efficiency of $L/D = 60$.

At the reference angle of attack,3.45°, ground clearance of $h/c = 1$ and Reynolds number of $\mathrm{Re} = 7.77 \times 10^5$, the inverted wing under test has a lift coefficient of $C_L = -0.651$, a drag coefficient of $C_D = 0.0217$ and efficiency of

$L/D = 30$. At a comparable incidence the findings of [84] are approximately $C_L = 0.92$ and $C_D = 0.013$,although at a greater Reynolds number, $2{\times}10^6$.This disparity can be attributed to the reduced aspect ratio. From finite wing theory we can expect the lift and drag to differ from the results of the aerofoil.

Along with the reduced aspect ratio the fitting of end plates also has a significant effect. The end plates increase lift by reducing downwash and increasing the effective wing span. Using the numerical analysis tool XFOIL[92] the equivalent aspect ratio of approximately 4.5 produces the lift coefficient under the conditions tested. The end plates have a more marked effect on drag. As they separate the high and low pressure regions on the pressure and suction surfaces of the wing, thus preventing flow from passing between the two. Downwash and hence induced drag are therefore reduced. The XFOIL generated equivalent aspect ratio is an order of magnitude higher at approximately 40. Although this finding is interesting it is not directly relevant to the research here as all tests are performed with end plates fitted and hence is not explored further.

Comparisons of numerical simulation section pressure coefficient profile and experimental results for wing at the reference incidence can be seen in figure 6.2.

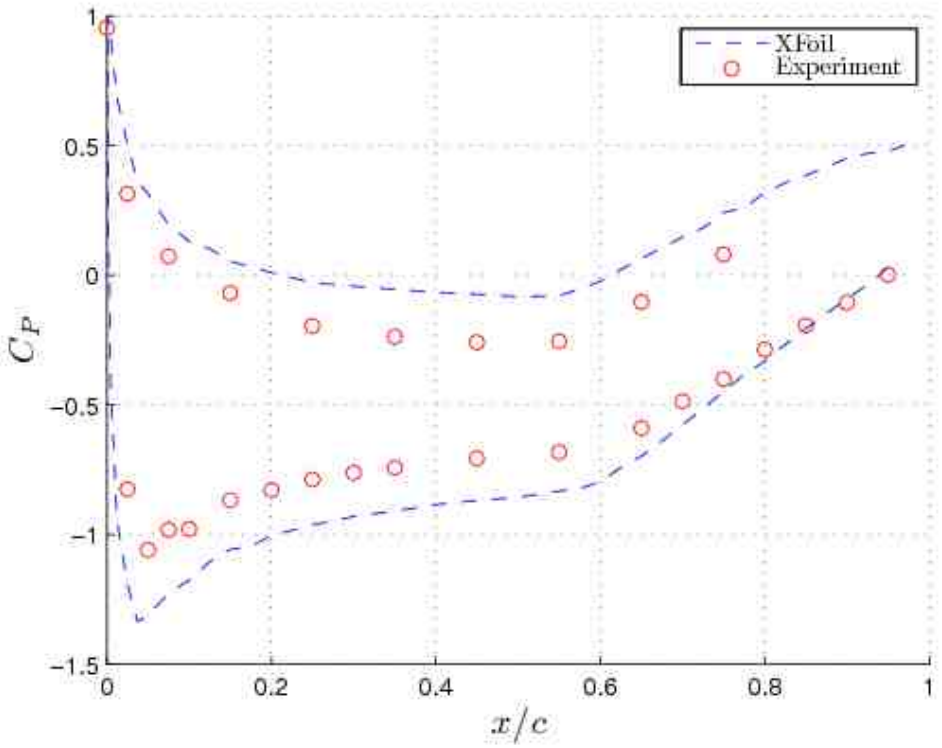

Figure 6.2: Comparison of numerical and experimental pressure profiles

Flow visualisation, detailed in the following sections, showed no separation and minimal spanwise flow and edge vortices on the suction side. On the pressure side a laminar separation bubble is present at the cusp toward the trailing. The initial NASA design study found trailing edge separation occurs from an angle of attack of approximately 8°. Only with incidence increasing to 20° did separation extending forward, to $x/c = 0.7$. The lack of significant end plate vortices was further determined by observing the behaviour of a wool tuft and the rear lower corner of the end plate, further reinforcing the effectiveness of the end plates.

In comparison to other research Knowles [93], employed the same wing profile during ground effect studies with large end plates and again with PIV experiments [94]. In the latter also with a low aspect ratio of 3. In that case no end plates were employed. Force data was not acquired so comparisons cannot be made. Soso [95] used a the GAW(1) wing with aspect ratio of 2.5 and end plates similar to those used in this research, to study interaction effects from upstream bluff bodies. The tests extended to a maximum ground clearance of $h/c = 0.833$. Here lift and drag was $C_L = 0.75$ and $C_D = 0.06$. The greater lift coefficient than this study can be attributed to the lower wing height, whilst the higher drag value is likely due to the lower aspect ratio.The general behaviour of the wing is in line with a finite wing in freestream with the additional influence of end plates. The wing therefore cannot be considered as being in ground effect at a ground proximity of $h/c = 1$.

6.3 Lift Behaviour with ground proximity

To determine the behaviour of the lift force with varying ground proximity data was acquired at a range of heights from $h = 1c$ to $h = 0.08c$. Results are shown in figure 6.3. It can be clearly seen that downforce increases with reducing ground clearance.

Three distinct regions were found in agreement with those found in Zerihan and Zhang[16] and Soso and Phillips [95]. Reducing ground clearance from $h = 1c$ to $h = 0.3c$ the increase is approximately 50%. This behaviour is termed the force enhancement region. The increase slows sharply at $h = 0.18c$, followed by a short region, the plateau, containing a hump with the peak in downforce at its midpoint at $h = 1.4c$. At its peak the wing has reached approximately twice the downforce generated at $1c$. At approximately $h/c = 0.1$ a significant reversal in the previous trend is found with downforce showing a sharp drop that continues down to the lowest ground clearance tested. This is the force reduction region.

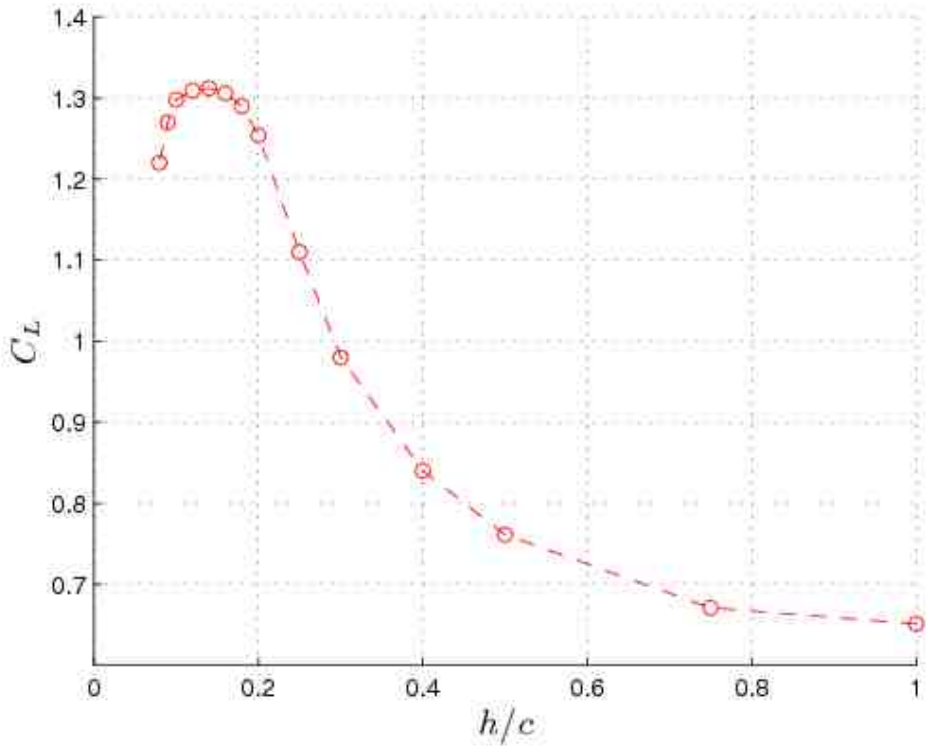

Figure 6.3: Lift coefficient variation with ground proximity.

6.4 Drag Behaviour with ground proximity

The relationship between drag and varying ground clearance is shown in figure 6.4. Drag is found to increase continuously with reducing ground clearance. The increase in drag can be seen to consist of two regions. Firstly a moderate increase is found from the highest ground clearance down to $h = 0.3c$. From this point the greater rate of increase is found and results in a maximum drag more than three times that at $h = 0.1c$. Both regions have shown an approximately linear variation of drag with ground proximity. The flow features leading to both the lift and drag variation with ground proximity will be determined with analysis of the surface pressure and flow visualisation data.

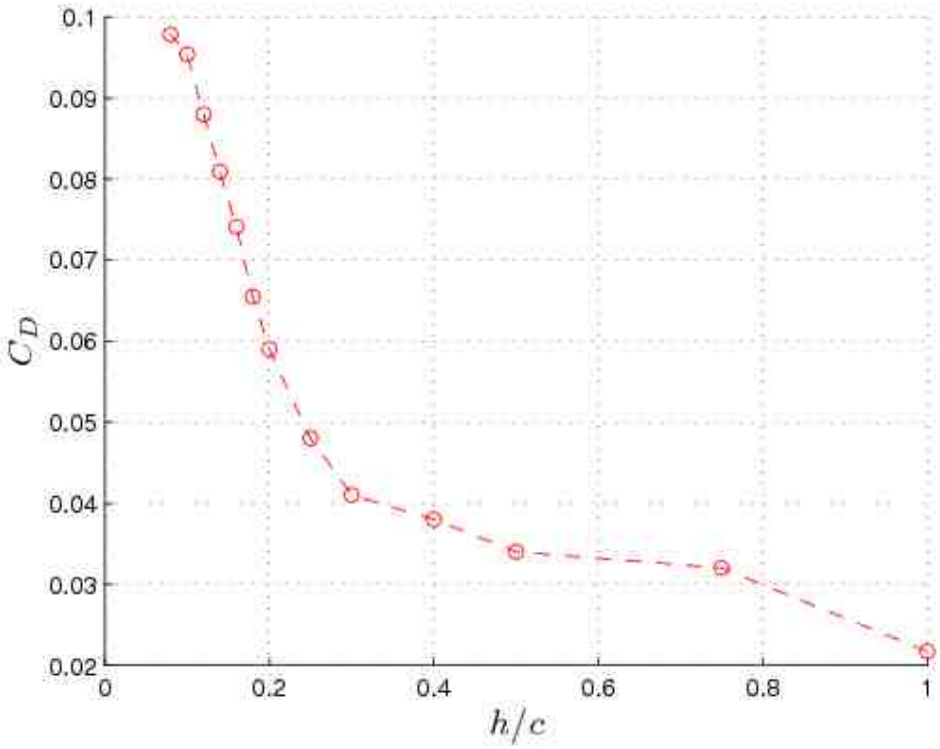

Figure 6.4: Drag coefficient variation with ground proximity.

The efficiency of the wing with varying ground proximity can be seen in figure 6.5. A sharp increase is drag is initially experienced as the wing is moved from $h/c = 1$ to 0.75 due to the minimal gain is lift. Throughout the force enhancement region to $h/c = 0.25$ a linear type relationship if found. A slight reduction in efficiency occurs at $h/c/ = 0.2$. Below this height, the plateau and force reduction regions, an inflection is found as lift reaches a maximum whilst drag continues to rise.

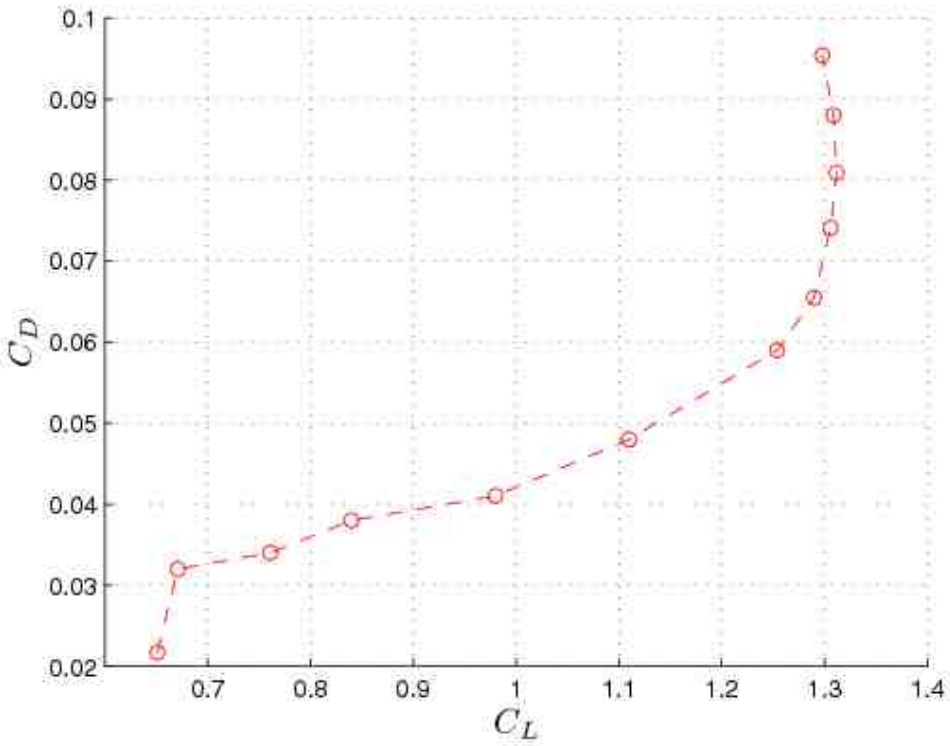

Figure 6.5: Drag polar variation with ground proximity.

6.5 Reynolds Number effects

To investigate the wings behaviour with Reynolds number, further tests were performed at 20 ms^{-1} and 30ms^{-1}. These results are compared with the static test at reference test velocity of 40 ms^{-1}. These results can be seen in figures 6.6 and 6.7. These velocities equate to Reynolds numbers of 3.88×10^5, $5.82 \times 10^5$and 7.77×10^5 respectively.

The effect that Reynolds number has upon lift is negligible in the force enhancement region. When the force enhancement region is reached, lift at the highest Reynolds number plateau is as previously described. However at the middle Reynolds number lift continues to increase.The plateau is formed at $h = 0.14c$. Here lift is 8% greater than the reference case. Following a short plateau, lift reduction commences at the same ground clearance,although the loss in downforce is far less severe, 1% compared to 6%.

At the lowest Reynolds number,again lift continues to increases further with reduced height, up to the highest maximum coefficient of the three Reynolds number test cases. A peak value is reached at 0.12 with lift having increased by 11%. Downforce reduces to a value that remains relatively stable down to the lowest ground proximity. The effect of decreasing Reynolds number results

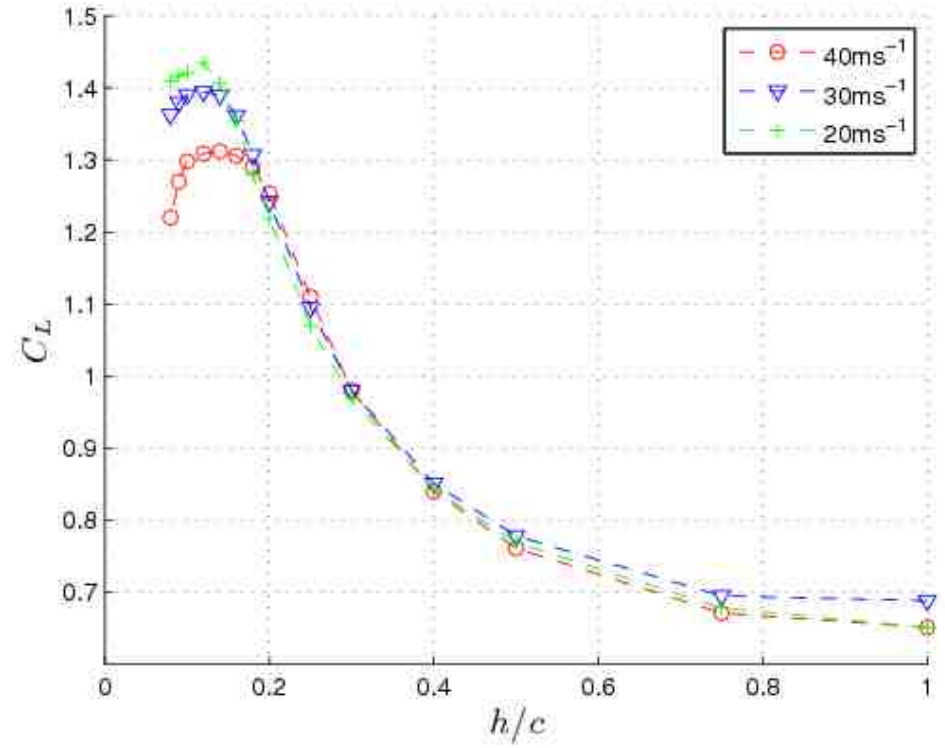

Figure 6.6: Lift coefficient variation with ground proximity.

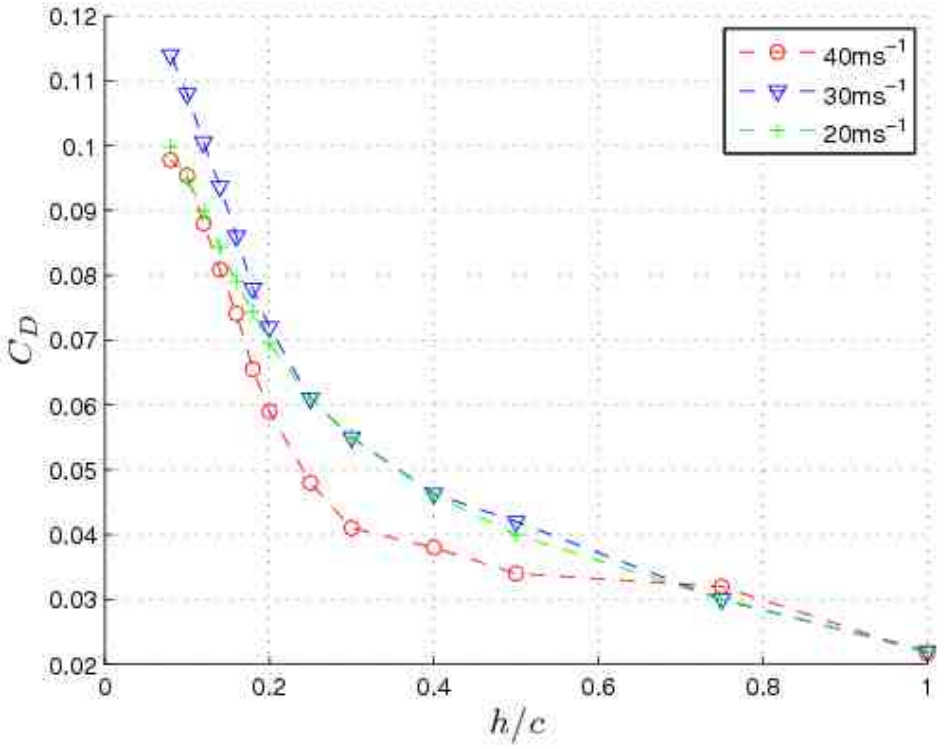

Figure 6.7: Drag coefficient variation with ground proximity.

is a shortening of the force plateau and a reduction in the severity of the force reduction.

The behaviour of drag with Reynolds Number is also to produce an increase above the reference case.As ground clearance is reduced, at the two lower Reynolds numbers the rate of increase in drag remain constant and drag is greater across the force enhancement region. This continues to the plateau where the gradient of lowest test velocity reduces and reaches a similar value as the highest Reynolds number. The middle test speed reaches a maximum drag value 17% greater.

The relationship between lift and drag over the range of ground proximities is shown in figure 6.8. The two lower test speeds have a near identical efficiency throughout the lift enhancement region. This is lower than the highest test speed. As the drag increase remains essentially linear for all Reynolds numbers from $h/c = 0.3$ to lowest height sharp upturn in drag polar is due to the wing reaching the plateau where lift no longer increases.

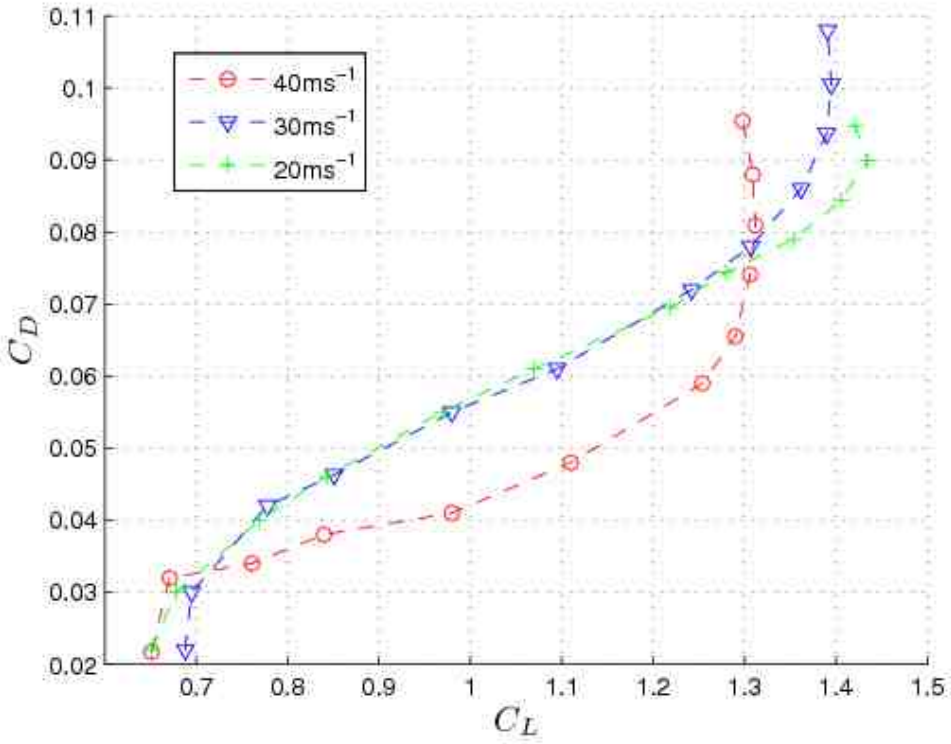

Figure 6.8: Lift Drag polar with variation of Reynolds number.

The behaviour of the wing with varying Reynolds number can be explained by the state of the boundary layer on the wing. At the reference test velocity the suction surface is entirely laminar. On the pressure side a laminar separation bubble is present at the cusp toward the trailing edge. As the ground

is approached suction is increased, which produces an adverse pressure gradient towards the rear of the wing. Upon encountering the adverse pressure gradient the laminar boundary layer may separate. A region of recirculating flow forms a bubble. Whilst separated, the laminar boundary layer undergoes transition to a turbulent boundary layer and reattaches to the wing at some point downstream.

The size and extent of the separation bubble depend on a number of properties of the wing and flow. With all other conditions fixed and only the Reynolds number altered the effect is to decrease the size of the bubble with increasing Reynolds number. The bubble has the effect of increasing the effective wing thickness, being the combination of the aerofoil profile and the boundary layer displacement thickness. This can have an effect on lift either beneficial or detrimental dependent upon the Reynolds number and aerofoil and flow characteristics. As a result of the thicker boundary layer drag is increased.

The effect this had upon this wing is that as the wing moves into ground effect, suction increased providing a sufficiently adverse pressure gradient to develop a laminar separation bubble. The separation bubble increases drag and augments the generation of downforce. The laminar separation bubble increases in size with reducing Reynolds number and is therefore the likely mechanism for the increase of drag and downforce with decreasing Reynolds number.

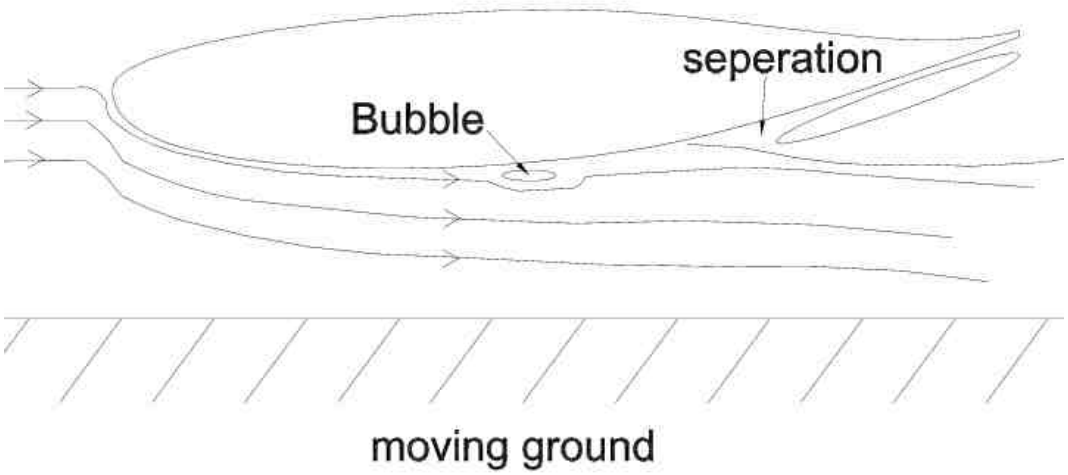

Figure 6.9: Schematic of suction surface flow

6.6 Surface pressure measurements

Surface pressure data provides an insight into the flow mechanisms behind the behaviour of ground effect. The surface pressures for the three spanwise and four chordwise rows of tappings can be seen in figures 6.10 to 6.13 for 7 ground clearances, varying from $h/c = 0.5$ to 0.06. The effect of ground proximity is best illustrated by the chordwise row nearest the wing centreline $z = 0.45b$ in figure 6.10. The first pressure tapping, on the very leading edge of the wing, provides insight in to the behaviour of the stagnation point. Away from the ground, at a h/c of 1 to 0.25, this point has a C_p of less than 1. As height is reduced this value increase to unity at $h/c = 0.14$. Below this height a significant reduction in pressure is found in the force reduction region, being 0.89 and 0.75 at $h/c = 0.08$ and 0.06 respectively.This indicates that the stagnation point moves around the blunt nosed leading edge with increasing ground proximity and that at the lowest force region the surface velocity about the nose has reduced significantly.

The pressure distribution at the largest ground clearance shown, $h/c = 0.5$, is analogous to the wing in a freestream flow. On the suction surface the static pressure rapidly decreases after the stagnation point near the leading edge to a minimum in the region of $x = 0.05c$. The pressure profile remains uniform across the remainder of the chord up to $x = 0.65c$ where a gradual recovery occurs. As the design intent the pressure at the trailing edge on the both wing surfaces is very similar. As the ground proximity is reduced, $h/c = 0.25$, suction increases across almost the entire chord, being approximately a 50% increase in pressure coefficient across the central section of the chord, $c = 0.2$ to 0.5. The profile has flattened, only after mid-chord does a gradual pressure rise occur, eventually leading to a single base pressure as the higher case. As the ground is further approached, $h/c = 0.18$, the initial flow acceleration about the leading edge is maintained, the most significant change is the increase in suction across the center section of the chord. The peak suction is now at $c = 0.3$ and is now approximately double that of $h/c = 0.5$. The pressure recovery now commences earlier, from $x = 0.55c$ to $x = 0.45c$. Trailing edge separation is evident, a region of constant pressure from $x = 0.75c$.

A further increase in ground proximity to $x = 0.75c$, at the center of the force plateau, finds a reduction in negative pressure about the nose leading on the suction surface from $x = 0.05c$ to $x = 0.1c$. The suction on the central section of the chord has continued to increase. However, this is at a lower rate, being a gain of %15. The sharp pressure recovery commences as the previous height and again trailing edge separation is found. This how now extended

upstream to $c = 0.7$.

At the lowest height, $h/c = 0.1$, defining the lower boundary of the force plateau and the onset of the reduction region. Here the loss of suction about the nose is exaggerated further. At $c = 0.025$ being only 1/3 of that at $h/c = 0.5$, 0.25 and 0.18. The suction peak has continued to develop, reaching approximately 2.5 the value off $h/c/ = 0.5$. The pressure recovery and separation locations are as the previous height.

Once into the force reduction region, the $x = 0.08c$ to $x = 0.06c$, the pressure profile continues to develop as that of the force plateau. The pressure about the nose continues to rise whilst the suction peak increases, reaching three times greater than that found at the highest presented case. The maximum negative pressure is found to have moved downstream to $c = 0.35$. Pressure recovery and trailing edge separation both occur at the previous chord point.

Along with the suction surface, the variation of pressure coefficient on the pressure surface can be seen in figure 6.10. At a $h/c = 0.5$ pressure reduces after the stagnation point as the flow accelerates over the nose. The acceleration continues over the pressure surface up to $z = 0.55c$. The peak in velocity and lowest pressure occur at $z = 0.35c$. After $z = 0.55c$. The wing profile begins its transition into a cusp. Here the flow is retarded by the geometric inclination, pressure rises reaching a maximum at the final pressure point at $z = 0.75c$. With increasing ground proximity surface pressures are seen to further reduce and is indicative of the increasing flow velocity over the pressure surface.

The general form of the pressure profile remains consistent with all ground clearances with the exception of the most forward point where negative pressure coefficient increases at a greater rate and supports the theory that the stagnation point moves toward the suction surface with decreasing height. The presence of the wing support is likely to have an effect on the pressure surface at the central row of tapping, by acting as a blockage and further accelerating the flow over the side.

The variation of surface pressure across the span of the wing can be seen in figures 6.11to 6.13. At $z = 0.25b$ the flow topology is as that of the $z = 0.45b$ row. The magnitude of the pressure reduction on both wing surfaces is lower. The first indication of trailing edge separation has also been delayed from $h/c = 0.25$ to 0.18. By comparison to the previous row the pressure surface has a more uniform profile, this is likely due to the interference effect described above.

Closer to the wing tip, $z = 0.1b$, again the general form is maintained but

at a lower magnitude. Now 25% less than that at $z = 0.4b$. Trailing edge separation occurred in the force reduction region only. Nearest the full span the movement of the stagnation point has been reduced, only occurring at the lowest height. The pressure surface experiences the same flow accelerations and decelerations over the cambered and cusped sections. On the suction surface the suction peak has markedly reduced and is only halved from $z = 0.45b$. The peak is also broader with the suction continuing to increase toward the rear of the wing, up to $x = 0.65c$. From here a gentle rise is experienced at tall heights with the exception of those in the reduction region which see a sharp rise at $x = 0.7c$ and$0.45c$. This section shows evidence of the influence from the edge vortex.

Surface pressures at spanwise rows, $x = 0.25c, 0.75c$ and $0.95c$ are shown in figures 6.14 to 6.16. At the quarter chord spanwise row the effect of the wings finite span can be seen as a considerable reduction in the suction from $z = 0.15b$ to the wing tip. The progressive increases in suction with increasing ground proximity is also clearly seen.

At $z = 0.75b$, at the highest ground clearance the flow is uniform across the entire span. A marginal decrease pressure coefficient is found at the tip. With reducing height two distinct features become evident. A distinct wavy profile is formed for all heights except the highest. The data does not make it clear what mechanism is leading to this wavy profile. It is however indication that a spanwise effect is present that varies with ground proximity. The second visible feature is the sudden reduction in pressure at the tip, outboard of $z = 0.2B$. This is the influence of the edge vortex. At the most outboard tapping pressure progressively reduces throughout the force enhancement region. A small variation is found across the plateau which is followed by an immediate loss in suction in the force reduction region to the point where the pressure coefficient is as $h/c = 0.5$. This point has minimal edge vortex indicating that in the force reduction region the edge vortex is no longer present.

At the furthest rearward row, $x = 0.95c$, the base pressure variation can also be seen. No evidence of the low pressure vortex interaction is found. The form of the waves is now much more aligned across all but the highest ground clearance. This is an indication of a spanwise flow feature that was explored with flow visualisation techniques.

The surface pressure analysis can be summarised as follows. At the reference height the wing exhibits a pressure profile in line with that of a wing freestream. With increasing ground proximity the suction peak reduces about the nose and is greatly increased at one third chord. The associated pressure recovery increases to the point where trailing edge separation occurs. This

constant pressure region is found to extend further upstream across the mid and quarter span rows as height is reduced. Strong edge effects are highlighted. Both reduction in suction due to the finite span and also the development and bursting of an edge vortex.

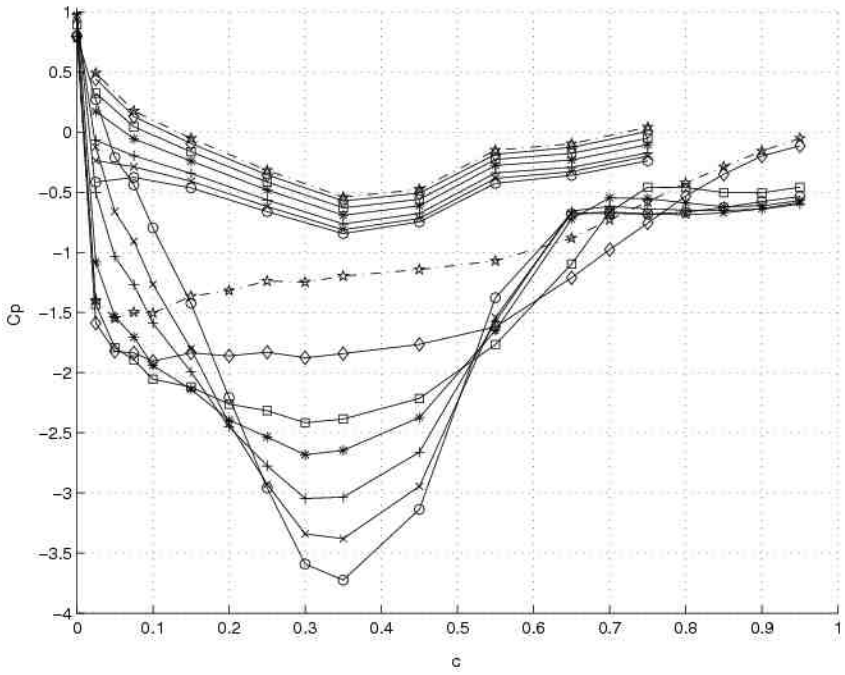

Figure 6.10: Chordwise surface pressure coefficient at 0.45b $-.-\bigstar 0.5c$ $-\Diamond 0.25c$ $-\Box 0.18c$ $-*0.14c$ $-+0.1c$ $-\times 0.08c$ $-\circ 0.06c$

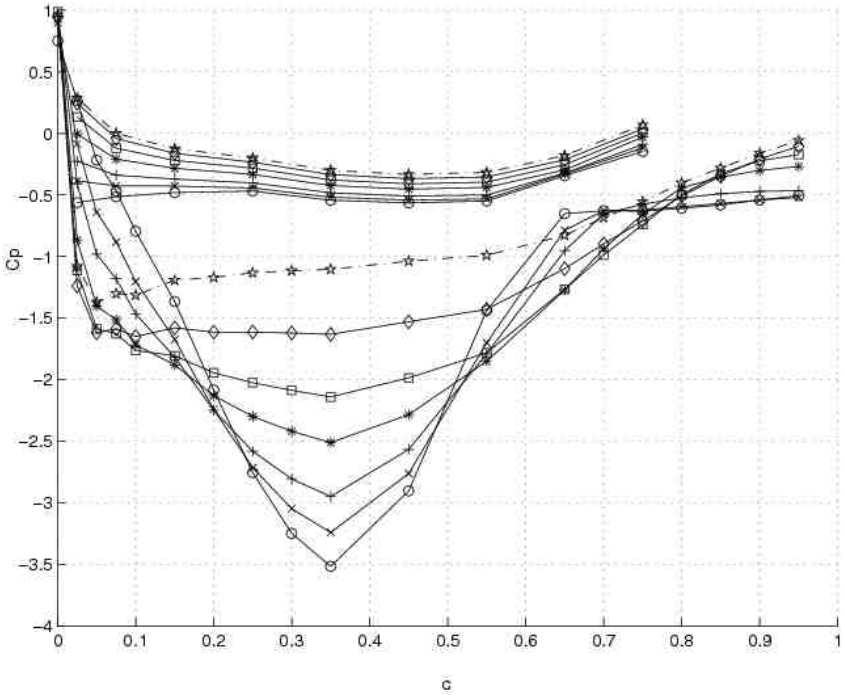

Figure 6.11: Chordwise surface pressure coefficient at 0.25b

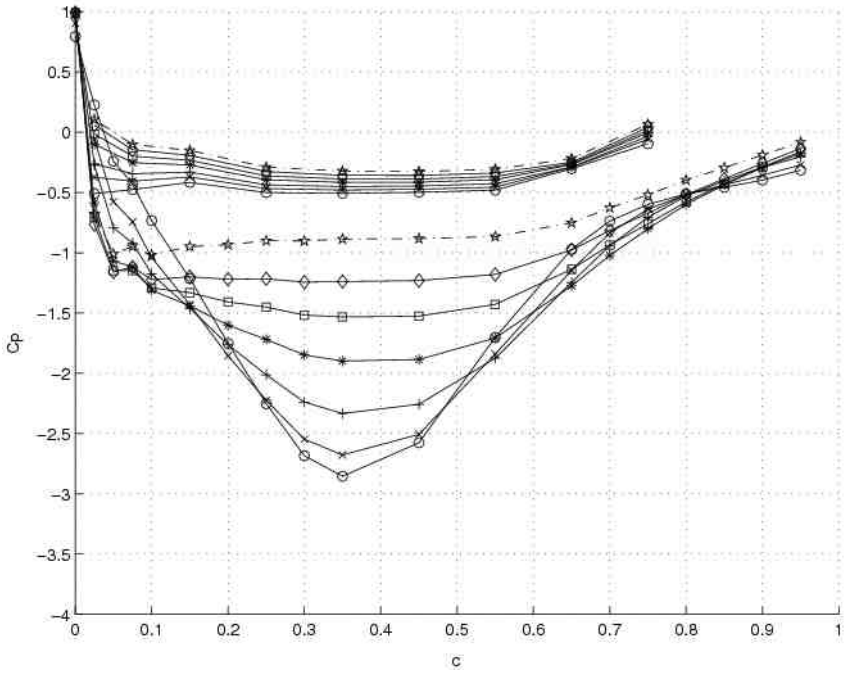

Figure 6.12: Chordwise surface pressure coefficient at 0.01b

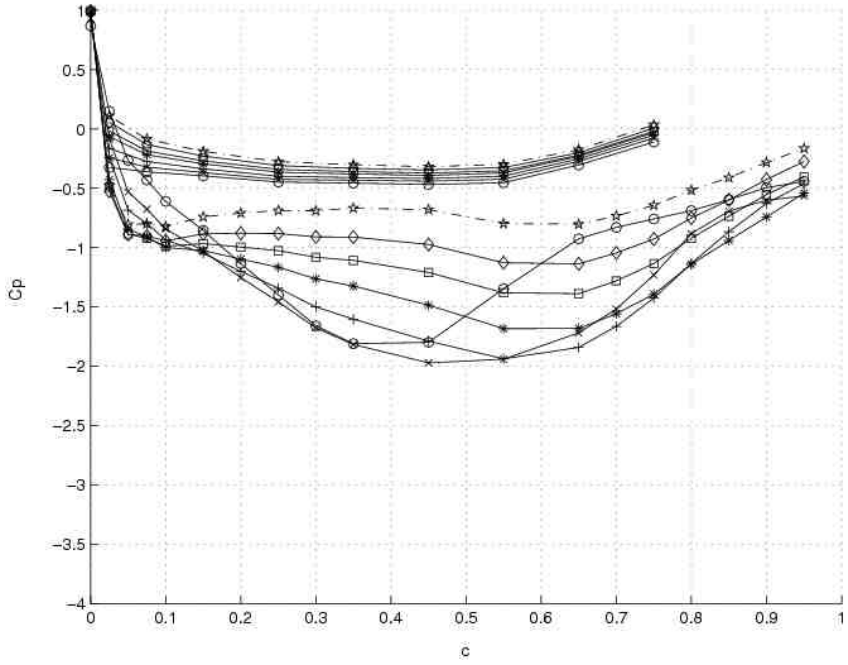

Figure 6.13: Chordwise surface pressure coefficient at 0.025b

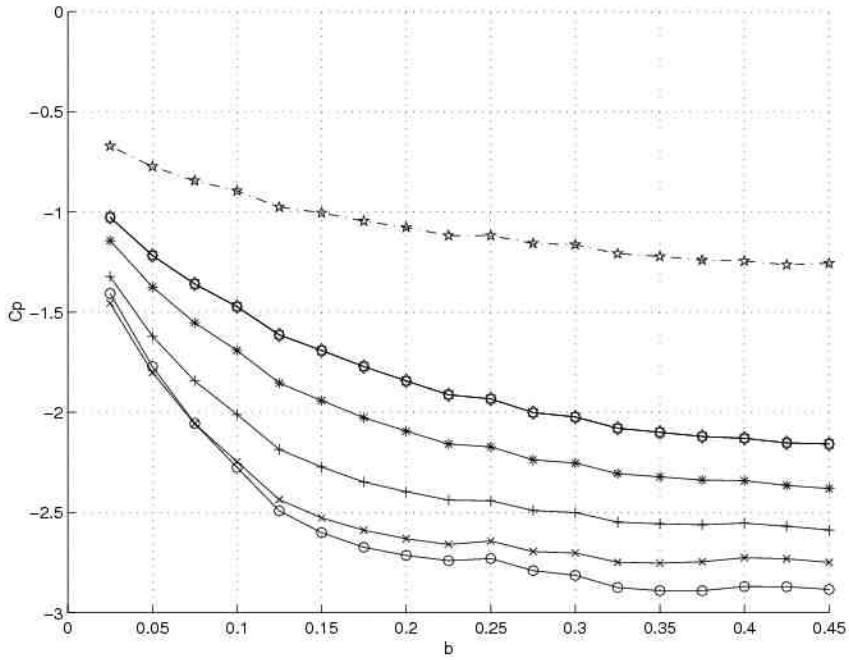

Figure 6.14: Spanwise surface pressure coefficient at 0.25c

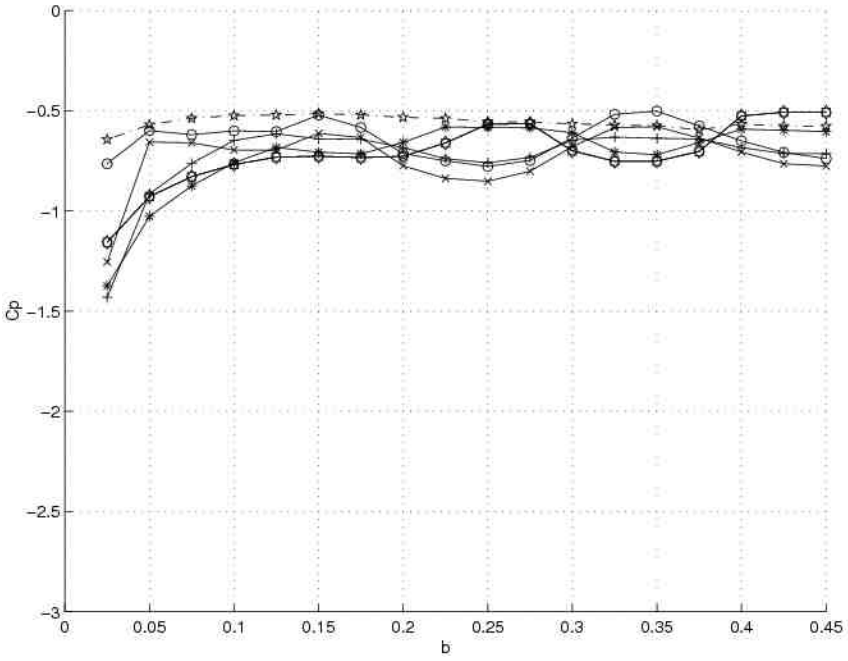

Figure 6.15: Spanwise surface pressure coefficient at 0.75c

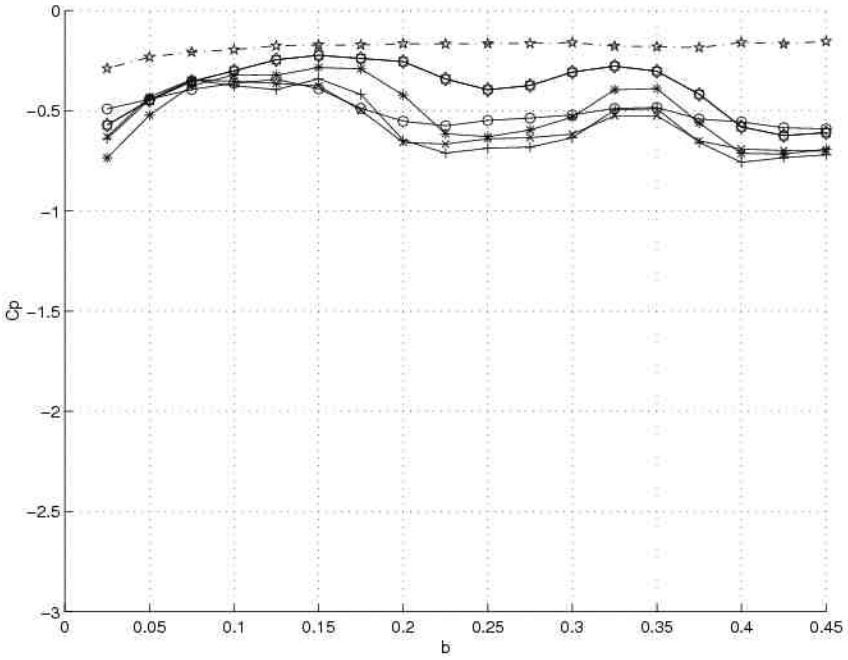

Figure 6.16: Spanwisewise surface pressure coefficient at 0.95c

6.7 Canonical Pressure

The Canonical pressure coefficient provides a good method for examining pressure recovery and separation. It is a scaling method that uses the point on the chord where pressure is at a minimum and the rise commences to normalise the pressure recovery profile and is defined as equation 6.1. Canonical pressures are examined for three ground clearances, $h/c = 0.5, 0.25$ and 0.06 at a spanwise location of $z = b/2$, figure 6.17. The highest has a freestream type pressure profile, having a suction peak immediately after leading edge, and a uniform pressure across the majority of the chord prior to a gradual rise toward the trailing edge. At $h/c = 0.25$ the wing is at the transition from freestream to full ground effect. The suction peak has shifted to $0.3c$ and is the height at which trailing edge separation is first observed at the semi-span.The maximum value of $\overline{C}_P$ =1 is one, this occurs at where the surface velocity is zero, i.e. the stagnation point. $\overline{C}_P$ =0 is the chord location where suction has peaked and pressure recovery begins.

$$\overline{C}_P = \frac{C_P - C_{Pmin}}{1 - C_{Pmin}} \tag{6.1}$$

At the highest ground clearance the pressure recovers over a greater extent of the chord at a lower rate up to $x/c = 0.55$. From here to the trailing edge the gradient in pressure recovery increases. A step recovery gradient is formed at a h/c of 0.25, with the point of greater suction having moved downstream, once the breadth of the suction peak is passed, also at $x/c = 0.55$. This appears to be the value beyond which increasing pressure recovery leads to trailing edge separation. This effect is amplified at the closest ground proximity where the extent of the separation and enlarged gradient are clearly visible. The Canaonical pressure coefficient is shown for the force plateau and reduction regions in figure 6.19. Canonical pressures have highlighted the mechanism of separation as being the magnitude of the pressure recovery resulting from the magnitude of the suction peak, the chord location of the peak and the resultant distance over which to recovery all contributing to the severity of the adverse pressure gradient and hence trailing edge separation.The pressure coefficient figure for the three heights are repeated here for clarity 6.18.

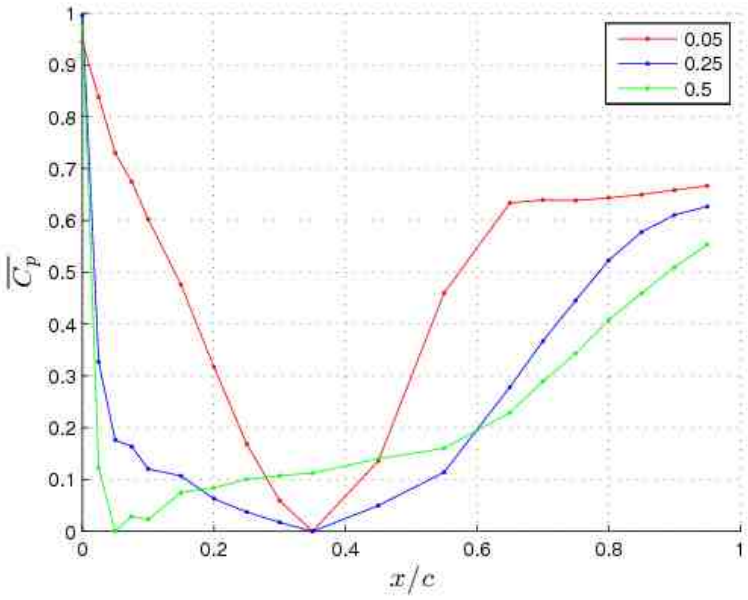

Figure 6.17: Canonical pressure coefficient along chord at 0.25b for ground clearances h/c of 0.005, 0.14 and 0.5

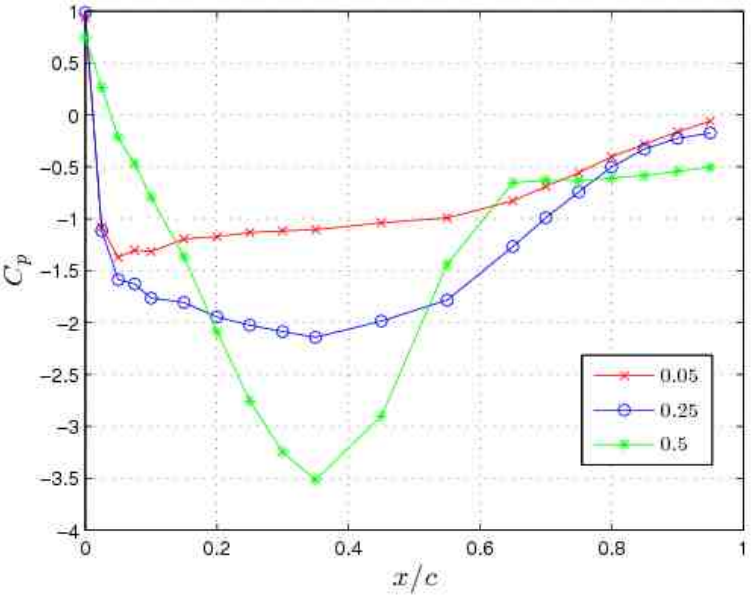

Figure 6.18: Surface pressure coefficient at 0.25b for ground clearances h/c of 0.005, 0.14 and 0.5

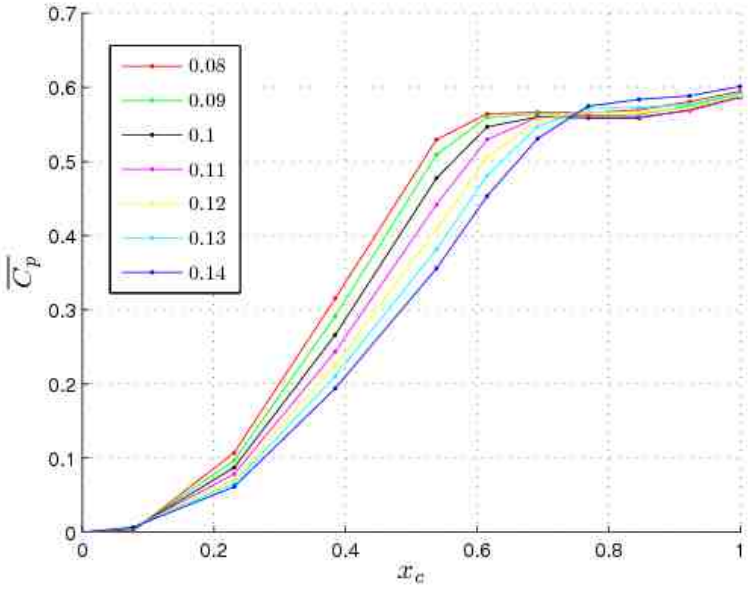

Figure 6.19: Canonical pressure coefficient at 0.45b for ground clearances h/c of 0.08 to 0.14

6.8 Flow Visualisation

Flow visualisation provides a means of illuminating the flow on the surface and in the domain of its influence. It offers the potential to provide considerable insight into flow features, including boundary layer transition, separation and unsteadiness, and is therefore an invaluable tool for experimental aerodynamics. Oil, a mixture of paraffin and titanium dioxide, is applied to the wing surface with a brush. Care is taken to ensure an even distribution and consistency of mixture. An uneven mixture can artificially induce transition and separation [95] [16]. The wind tunnel is brought up to speed as quickly as possible and maintained at the test ground clearance until the fluid has dried. Flow visualisation tests were performed at $h/c = 1, 0.25, 0.25, 0.1$ and 0.8.

At the reference height of $h = 1c$ a uniform flow exists across the entire suction surface with the exception of two regions of undried fluid at the trailing edge. The first of these was caused by a disturbance on the leading edge, the second was attributed to a combination excess fluid and premature completion of the test. As the ride height tested was the first of the series, the wing was cleared of imperfections and test run time was extended for subsequent flow visualisation tests.

A small region at the wing end is seen to exhibit a spanwise effect. The flow pattern shows a pathline commencing at the leading edge and progressively moving inboard to approximately $z = 0.05b$. On the pressure surface the flow is aligned with the freestream. However, it is not uniform, a separation bubble can be clearly seen in picture 6.20. There attachment line remains consistent at approximately $x = 0.7c$. However, separation and hence width of the bubble varies with the span, being 18c from mid-span to $z = 0.25b$.

The presence of the flow visualisation fluid within the bubble is likely to have had an effect of exaggerating the height of the bubble leading to its increasing width. Pressure distributions across the pressure surface have shown little variation spanwise so no flow mechanism heading to the increased bubble would be expected across the central span area. By monitoring the drying process, regions of turbulent flow could be identified [74]. The region after reattachment dried faster than that immediately prior to that ahead of the bubble indicating the boundary layer had indeed transitioned to turbulent during separation.

At the lower height of $h/c = 0.25$, where surface pressure data showed initial signs of trailing edge separation, the flow is no longer uniform across the suction surface. The spanwise flow at the outboard extremities of the wing has turned outboard toward the end plate over the last 1/4 of the chord. This

is the increasing effect of the edge vortices at the wing tip endplate junction. The highly three-dimensional nature of the vortex produces a distinct spanwise pattern that broadens as the vortex develops along the length of the chord.

A much greater effect has occurred inboard. At 7 points across the wing the formation of separation bubbles can be seen. The flow visualisation fluid has thickened for approximately $0.1c$ and is followed by a short region of flow that has turned to a right angle to the upstream flow. These occur across the central half of the span at approximately $x = 0.45c$. At the trailing edge separation is present with flow reversal pattern extending upstream to $x = 0.85c$; again, these occur across the central half of the chord. There is a clear relationship between the separation bubbles and trailing edge separation. The points of separation, 6 in total, are directly downstream of the gaps between the forming bubbles.

With a further small reduction in the ground proximity to $h/c = 0.2$, now within the regions of heights with trailing edge flow separation. The flow structure has remained consistent with the previous height. The outboard spanwise flow has continued to grow to a small extent, as has the extent of the trailing edge separated flow features. Their width has grown to the point where they are in contact with their neighbouring feature at the trailing edge. At mid-span the developing bubble has a clear area without flow visualisation fluid, indicating separation has now occurred. It proved difficult to ascertain if the bubbles had consistently changed across the span due to the irregular pattern they formed. On the pressure surface the flow was found to be relatively unchanged from that at $h/c = 1$.

A further increase in ground proximity to $h/c = 0.1$, on the boundary of the force plateau and force reduction regions. Spanwise flow has not encroached further inboard, however the flow on the outboard side is now turned through a greater angle toward the end plate. This effect has migrated further forward to approximately $x = 0.6c$. Separation bubbles have increased across the span, now covering 80%. These bubbles exhibit much clearer definition in form. Along with a wide central bubble, on the left side,bubbles have coalesced to form a single bubble. On the right hand side they remain as four separate bubbles with uneven width and spacing.The trailing edge separation has developed into a spanwise cellular pattern. 4 mushroom like features can be clearly seen in figure 6.25. These features are stall cells [96], each is formed by two counter-rotating vortices that, over time, produce the 'owl face' pattern. Only the wing tip, under the influence of the edge vortex, remaining attached. The separated region has now extended forward to approximately $z = 0.65c$.

The lowest height tested with flow visualisation was $h/c = 0.08$ figure 6.28.

Here, the edge vortex effect has an additional component of flow turned inboard at an angle of 45° across the rear quarter of the chord. The separation bubbles have developed further, increasing in width on the right hand side although gaps still exist. At the trailing edge the separation region have extended further forward to $z = 0.6c$. The third cell has lost its previous form and now contains only reversed flow from the trailing edge. Again on the pressure surface the flow was found to be relatively unchanged from that at $h/c = 1$.

The flow visualisation study has identified a number of key flow features and their behaviour with varying ground proximity. Principally these are: the size and extent of the edge vortex, to be discussed in the following section 6.9, the development of separation bubbles on the suction n surface and most crucially, the nature of trailing edge separation.

Of these the presence of stall cells provides the greatest potential insight into the underlying flow physics. This has implications for the wing undergoing dynamic motion. The formation of these vortex pairs provides evidence of large scale three-dimensional flow across the span of the wing. These structures, although present throughout the range of heights of interest for the dynamic study, produce a consistent form during steady state are none the less highly unsteady.

The time averaged analysis employed so far has identified their presence, despite potential fluctuations in pressure the mean pressure has been found to be essentially constant [96]. In that research a dynamic behaviour within the cells described as 'jostling', fluctuations varying from slight to vigorous, was only discovered with the use of a high response measurement technique.

The stall cells are initial formed downstream of gaps between developing bubbles. This indicates that the laminar boundary layer, having not undergone transition via the bubble, is separating prior to the trailing edge. From the pressure data it is known that with increasing ground proximity the pressure gradient increases markedly. It can therefore be deduced that the mechanism driving separation is that of a laminar boundary layer in a strong adverse pressure gradient experiencing trailing edge separation. This exists across the range of heights experiencing separation, $h/c = 0.25$ to 0.08. Only within the force reduction region did the presence of a wide transition bubble prevent the development of vortices and hence the stall cell. This only occurred at one location.

Photographs are shown in figures 6.20 to 6.28.

Figure 6.20: Surface flow visualisation at h/c=1. Pressure surface viewed with leading edge at the bottom of the image.

Figure 6.21: Surface flow visualisation at h/c=1. Suction surface viewed with leading edge at the bottom of the image.

Figure 6.22: Surface flow visualisation h/c=0.25.Suction surface viewed with leading edge at the bottom of the image.

Figure 6.23: surface flow visualisation h/c=0.25. Mid-span suction surface viewed with leading edge at the bottom of the image.

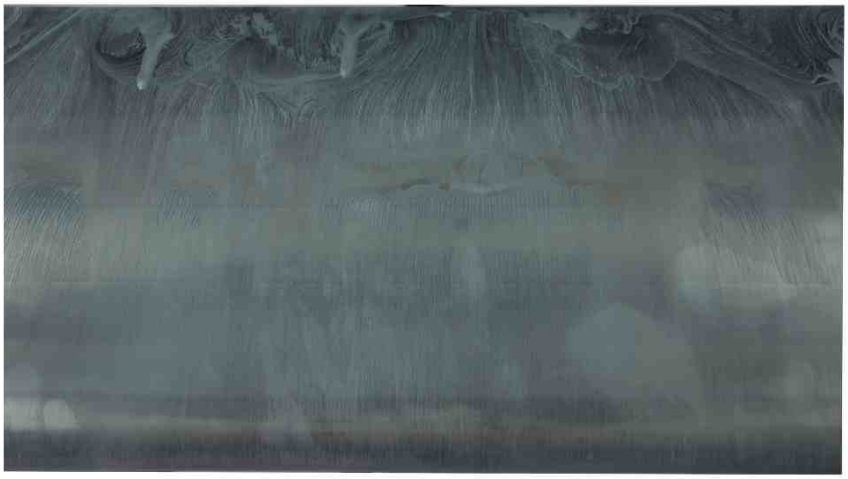

Figure 6.24: surface flow visualisation h/c=0.2.Mid-span suction surface viewed with leading edge at the bottom of the image.

Figure 6.25: surface flow visualisation h/c=0.1.Suction surface viewed with leading edge at the bottom of the image.

Figure 6.26: surface flow visualisation h/c=0.1.Mid-span suction surface viewed with leading edge at the bottom of the image.

Figure 6.27: surface flow visualisation h/c=0.08. Righthand suction surface viewed with leading edge at the bottom of the image.

Figure 6.28: surface flow visualisation h/c=0.08. Suction surface viewed with leading edge at the bottom of the image.

6.9 Edge Vortex

The presence of the edge vortex has been identified with both surface pressure and flow visualisation data. It is created by the pressure difference across the end plates. The higher pressure flow on the outboard side of the plate is drawn beneath the end plate forming a separated shear layer that 'rolls up' in to the vortex. This remains attached to the inboard side of the end plate and the wing suction surface. Figure 6.29 shows an illustration of its expansion downstream from the wing.

The edge vortex has a positive effect in that it provides induced suction that augments downforce. This gives an indication that the peak in vorticity is linked to the highest gradient in the downforce enhancement curve. The vortex also induces upwash that increases toward the wing tip figure 6.30. This leads to a reduction in local angle of attack and in turn is likely to delay separation. The edge vortex effect is not solely positive. The increased suction comes with a drag penalty. The increase in gradient of drag with ground proximity can be attributed to the vortices induced drag. This coincides with the highest downforce increase gradient. At heights below this, the vortex begins to diffuse, evident in the pressure and flow visualisation data, being larger with reduced vortices.

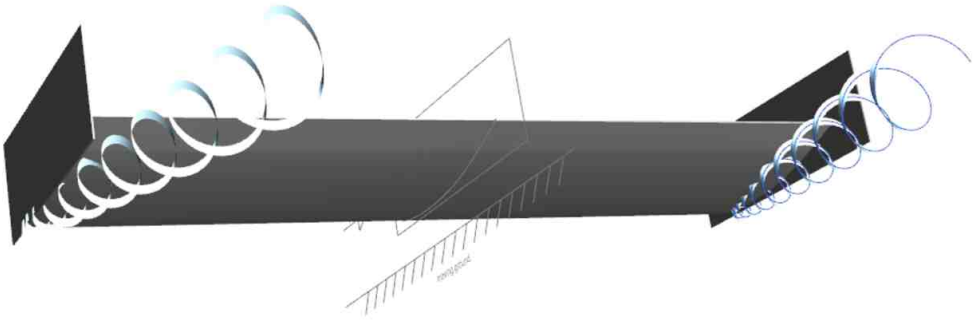

Figure 6.29: Schematic of edge vortex

The surface oil flow visualisation study cleared showed the highly three-dimensional nature of the vortex produces a distinct spanwise pattern that broadens as the vortex develops along the length of the chord. Its increasing magnitude is clearly visible throughout the photographs as ride height reduces. In addition to this method surface flow visualisation was performed using wool tufts. These were placed at the lower rearmost corners of the endplates making the edge vortex behaviour evident. It was found that the edge vortices

grew in size with increasing ground proximity until fully formed in the force enhancement region until their subsequent complete breakdown at h/c = 0.07 in the force reduction region.

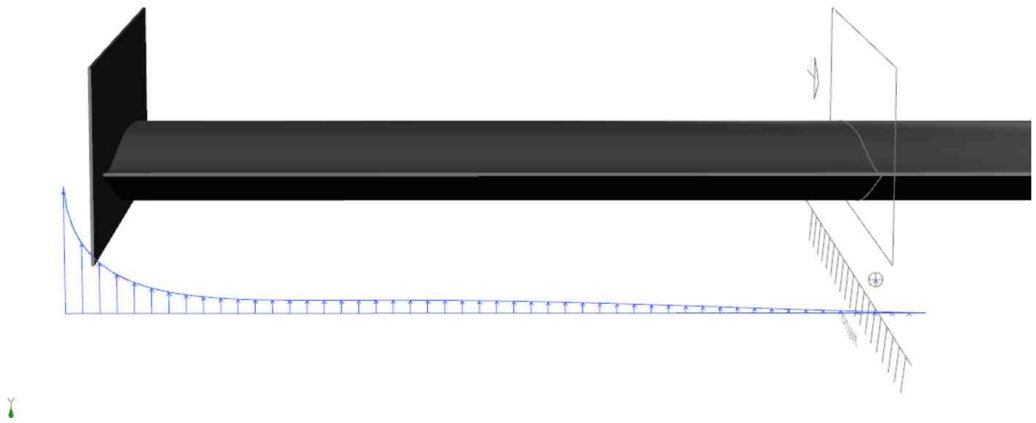

Figure 6.30: Schematic of upwash

The mechanism of breakdown is not clear in this case. An alternative method of flow visualisation such as PIV would be required to ascertain this. The increase in size and movement inboard at the lower heights indicate diffusion may be linked to the high mid-span suction and strong adverse pressure gradient. As the vortex breaks down this effect is reduced, leading to an increase in separation across the wing.

6.10 Summary of Static Testing

The static test was performed in order to determine the wings aerodynamic characteristics and provide a comparison for dynamic results. Away from the ground, at $h/c = 1$ the wing can be considered to have minimal effect from the ground. As ground proximity increases the flow is constrained between the wing and the ground. This produces a significant increase in the suction with the suction peak shifting rearwards to 1/3 chord. The increased suction increased downforce significantly. Drag is also increased. The development of edge vortices further increases downforce, however they also develop an increase in the drag gradient. The spanwise intermittent formation of separation bubbles and trailing edge separation occur at $h/c = 0.25$.

As ground clearance reduces, trailing edge separation extends across the span and further upstream as a results of the strengthening adverse pressure gradient. Suction continues to increase, however this is balanced by the increased separation and diffusion of the edge vortices and a downforce plateau is formed. As height reduces a sharp loss in downforce occurs as the edge vortices burst and separation extends over a large portion of the wing.

The characterisation of the wing was successful in identifying strong three-dimensional features; edge vortices, separation bubbles and stall cells, each of this can be considered potentially unsteady even during time averaged experiments. Their subsequent behaviour during dynamic testing is the motivation of this research. Having established the static aerodynamic behaviour of the wing an investigation onto the transient aerodynamics effects can be undertaken.

Chapter 7

Future Work and Conclusion

7.1 Conclusion

The principal goal of the research programme was to investigate transient aerodynamic effects of a wing in ground effect. In order to achieve this it was first necessary to develop novel apparatus and methodology. A data acquisition and motion system was required for the oscillating wing investigation. However to develop the capability to perform future investigations with scale car models it was necessary to consider the performance of the wind tunnel. The research was therefore formed of two distinct but related branches. Firstly the development of an improved wind speed control system at the R.J. Mitchell Wind Tunnel. Secondly a dynamic testing system.

Gaining the necessary knowledge to develop an improved controller was achieved with suitable stimuli during a system identification exercise. Once acquired the results were used to develop a model of the tunnel performance. The key finding during this stage was the non-linearity of the relationship between command signal, fan and wind speed. Gain scheduling was adopted as a suitable method to deal with this non-linearity. A family of controllers was developed that, when accessed with simulation tools achieved the desired performance.

The implementation of the controller system, although troublesome and demanding in terms of safety, proved to have little impact on the desired controllers performance. Overall results were found to agree with their modelled counterparts. The wind tunnel performance was greatly improved. Settling time, steady state error and disturbance rejection were all significantly improved providing gains in both cost and performance.

The dynamic testing system was developed in two parallel work streams. The first concentrated on the creation of data acquisition and motion system whilst the second established the experimental apparatus and procedures.

With a motor system correctly specified and tuned a motion strategy was developed that allowed the desired motion trajectories to be accurately followed. A data acquisition system was created that incorporated the motion controller to provide synchronised position, pressure and force measurements.

Measuring forces during dynamic testing was identified at the outset of this research as a challenging task. The development of this capability focused on determining the dynamic response of the force balance. As this represented a significantly demanding undertaking the unsteady pressure measurement system was established first. A method was developed that extended the performance of a multichannel pressure sensor that allowed a sample rate only previously possible with individual high response transducers. As with the tunnel controller, system identification was employed with an appropriate stimulus. The system was evaluated in the laboratory and when installed in the model. This allowed a transfer function to be developed that compensated for the transmission characteristics of the pressure measurement system. With the knowledge and confidence gained during the unsteady pressure system development the dynamic response of the force measurement system was then tackled.

This represented the most critical part of the research. As such a great deal of effort and time was concentrated on this task. Several approaches were trialled before a method was employed that provided the necessary stimulus and response. Much of the difficulty with satisfying this requirement was in producing and most crucially measuring small amplitude and low frequency stimuli and response.

During the various investigations a number of factors were determined; principal amongst them was establishing the frequency response of the force balance. Crucially its limits lay beyond that of the aerodynamic investigation. This was critical to the success of the experimental investigation. When completed these two streams were combined to provide the necessary dynamic testing system. Finally a method of isolating the transient aerodynamic measurements was developed.

A post processing routine was created that following data gathering produced an ensemble average of the oscillating data set. Experiments were performed with the wind on and repeated with the wind off. The later was subtracted to provide the desired transient data. It was vital to assess the effectiveness of this complete system, as such the uncertainty of the data was determined.

In establishing the system provided all the necessary components of dynamic testing system it was possible to proceed with the experimental investi-

gation. Much of the work undertaken during the research was underpinned by an advanced level of understanding of the National Instruments family of hardware and software products acquired throughout the duration of the project and from professional training. This reflects the applied nature of the research and was necessary to deliver operational systems that satisfied the academic and commercial requirements of the R.J. Mitchell Wind Tunnel.

With the dynamic system complete an experimental investigation was conducted. It sought to identify the differences between static and transient wing in ground effect aerodynamics. The features of a static wing in ground were first established. Distinguishing features included significant trailing edge separation, strong edge vortices. The behaviour with increasing ground proximity can be characterised as force enhancement prior to reaching a plateau and finally significant reduction. To gain an insight into this complex flowfield tests were conducted with the aim of isolated individual features. Tests were performed out of ground effect at varying amplitudes, frequencies and ground proximities. Major differences were found between static and dynamic testing results. When motions were performed out of ground effect a gain in downforce found during the upstroke and a loss during the downstroke. This was attributed to changes in the effective angle of attack. Oscillations across the force enhancement region also prodcued a gain in downforce during the upstroke and a loss during the downstroke. This is due to an increase in flow beneath the wing at the end of the downstroke that is mainted throughout the upstroke. When performed across the force plateau a stark change occurred. This was attributed to strong three-dimensional effects reducing the flow beneath the wing and significant hysteresis being experienced and downforce was lost during the entire motion.

In conclusion the research was successful in developing the necessary techniques and technology to perform an experimental investigation into transient ground effect aerodynamics. The relationship between force behaviour and motion parameters for a range of mean heights, frequencies and amplitudes was established.

7.2 Future Work

This research programme was successful in developing the dynamic testing capability and performing an exploratory investigation. A full investigation in to transient ground effect aerodynamic was beyond the scope of this project. The primary recommendation for future work is a full investigation into the underlying flow physics of a transient wing in ground effect. As part of the

dynamic testing system a number of capabilities were developed that offer the potential for further in-depth investigations.

A lever mechanism was manufactured that connected the wing mounting point to the rear strut and allowed the wing to be pitched, either independently or in conjunction with heave. This allows an investigation of pitching and combined pitch and heave. The PIV system was synchronised with motion system allowing investigations into off surface features, in particular the edge vortex and wake. The full capability of the unsteady pressure transducer system can also be exploited allowing the spectral components of pressure measurements to be analysed. The data acquisition system also has the potential to accommodate additional instrumentation. Surface hot film was identified as a potential method of investigating the behaviour of the boundary layer during dynamic motions and a compatible data acquisition device was determined. As test were conducted transition free, it is suggested that leading edge roughness is applied to fix transition. This will provide greater insight into the role of laminar seperation and allow corrolation with potential CFD studies.

Although not presented in the thesis an in-model and overhead motion system was also developed for research into yawing rally car aerodynamics. This system has the potential to provide motion to other vehicle types.

With the dynamic motion of a scale model vehicle comes the potential of sever blockage variation. A possible enhancement of the control system would be a predictive controller linked to the motion system to counter the varying blockage.

Bibliography

[1] A. Lock. *Unsteady Aerodynamics - Its Simulation, Measurement and Effect on the Driver*, chapter 7, pages 89–106.

[2] T. Lee and P. Gerontakos. Investigation of flow over an oscillating airfoil. *Journal of Fluid Mechanics*, v 512:p 313–341, Aug 10 2004.

[3] R. M. Hall, S. H. Woodson, and J. R. Chambers. Overview of the abrupt wing stall program. *Progress in Aerospace Sciences*, 40(7):417 – 452, 2004.

[4] N. Lindener and G. Wickern. The audi aeroacoustic wind tunnel: Final design and first operational experience. *SAE*, (Technical Paper 2000-01-0868), 2000.

[5] W.H. Hucho. *Aerodynamics of Road Vehicles*. SAE International, 1998.

[6] P. Wright. *Formula 1 technology*. Society of Automotive Engineers, 2001. ISBN 9780768002348.

[7] W.F. Milliken and D.L. Milliken. *Race car vehicle dynamics*. Society of Automotive Engineers, 195.

[8] A. Chadwick, K. P. Garry, and J. Howell. Transient aerodynamic characteristics of simple vehicle shapes by the measurement of surface pressures. *SAE*, (2001-01-0876), March 2000.

[9] C. Noger, C. Regardin, and E. Szechenyi. Investigation of the transient aerodynamic phenomena associated with passing manoeuvres. *Journal of Fluids and Structures*, v 21(n 3):p 231–241, November 2005.

[10] A. F. Abdel-Azim. An experimental study of the aerodynamic interference between road vehicles. *SAE*, (940422), March 1994.

[11] L. Tsuei and O. Savas. Transient aerodynamics of vehicle platoons during in-line oscillations. *Journal of Wind Engineering and Industrial Aerodynamics*, v 89(n 13):p 1085–1111, October 2001.

[12] J. Michael Summa. Steady and unsteady computational aerodynamics simulations of the corvette zr-1. *SAE*, (921092), 1992.

[13] J. Wiedemann and W.H. Hucho, editors. *Unsteady Flow Effects*. Progress in Vehicle Aerodynamics III. Expert Velang, 2004. ISBN 3-8169-2380-1.

[14] U. Knornschild. *Influence of Unsteady Pitch Angle Changes on a Race Car*, chapter 9, pages 121–132.

[15] P. Aschwanden, U. Knornschild, and J. Muller. Experimental study on the influence of model motion on the aerodynamic performance of a race car. *SAE*, (2006-01-0803), April 2006.

[16] J. Zerihan and X. Zhang. Aerodynamics of a single element wing in ground effect. *Journal of Aircraft*, 37(6):1058–1064, November December 2000.

[17] J. Zerihan and X. Zhang. Unsteady turbulent wake behind a single element wing in ground effect. 10th International Symposium on Applications of Laser Techniques to Fluid Mechanics, Lisbon,Portugal, July 10-13 2000.

[18] X. Zhang and J. Zerihan. Off-surface aerodynamic measurements of a wing in ground effect. *Journal of Aircraft*, vol.40(no.4):p 716–725, July-August 2003.

[19] X. Zhang and J. Zerihan. Aerodynamics of a double-element wing in ground effect. *AIAA Journal*, vol.41(no.6):p 1007–1016, June 2003.

[20] X. Zhang and J. Zerihan. Edge vortices of a double element wing in ground effect. *Journal of Aircraft*, vol.41(no.5):p 1127–1137, Sep-Oct 2004.

[21] A. Senior and X. Zhang. An experimental study of a diffuser in ground effect. *38th Aerospace Sciences Meeting and Exhibit Reno, NV*, (AIAA Paper-2000-118), Jan. 10-13 2000.

[22] A. Senior and X. Zhang. The force and pressure of a diffuser equipped bluff body in ground effect. *Journal of Fluids Engineering: Transactions of the ASME*, Volume 123(Issue 1):pp. 105–111, March 2001.

[23] A. Ruhrmann and X. Zhang. Influence of diffuser angle on a bluff body in ground effect. *Journal of Fluids Engineering*, Volume 125(Issue 2):pp. 332–338, March 2003.

[24] X. Zhang, A. Senior, and A. Ruhrmann. Vortices behind a bluff body with an upswept aft section in ground effect. *International Journal of Heat and Fluid Flow*, Volume 25(Issue 1):Pages 1–9, February 2004.

[25] S. Mahon, C. Gage, and X. Zhang. The evolution of edge vortices underneath a diffuser equipped bluff body. 12th International Symposium on Applications of Laser Techniques to Fluid Mechanics, pages p 1–10, Lisbon, Portugal, 12-15 Jul 2004.

[26] X. Zhang, W. Toet, and J. Zerihan. Ground effect aerodynamics of racing cars. *Applied Mechanics Reviews*, Volume 59(Issue 1):pp. 33–49, January 2006.

[27] W.R. Sears and Th. von Karman. Airfoil theory for non-uniform motion. *Journal of the Aeronautical Sciences*, vol 5(10)(379), 1938.

[28] B. D. Dore. The unsteady forces on finite wings in transient motion. part 1, initial aerodynamic forces following a sudden change of incidence. part 2, transient lift and moment functions for rectangular and delta wings. R&M 3456, Aeronautical Research Council, London, September 1964.

[29] R.H. Landon. Naca0012, oscillatory and transient pitching. In *Compendium of Unsteady Aerodynamic Measurements*, number AGARD-R-702, chapter Data Set 3, pages p. 3.1–3.25. ARGARD, 1982.

[30] R. C. Chang and V. U. Muirhead. Effect of sink rate on ground effect of low-aspect-ratio wings. *Journal of Aircraft*, 24(3):176–180, March 1987.

[31] R. Karkehabadi and D. T. Mook. Wing in heaving oscillatory motion. *Journal of Aircraft*, v 33(n 5):p 913–918, Sep-Oct 1996.

[32] S.A. Thompson, S.M. Batill, and R.C. Nelson. Separated flowfield on a slender wing undergoing transient pitching motions. *Journal of Aircraft*, v 28(n 8):p 489–495, Aug 1991.

[33] D. M. Birch and T. Lee. Tip vortex behind a wing undergoing deep-stall oscillation. *AIAA Journal*, vol.43(no.10):p 2081–2092, 2005.

[34] S. J. Schreck and H. E Helin. Unsteady vortex dynamics and surface pressure topologies on a finite pitching wing. *Journal of Aircraft*, v 31(n 4):p 899–907, July-Aug 1994.

[35] J. Katz and D. Weihs. Behaviour of vortex wakes from oscillating airfoils. *J of Aircaraft*, vol. 15(no. 12), 1978.

[36] D.M. Tang and E.H. Dowell. Experimental investigation of three-dimensional dynamic stall model oscillating in pitch. *Journal of Aircraft*, v 32(n 5):p 1062–1071, Sep-Oct 1995.

[37] D.S. Grismer and J.E. Jenkins. Critical-state transients for a rolling 65-degree delta wing. *Journal of Aircraft*, Vol. 34(No. 3):p 380–386, May-June 1997.

[38] B. Fraser, F.N. Coton, R.B. Green, R. Cannon, and R.A.McD. Galbraith. An analysis of high resolution pressure signals on an oscillating delta wing. 41st AIAA Aerospace Sciences Meeting & Exhibit, Reno, Nevada, U.S.A., 2003.

[39] B.H.K. Lee and F.C. Tang. Unsteady pressure and load measurements on an f/a-18 vertical fin. *Journal of Aircraft*, v 30(n 5):p 756–762, Sep-Oct 1993.

[40] R. Knoller. Die gesetze des luftwiderstandes. *Flug-und Motortechnik*, vol 3:1–7, 1909.

[41] A. Betz. Ein beitrag zur erklaerung des segelfluges. *Zeitschrift fuer Flugtechnik und Motorluftschiffahrt*, vol 3:269–272, 1912.

[42] I. E. Garrick. Propulsion of a flapping and oscillating airfoil. Technical Report NACA 567, 1936.

[43] K. D. Jones, C. M. Dohring, and M. F. Platzer. Experimental and computational investigation of the knoller-betz effect. *AIAA Journal*, 36: 1240–1246, 1998.

[44] J.C.S. Lai and M.F. Platzer. Jet characteristics of a plunging airfoil. *AIAA Journal*, vol. 37(No. 12):p 1529–1537, December 1999.

[45] J. M. Anderson, K. Streitlien, D. S. Barrett, and M. S. Triantafyllou. Oscillating foils of high propulsive efficiency. *Journal of Fluid Mech*, 360: 41–72, 1998.

[46] F. S. Hover, O. Haugsdal, and M. S. Triantafyllou. Effect of angle of attack profiles in flapping foil propulsion. *Journal of Fluids and Structures*, 19: 37–47, 2004.

[47] I. H. Tuncer and M. F. Platzer. Computational study of flapping airfoil aerodynamics. *Journal of Aircraft*, v 37(n 3):p 514–520, May 2000.

[48] G. Pedro, A. Suleman, and N. Djilali. A numerical study of the propulsive efficiency of a flapping hydrofoil. *International Journal for Numerical Methods in Fluids*, vol. 42:pp. 493–526, 2003.

[49] N. Vandenberghe, J. Zhang, and S. Childress. Symmetry breaking leads to forward flapping flight. *Journal of Fluid Mech*, 506, 2004.

[50] J. C. S. Lai and M. F. Platzer. Characteristics of a plunging airfoil at zero freestream velocity. *AIAA Journal*, vol.39(no.3):p 531–534, 2001.

[51] E. A. Becks, T. J. Bencic, and P. Z. Blumenthal. Improved speed control system for an 87,000 hp wind tunnel drive. Technical Memorandom 106840, NASA, 1195.

[52] G. Zhang, T. Chai, and C. Shao. A synthetic approach for control of intermittent wind tunnel. Proceedings of 16th American Control Conference, pages 203–7. American Autom. Control Council, 4-6 June 1997.

[53] N. Nguyen and M. Ardema. Optimal control of a flow recirculation in a wind tunnel. AIAA Guidance, Navigation, and Control Conference, pages p 116–129, Providence, RI, United States, Aug 16-19 2004. AIAA.

[54] Verbruggen H.B. Van Langen Pels, A.F. A predictive controller for the mach number in a transonic wind tunnel. *Control Systems Magazine*, v 11(n 1):63–72, Jan. 1991.

[55] K. J. Astrom and B. Wittenmark. *Adaptive Control*. Addison-Wesley Longman Publishing Co., Inc., Boston, MA, USA, 1994. ISBN 0201558661.

[56] Z. Vukic, L. Kuljaca, and D. Milinovic. Predictive gain scheduling autopilot for ships. In *Electrotechnical Conference, 1996. MELECON '96., 8th Mediterranean*, volume 2, pages 1133 –1136 vol.2, may 1996.

[57] J. S Shamma and M. Athans. Analysis of gain scheduled control for nonlinear plants. *IEEE Transactions on Automatic Control*, 35(8):898–907, 1990.

[58] R.A. Nichols, R.T. Reichert, and W.J. Rugh. Gain scheduling for h-infinity controllers: a flight control example. *Control Systems Technology, IEEE Transactions on*, 1(2):69 –79, jun 1993.

[59] W. E. Leithead D. J. Leith. On incorporating non-equilibrium plant dynamics into gain-scheduling design. *International Conference of Control*, pages 816 –821, September 1998.

[60] W. E. Leithead D. J. Leith. Gain-scheduled and nonlinear systems: dynamic analysis by velocity-based linearization families. *International Journal of Control*, 70(2):289 –317, 1998.

[61] S. Schuler, D. Schlipf, Po Wen Cheng, and F. Allgower. $\ell_1$optimal control of large wind turbines. *Control Systems Technology, IEEE Transactions on*, 21(4):1079–1089, July 2013.

[62] K.J. Hunt, T.A. Johansen, J. Kalkkuhl, H. Fritz, and T. Gottsche. Speed control design for an experimental vehicle using a generalized gain scheduling approach. *Control Systems Technology, IEEE Transactions on*, 8(3): 381–395, May 2000.

[63] M. Farhood and E. Feron. Obstacle-sensitive trajectory regulation via gain scheduling and semidefinite programming. *Control Systems Technology, IEEE Transactions on*, 20(4):1107–1115, July 2012.

[64] M. Postma and R. Nagamune. Air-fuel ratio control of spark ignition engines using a switching lpv controller. *Control Systems Technology, IEEE Transactions on*, 20(5):1175–1187, Sept 2012.

[65] Alexandra Moutinho and JosRaul Azinheira. A gain-scheduling approach for airship path-tracking. In JuanAndrade Cetto, Jean-Louis Ferrier, Jos Miguel Costa dias Pereira, and Joaquim Filipe, editors, *Informatics in Control Automation and Robotics*, volume 15 of *Lecture Notes Electrical Engineering*, pages 263–275. Springer Berlin Heidelberg, 2008. ISBN 978-3-540-79141-6.

[66] CameronR. Nott, SemihM. lmen, DanielR. Lewis, and Keith Williams. Supersonic, variable-throat, blow-down wind tunnel control using genetic algorithms, neural networks, and gain scheduled pid. *Applied Intelligence*, 29(1):79–89, 2008.

[67] Sakakibara S Takashima K Miwa H, Sato M. Closed-loop mach number control and measurement. In *Fluid control and measurement; proceedings of the international symposium*, pages pp 515–520, Tokyo, Japan, 1986.

[68] N. E. Okoro. Development of a supersonic wind tunnel rapid real-time data acquisition and control system. M.s.c. thesis, Mississippi State University, Mississippi State, U.S.A., December 2005.

[69] D. Hodges. Wind tunnel automation with labview. In *Proceedings of the 47th International Instrumentation Symposium*, volume v 47, pages p 1–10, Denver U.S.A., 2001. Instruments Systems and Automation.

[70] M. Lau, G. Seet, and C.Y. Wing. Recirculating wind tunnel measurement and control system optimising data bus communication and distributed processing. *Measurement and Control*, v 22(p 246-248):, 1989.

[71] Sh. S. Graves. Investigation of a technique for measuring dynamic ground effect in a subsonic wind tunnel. Technical Report CR-1999-209544, NASA, August 1999.

[72] E. H. D. Heim. Development of methods for improved data integrity and efficient testing of wind tunnel models for dynamic test conditions in unsteady and nonlinear flight regimes. M.s.c. thesis, Virginia Polytechnic Institute and State University, Virginia U.S.A., December 2003.

[73] P.A. Parker and R. DeLoach. Response surface methods for force balance calibration modeling. 19th International Congress on Instrumentation in Aerospace Simulation Facilities, pages p 283–294, Cleveland, OH, U.S.A., Aug 27-30 2001. IEEE.

[74] W. H. RAE and A. POPE. *Low-speed wind tunnel testing*. John Wiley, New-York, 1984. ISBN 0-471-87402-7.

[75] M.W. Foley, R.H. Julien, and B.R. Copeland. Proportional-integral-derivative x003bb;-tuning for integrating processes with deadtime. *Control Theory Applications, IET*, 4(3):425 –436, march 2010.

[76] K.J. Åstr˙System identificationa survey. *Automatica*, 7(2):123 – 162, 1971.

[77] D. A. Lawrence and W. J. Rugh. Gain scheduling dynamic linear controllers for a nonlinear plant. *Automatica*, 31(3):381–390, 1995.

[78] P. Apkarian and R.J. Adams. Advanced gain-scheduling techniques for uncertain systems. *Control Systems Technology, IEEE Transactions on*, 6(1):21–32, Jan 1998.

[79] T.A. Johansen, K.J. Hunt, and H. Fritz. A software environment for gain scheduled controller design. *Control Systems Magazine, IEEE*, 18(2):48 –60, apr 1998.

[80] S. Tavakoli, I. Griffin, and P.J. Fleming. Toward intelligent control. In *Control Applications, 2005. CCA 2005. Proceedings of 2005 IEEE Conference on*, pages 428 –437, 1989.

[81] C.C. Hang and K.K. Sin. On-line auto tuning of pid controllers based on the cross-correlation technique. *Industrial Electronics, IEEE Transactions on*.

[82] G.A. Dumont, C. Zervos, and P.R. Belanger. Automatic tuning of industrial pid controllers. In *American Control Conference, 1985*, 1985.

[83] W.E. Leithead. Survey of gain-scheduling analysis design. *International Journal of Control*, 73:1001–1025, 1999.

[84] R. McGhee and W. Beasley. Low-speed aerodynamic characteristics of a 17-percent-thick airfoil section designed for general aviation applications. *NASA Technical Note*, (D-7428), December 1973.

[85] A. Williams C Coe, D. Chipperfield. Transients ground effect aerodyanmics. In *6th MIRA Aerodynmics Conferance*, 2006.

[86] H Bergh and H Tijdeman. Theoretical and experimental results for the dynamic response of pressure measuring systems. Technical Report NLR-TR-F.238, 1965.

[87] G. Paniagua and R. Dnos. Digital compensation of pressure sensors in the time domain. *Experiments in Fluids*, Volume 32(Number 4):417–424, April 2002.

[88] C.B. Williams. *Experimental Investigations of the Unsteady Flow on Diamond and Lambda Planform Wings*. Phd thesis, Cranfield University, October 2001.

[89] Th. Bruns, R. Kumme, M. Kobusch, and M. Peters. From oscillation to impact: the design of a new force calibration device at ptb. *Measurement*, 32(1):85 – 92, 2002.

[90] Dr S. Newman. Unsteady aerodynamics lecture series. University of Southampton, Aerodynamic and Flight Mechanics group, 2009.

[91] Hugh W Coleman and W Glenn Steele. Engineering application of experimental uncertainty analysis. *AIAA journal*, 33(10):1888–1896, 1995.

[92] Mark Drela. Xfoil: An analysis and design system for low reynolds number airfoils. In ThomasJ. Mueller, editor, *Low Reynolds Number Aerodynamics*, volume 54 of *Lecture Notes in Engineering*, pages 1–12. Springer Berlin Heidelberg, 1989.

[93] K. Knowles, D. Donahue, and M. Finnis. A study of wings in ground effect. Loughborough University Conference on Vehicle Aerodynamics, pages 22.1–22.13, Loughborough, 1994.

[94] R J E Hart J N Wray N J Lawson, K Knowles and J M Eyles. An experimental investigation using piv of the underflow of a ga(w)-1 aerofoil section in ground effect. 5th MIRA International Vehicle Aerodynamics Conference, page Session 6b, Warwick, 2004.

[95] M.D. Soso and P.A. Wilson. Aerodynamics of a wing in ground effect in generic racing car wake flows. *Journal Proceedings of the Institution of Mechanical Engineers, Part D: Journal of Automobile Engineering*, 1: 1–13, 2006.

[96] Steven A Yon and Joseph Katz. Study of the unsteady flow features on a stalled wing. *AIAA journal*, 36(3):305 – 312, 1998.